# 論文 / 著書情報
# Article / Book Information

| | |
|---|---|
| 題目(和文) | アルミン酸ストロンチウムの溶液燃焼合成と関連プロセスに関する研究 |
| Title(English) | Study on Strontium Aluminates Solution Combustion Synthesis and Related Process |
| 著者(和文) | 田中大基 |
| Author(English) | Hiroki Tanaka |
| 出典(和文) | 学位:博士（工学）,<br>学位授与機関:東京工業大学,<br>報告番号:甲第10177号,<br>授与年月日:2016年3月26日,<br>学位の種別:課程博士,<br>審査員:小田原 修,吉本 護,東 正樹,和田 裕之,長井 圭治 |
| Citation(English) | Degree:,<br>Conferring organization: Tokyo Institute of Technology,<br>Report number:甲第10177号,<br>Conferred date:2016/3/26,<br>Degree Type:Course doctor,<br>Examiner:,,,, |
| 学位種別(和文) | 博士論文 |
| Type(English) | Doctoral Thesis |

A doctoral dissertation

# Study on Strontium Aluminates Solution Combustion Synthesis and Related Process

（アルミン酸ストロンチウムの溶液燃焼合成と関連プロセスに関する研究）

Department of Innovative and Engineered Materials

Interdisciplinary Graduate School of Science and Engineering

Tokyo Institute of Technology

Hiroki Tanaka

March 2016

# Table of Contents

# Chapter 1
# General Introduction

## 1.1 Combustion synthesis and self-propagating high-temperature synthesis

### 1.1.1 Combustion wave propagation

Combustion synthesis technology was originated from an epoch making discovery of self-propagating high-temperature synthesis (SHS) named by A.G. Merzhanov et al. through research on combustion wave propagation in condensed matter [1-3]. The characteristic of SHS is mainly in stable combustion wave propagation with a propagation rate in the range of mm/s~cm/s. In this range of a propagation rate, the product can be synthesized in a high-temperature zone after combustion wave propagates. The products which have high conversion ratios can be synthesized by stabilizing this high-temperature zone. Research of SHS stands on the view point of propagation as a key factor. In the case of SHS, combustion wave propagation is controlled in one direction with suppressing gas generation.

With recent progress of combustion synthesis research, many types of material synthesis technologies used a combustion reaction have been reported. Not only the synthesis technology used a combustion reaction in condensed matter, but also the technologies in gas and solution have been performed. In the case of reaction systems of gas and solution, the condition of combustion wave propagation would be complicatedly disturbed by pressure and temperature change derived from gas phase through phase transition and heat transfer. This phenomena induced disturbance of the

combustion wave front and complication of the reaction propagation rate. Therefore, the characteristics of combustion wave propagation in SHS cannot apply to the reaction system included pressure and temperature change, because combustion wave propagates intricately. A.G. Merzhanov et al. called this reaction system with pressure and temperature change, “thermal explosion (TE)”.

Combustion synthesis means material synthesis technology used in the combustion reaction. Combustion synthesis includes both SHS and TE. SHS is the stable combustion process governed with a propagation rate, and TE is the combustion phenomena governed with complex combustion wave propagation. The relationship between combustion synthesis and SHS is shown in Figure 1.1.

In the case of solution combustion synthesis (SCS) [4] shown in Figure 1.1, the combustion reaction starts almost simultaneously in whole volume, thus combustion wave propagation is not the main characteristic of solution combustion synthesis. The structure formation process after combustion wave propagation is an important factor to clarify the SCS process.

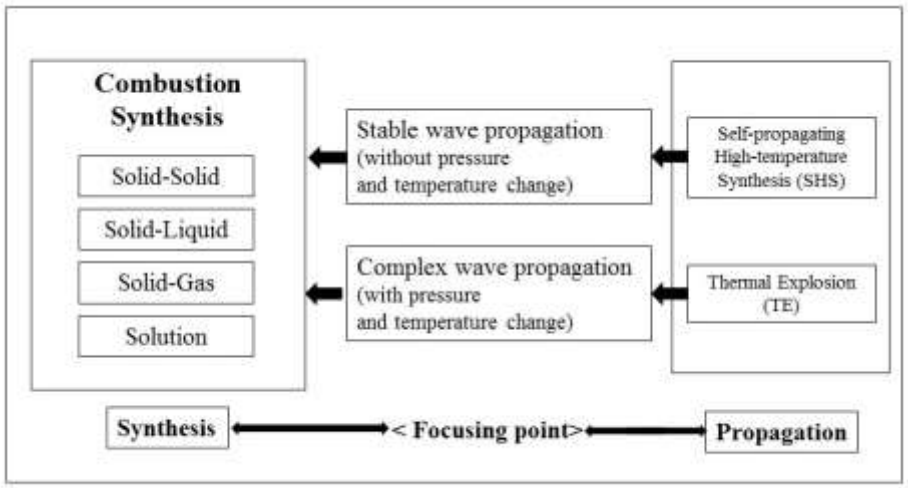


**Figure 1.1 Relationship between combustion synthesis and self-propagating high-temperature synthesis**

In 1967, SHS was discovered with the $TiB_2$ system [1, 2]. In this system, pure $TiB_2$ products are synthesized. In the past, $TiB_2$ could be synthesized by solid-state reaction method in an electric furnace at about 2300 K in a several hours [2].

The combustion reaction of $TiB_2$ is shown in the Equation (1.1).

$$Ti+2B \rightarrow TiB_2$$

$$\Delta H_{298\,K} = -320\ \text{kJ/mol} \qquad (1.1)$$

Here, "$\Delta H_{298\,K}$" is heat of formation of the system.

Adiabatic temperature of the combustion reaction of $TiB_2$ is 3173 K, and thermochemical data of combustion synthesis are shown in Table 1.1.

**Table 1.1 Thermochemical data of starting materials and products in combustion synthesis of $TiB_2$ [5]**

| | | |
|---|---|---|
| $TiB_2$ | Adiabatic temperature | 3173 K |
| | Melting point | 3173 K |
| Ti | Melting point | 1941 K |
| | Boiling point | 3560 K |
| B | Melting point | 2453 K |
| | Boiling point | 3923 K |

In the case of $TiB_2$, the adiabatic temperature is equal to the melting point of $TiB_2$ which is product, and is less than the boiling points of all starting materials (Ti and B), thus the reaction conducted mainly under the gasless system.

The combustion synthesis process of $TiB_2$ is as follows [6]. When a combustion wave front is approaching and temperature of starting materials increase, titanium powders melt and boron atoms are diffused into liquid titanium, which is an exothermic reaction. Then, nuclei of $TiB_2$ are formed in liquid titanium. After the combustion front passes, a structure formation process which recrystallization occurs. The combustion synthesis process of $TiB_2$ is shown in Figure 1.2.

It was reported that in the case of combustion synthesis of the Ti-B system which grain sizes of starting powders of titanium and boron are 50 μm and 0.6 μm, respectively, fine $TiB_2$ in grain size of 0.5 μm can be synthesized [7]. It is because boron diffused into melting titanium would become the nucleus of crystal.

In the combustion process of the Ti-B system, two combustion fronts occur. First, the exothermic reaction of the powder particle surface causes a rapid temperature rise, resulting in rapid reaction propagation. Then, the reaction with phase transition

of the particle inside occurs. This reaction causes slow reaction propagation. Therefore, the reaction of $TiB_2$ can divide into two modes; incomplete reaction with fast propagation and complete reaction with slow reaction. In the case of the Ti-B and Zr-B system, this type of combustion occurs.

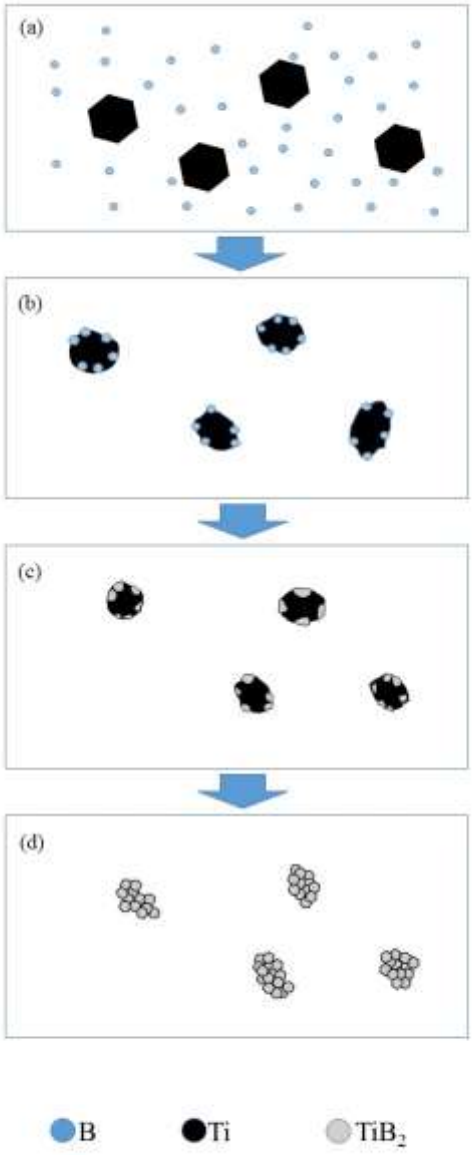


**Figure 1.2 Combustion synthesis of the Ti-B system**

**(a) Starting powder mixture of Ti and B**

**(b) Melting of Ti and diffusion of B into liquid Ti**

**(c) Nucleation of $TiB_2$ in liquid Ti**

**(d) Crystal growth of $TiB_2$**

Combustion synthesis of the Ti-C system was also reported [1, 2]. The combustion synthesis reaction of the Ti-C system is shown in the Equation (1.2).

$$Ti+C \rightarrow TiC$$

$$\Delta H_{298\ K} = -181\ kJ/mol \qquad (1.2)$$

The adiabatic temperature is 3423 K, and thermochemical data of Ti, C, and TiC are shown in Table 1.2. In this case, the adiabatic temperature of the system is lower than the sublimation point of carbon, and between the boiling point and melting point of titanium. Therefore, the combustion reaction would start where melting titanium contacts with solid carbon.

**Table 1.2 Thermochemical data of combustion synthesis of TiC [5]**

| | | |
|---|---|---|
| TiC | Adiabatic temperature | 3423 K |
| | Melting point | 3423 K |
| Ti | Melting point | 1941 K |
| | Boiling point | 3560 K |
| C | Sublimation point | 3913 K |

In addition to combustion synthesis of $TiB_2$ and Ti-C, another type of combustion synthesis was reported [8, 9]. For example, in the case of the Mo-B, Ta-C, and Nb-B system, the adiabatic temperature is lower than all substance included combustion process, gasless combustion mainly occurs.

Combustion synthesis of the Ta-C system is shown in the Equation (1.3).

$$Ta+C \rightarrow TaC$$

$$\Delta H_{298\ K} = 146.4\ kJ/mol \qquad (1.3)$$

Thermochemical data of combustion synthesis are shown in Table 1.3. The adiabatic temperature of TaC is lower than the melting or sublimation points of product (TaC) and starting materials (Ta and C), however, in this system, carbon atoms are diffused into solid Ta. This type of combustion is called solid state combustion. Normally, a reaction propagation rate of solid-state reaction is lower than combustion synthesis of the Ti-B or Ti-C system which starting materials melt in the combustion synthesis process.

**Table 1.3 Thermochemical data of starting materials and products in combustion synthesis of TaC [5]**

| | | |
|---|---|---|
| TaC | Adiabatic temperature | 2800 K |
| | Melting point | 4270 K |
| Ta | Melting point | 3270 K |
| C | Sublimation point | 3915 K |

Combustion synthesis in condensed matter of Ti-B, Ti-C, and TaC was discussed, so far. Difference among these systems is shown in Table 1.4. In the case of combustion synthesis of Ti-B and Ti-C, adiabatic temperatures are equal to the melting points of products. In the case of the Ti-B system, all starting reactants would melt, however, in the case of the Ti-C system, only titanium would melt. Therefore, the reaction propagation rate of the Ti-B system is higher than that of the Ti-C system. In contrast, the adiabatic temperature of the Ta-C system is lower than melting or

sublimation points of all reactants and products, therefore, the reaction proceeds in solid phase and a reaction propagation rate is low compared with combustion synthesis which conducts in liquid phase, such as Ti-C and Ti-B.

**Table 1.4 Combustion synthesis of the Ti-B, Ti-C, and Ta-C system**

| **Systems** | **Adiabatic temperatures comparison with transition points** |
|---|---|
| Ti-B | $T_m$ (Ti) <$T_m$ (B) <$T_m$ ($TiB_2$) =$T_{ad}$ |
| Ti-C | $T_m$ (Ti) <<$T_m$ (TiC) =$T_{ad}$<$T_s$ (C) |
| Ta-C | $T_{ad}$<$T_m$ (Ta) <$T_s$ (C) <$T_m$ (TaC) |

The schematic illustration of SHS process is shown in Figure 1.3 [10]. In this figure, the reaction initiates on the right side, and the combustion wave propagates from right to left. The pre-heating zone is the zone that the temperature increases because of heat from the reaction zone. In the reaction zone, the main combustion reaction occurs, and the temperature of the sample reaches very high, which is referred to the adiabatic temperature of the system, by heat of formation which the reaction system itself have. In the post-combustion zone, high temperature is kept because of heat from the reaction zone. In this zone, recrystallization and structure formation of samples occurs, resulting in synthesizing final products.

Generally, the combustion synthesis consists in two processes, the reaction propagation process and structure formation process. The pre-heating zone and reaction zone relate to the reaction propagation process. Thermo-gravitational transportation and fluctuation of the liquid phase are considered to affect the combustion propagation rate in this reaction propagation process. This reaction

propagation process subsequently affects the latter, the structure formation process, which relates to the post-combustion zone, resulting in final products. Typical values of combustion synthesis are shown in Table 1.5 [2].

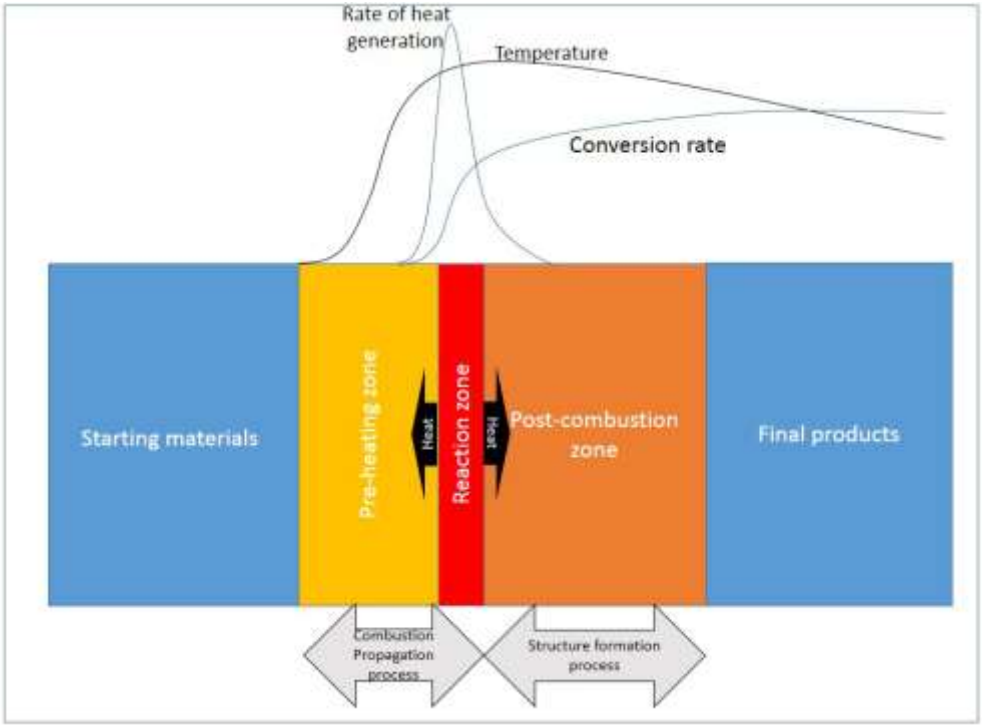


**Figure 1.3 Schematic illustration of self-propagating high-temperature synthesis (SHS)**

**Table.1.5 Typical values of parameters of**

**self-propagating high-temperature process [2]**

| **Parameters** | **Values** |
|---|---|
| **Maximum temperature** | 1000 K~4300 K |
| **Reaction propagation rate** | 0.1-15 cm/s |
| **Thickness of synthesis zone** | 0.1~5.0 mm |
| **Rate of heating** | 1000~1000000K/s |
| **Intensity of initiation** | 42~4200 J/cm$^2$s |
| **Duration of initiation** | 0.05-4 s |

As an example of gas included combustion synthesis, synthesis of metal nitrides is a typical system. Starting samples are a metal powder compact and $N_2$ gas [11]. The combustion reaction is shown in the Equation (1.4).

$$M+1/2 \cdot N_2 \rightarrow MN \qquad (1.4)$$

Here, M is the metal element.

When the adiabatic temperature of the system is higher than the melting point of the product, a nitridization rate is not so high, because the melting product prevents $N_2$ gas from penetrating into products. When the adiabatic temperature is equal to or lower than the melting point of the product, $N_2$ gas can penetrate into the center of the sample.

In the case of combustion synthesis of TiN with $N_2$ gas, the compact which is the composition of Ti about 40% would be only nitridization under an atmospheric pressure, because $N_2$ gas penetration inside of Ti compact is suppressed by melting

titanium in the zone, where reactions between Ti and $N_2$ occur. Decreasing packing density of Ti compact is one of the methods for improving low conversion ratio. However, this method would cause to increase to a propagation rate, resulting in decreasing a conversion rate. In order to increase the conversion ratio of combustion synthesis of nitrides, some attempts were reported. J.B. Holt and his colleagues were using sodium azide as a nitrogen source. The combustion reaction of the Ti-N system used sodium azide is shown in the Equation (1.5) [12].

$$3Ti+NaN_3 \rightarrow 3TiN+Na \quad (1.5)$$

In this case, sodium is easily volatized, and pure nitrides are obtained.

Another unique combustion synthesis used liquid nitrogen also has been reported. Liquid nitrogen has a characteristic of high density, which contributes to increase in the amount of the nitrogen for the reaction. This result shows that liquid nitrogen is effective for improving conversion. It is reported about 90 % of TiN could be obtained [13, 14].

In the case of combustion synthesis of ZnS, the adiabatic temperature of the system is 2200 K, and the sublimation point of ZnS is 1655 K [5]. Therefore, products are easily sublimated under atmospheric pressure. To avoid product sublimation, the combustion synthesis process can be performed under high pressure. It is reported that the combustion reaction of the ZnS system in condensed matter is conducted under 4 MPa in argon atmosphere [15, 16]. In this case, α-ZnS was synthesized. However, combustion synthesis of ZnS in atmospheric pressure had not been reported, because the starting materials (Zn and S) and product (ZnS) would vaporize in atmospheric pressure. Combustion wave propagation in the vapor phase is interesting theme

because solution combustion synthesis is also gas-included combustion synthesis. Combustion synthesis of ZnS in atmospheric pressure will be described in Chapter 5.

Almost every inorganic compound can be synthesized by combustion synthesis. Products of combustion synthesis are shown in Table 1.6 [17]. Those of the compounds listed in Table 1.6 are just only examples of combustion synthesized products.

**Table 1.6 Combustion synthesized products**

| Compounds | Products | Systems of Starting materials |
|---|---|---|
| **Borides** | $MgB_2$, $TiB_2$, $AlB_2$, $ZrB_2$ | Solid-solid |
| **Carbides** | TiC, $CaC_2$, SiC, TaC, VC, WC | Solid-solid |
| **Silicates** | TiSi, $NbSi_2$, $TaSi_2$, $MoSi_2$, $Mo_3Si$ | Solid-solid |
| **Intermetallics** | NiAl, NiTi, TiAl | Solid-solid |
| **Sulfides** | ZnS, CaS, $TiS_2$, $ZrS_2$ | Solid-solid |
| **Phosphides** | InP, GaP | Solid (liquid)-solid |
| **Nitrides** | TiN, AlN, $Si_3N_4$, | Solid-liquid, Solid-gas |
| **Hydrides** | $TiH_2$, $ZrH_2$, $HfH_2$, YH | Solid-gas |
| **Oxides** | $Al_2O_3$, $Fe_2O_3$, $Y_2O_3$, $MgAl_2O_4$, $SrAl_2O_4$ | Solution |

In 1988, a new combustion synthesis method of synthesizing oxides was reported, which was called “solution combustion synthesis (SCS)” [4, 18]. With this technology, oxide nano particles can be synthesized with heating of starting solution by

heating devices. Solution combustion synthesis is based on initiation by volume heating of the highly exothermic and fast redox reaction between metal nitrates and organic fuels. In the case of SCS, starting materials are mixed in molecular level in starting solutions.

## 1.1.2 Ignition

The ignition process of SCS is completely different from that of SHS. These two types of combustion synthesis are shown in Figure 1.4 [19]. In the case of SHS, the reaction will start by partial heating by heating device such as filament, laser, and chemical oven. On the other word, in the case of SCS, the reaction will start by volume heating by heating device such as electric furnace, hotplate, and microwave.

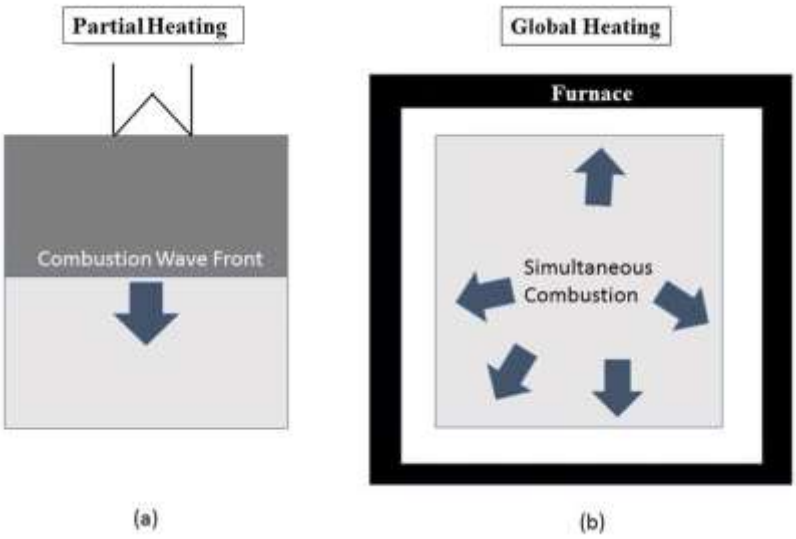


**Figure 1.4 Ignition of**

**(a) Self-propagating high-temperature synthesis (SHS)**

**(b) Solution combustion synthesis (SCS)**

In the case of SHS, combustion wave can propagate in one direction. On the other hand, in the case of SCS, the combustion reaction occurs in whole samples almost simultaneously, then the combustion reaction finished almost simultaneously, and after combustion finished, the temperature of the sample decreases rapidly with large amount of heat of evaporation with releasing the gas. Schematic illustrations of these temperature profiles are shown in Figure 1.5.

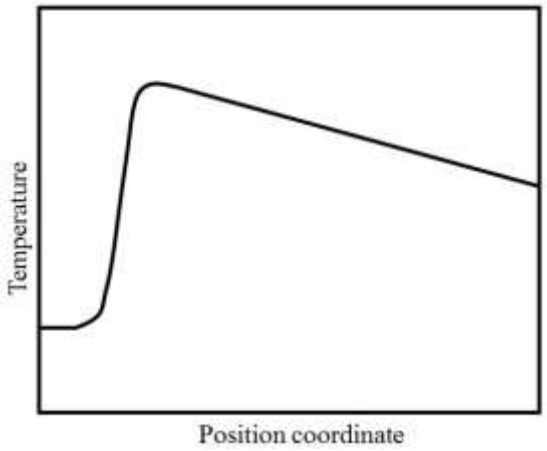


(a)

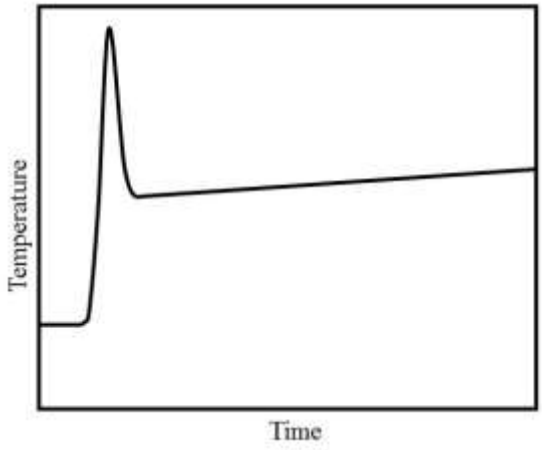


(b)

**Figure 1.5 Temperature profile of the combustion synthesis process**

**(a) Self-propagating high-temperature synthesis (SHS)**

**(b) Solution combustion synthesis (SCS)**

The theory of a reaction propagation rate in solid and gas was already proposed [17, 20-22]. The outline of this theory is as follows. The schematic illustration of combustion synthesis of particles is shown in Figure 1.6.

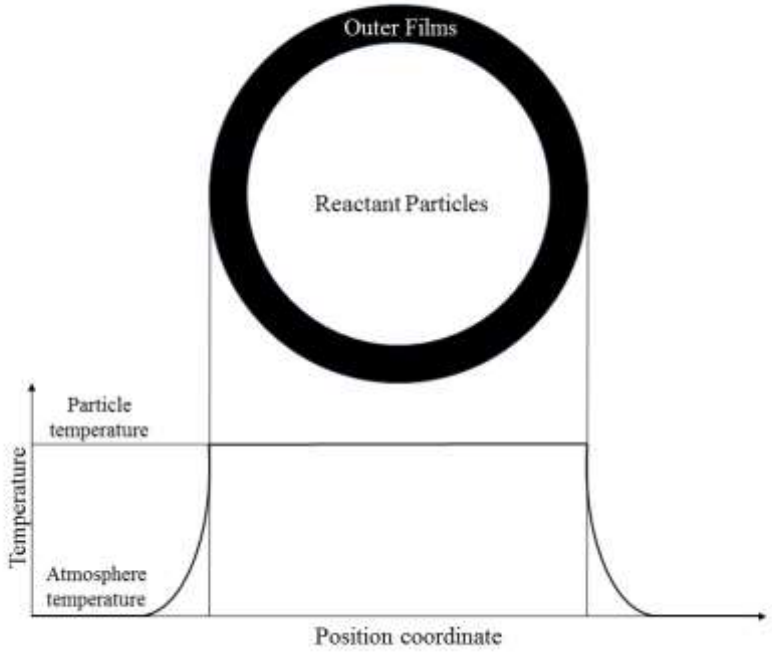


**Figure 1.6 Schematic illustration of ignition process [17]**

In combustion synthesis process, the micro reaction in small particle leads to the macro reaction of the large zone propagation. Therefore, the mechanism of ignition propagation in the powder particles should be investigated.

The Equation (1.6) shows the ignition of metal particles.

$$C \cdot m \cdot dT/dt = Q \cdot m \cdot d\eta/dt - \alpha \cdot S(T-T_0) - \varepsilon \cdot \sigma \cdot S(T^4-T_0^4) \qquad (1.6)$$

Where, *"Q"* is the heat of the reaction, *"m"* in the mass of the particle. *"η"* is the decree of particle conversion into the products, *"α"* is the heat transfer coefficient, "ε" is the degree of blackness, *"σ"* is the Stefan-Boltzmann constant, *"S"* is the surface

area of the particle, *"C"* is specific heat, *"T"* is the particle temperature, *"$T_0$"* is the gas temperature, and *"t"* is the time.

By the model of a zero order reaction, the Equation (1.7) is derived from the Equation (1.6) with Arrhenius type reaction.

$$d\theta/d\tau = e^{\theta} - \theta/K \tag{1.7}$$

Where, K is the Semenoff parameter ($=Q \cdot m \cdot E/\alpha \cdot S \cdot R \cdot T_o^2$), and $\theta$ ($=E(T-T_o)/RT_o^2$) and $\tau$ ($=Q \cdot E \cdot t/C \cdot R \cdot T_o^2$) are the dimensionless variables in temperature and time, respectively, *"E"* is the activation energy, and *"R"* is the gas constant.

The combustion reaction type is changed at $K=e^{-1}$. When $K$ is more than $e^{-1}$, combustion propagated spontaneously, and $K$ is less than $e^{-1}$, combustion does not occur.

With respect to the reaction propagation, it is derived from Equations (1.8) and (1.9) which is considered to one-dimensional thermal and mass balances.

$$\lambda\, d^2T/dx^2 - CV \cdot dT/dx + Q\rho[Ko \cdot \exp(-E/RT)](1-\eta)^n = 0$$

$$x=-\infty \rightarrow T=T_0,\ \rho=0$$

$$x=+\infty \rightarrow T=T_m=T_0+Q/C,\ \rho=1 \tag{1.8}$$

$$D \cdot d^2\rho/dx^2 - V \cdot d\rho/dx + [K_0 \cdot \exp(-E/RT)](1-\rho)^n = 0 \tag{1.9}$$

Where, *"$\lambda$"* is the thermal conductivity, *"$\rho$"* is the density, *"V"* is the combustion rate, *"$T_m$"* is the highest temperature attainable with complete conversion of the reactant, *"D"* is the diffusion coefficient, *"$K_0$"* is the pre-exponential factor, and "*n*" is the

reaction order.

In the case of gasless combustion, evaporation and chemical gas-forming reactions are absent. Therefore, it is characterized by the absence of diffusion and constancy in substance density. The expression for combustion rate is described as the Equation (1.10).

$$V^2=\mathrm{F}(n)\cdot(\lambda/Q\rho)\cdot(RT_m^2/E)\ K_o\exp(-E/RT_m)$$

$$F(n)=2[\Gamma(n/2+1)]^{(1-n/2)}(n/2\mathrm{e})^{n2/4}$$

$$\Gamma(Z)=\int_0^{\infty}e^{-1}t^{(Z-1)}dt \qquad (1.10)$$

In the case of gasless combustion, combustion rate is inversely proportional to the square root of the reactant density.

In the gas phase combustion, the diffusion coefficient is considered to be thermal diffusivity ($D=\lambda/C$) and the density is constant. The combustion rate is expressed as an Equation (1.11).

$$V^2=2n!\ (CRT_m^2/QE)^{n+1}(\lambda/C_\rho)\cdot K_0\exp(-E/RT_m) \qquad (1.11)$$

In the combustion process due to violent gassing in the condensed phase as a result of thermal decomposition and dispersing of liquid form, the large increase in volume causes that the pressure of "$P$" affects the reactant density (D=0) and $\rho=\rho_c[1+\eta B(\rho_c RT/MP-1)]$. The Equation (1.11) can be expressed for the combustion rate $n$=1 as shown in Equation (1.12).

$$V^2=2(\lambda MT_m/QEB)PK_0\exp(-E/RT_m)/\rho^2 \quad (1.12)$$

Where, "*M*", "*B*" and "$\rho_c$" are the molecular mass of the gaseous product, the fraction of the gaseous products in substance decomposition, and the density of the condensed phase, respectively.

The combustion rate is inversely proportional to the density in this dispersing combustion. These results of gasless combustion and gas included combustion are summarized in Table 1.7.

The combustion process of metal particles is shown in Figure 1.7. In this figure, particle size and particle temperature are taken into consideration. In the combustion process of metal particles, the oxide film formed on the particle surface plays a predominant role regarding the combustion characteristics. The relation between surface temperature and the melting point of oxide produced particle surface is an important factor of the morphology of product particles.

**Table 1.7 Combustion rates of gasless combustion and gas included combustion**

**"$V_c$" is combustion rate, d is the density of reactant.**

| **Combustion type** | **Gasless systems** | **Gas included systems** |
|---|---|---|
| **Combustion rate** | $V_c \propto \frac{1}{\sqrt{d}}$ | $V_c \propto \frac{1}{d}$ |

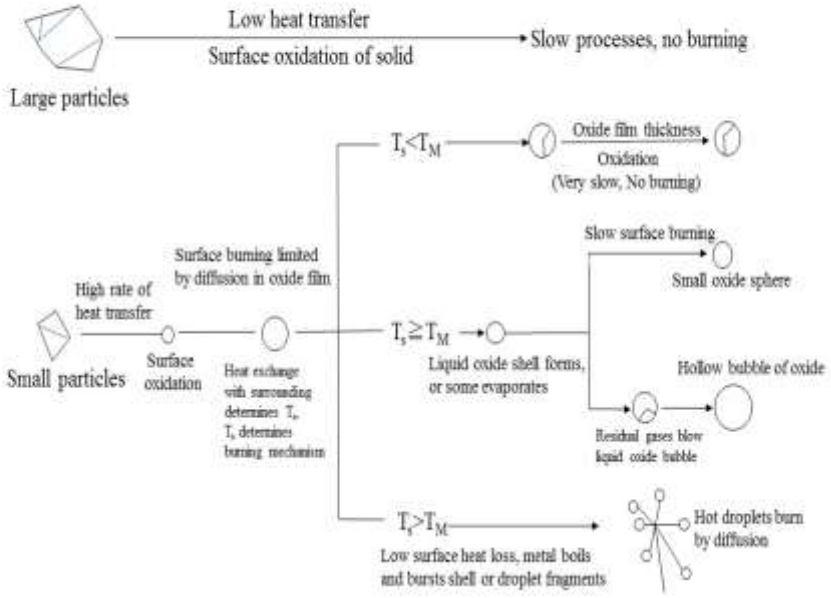


**Figure 1.7 Combustion of metal particles**

**(O. Odawara et al. (1988) [17])**

**$T_s$ is surface temperature and $T_m$ is melting point of oxide produced.**

# 1.2 Solution combustion synthesis

The solution combustion synthesis reaction is the redox reaction between nitrates and fuel. For example, solution combustion synthesis of $Al_2O_3$ using urea is shown in the Equation (1.13) which was reported by K.C. Patil in 1988 [4].

$$2Al(NO_3)_3 \cdot 9H_2O+5CO(NH_2)_2$$

$$\rightarrow Al_2O_3+5CO_2+10H_2O+8N_2 \qquad (1.13)$$

Schematic illustration of the solution combustion synthesis is shown in Figure 1.8. Oxide nano particles can be synthesized only heating solution of nitrides and fuel [23-30]. In starting solution, starting materials are mixed in molecular level, therefore combustion synthesis process is performed in the reaction field of molecular level, resulting in a uniform composition of products. Examples of the products of solution combustion synthesis are shown in Table 1.8.

Solution combustion synthesis is also the gas included system. Because part of organic fuels and some kind of nitrates are gasified. Therefore, the correlation between the amount of starting materials and the products is an interesting theme. Moreover, in the research field of solution combustion synthesis, there are not many reports about the solution combustion synthesis process. It needs to clarify the process of the solution combustion synthesis process.

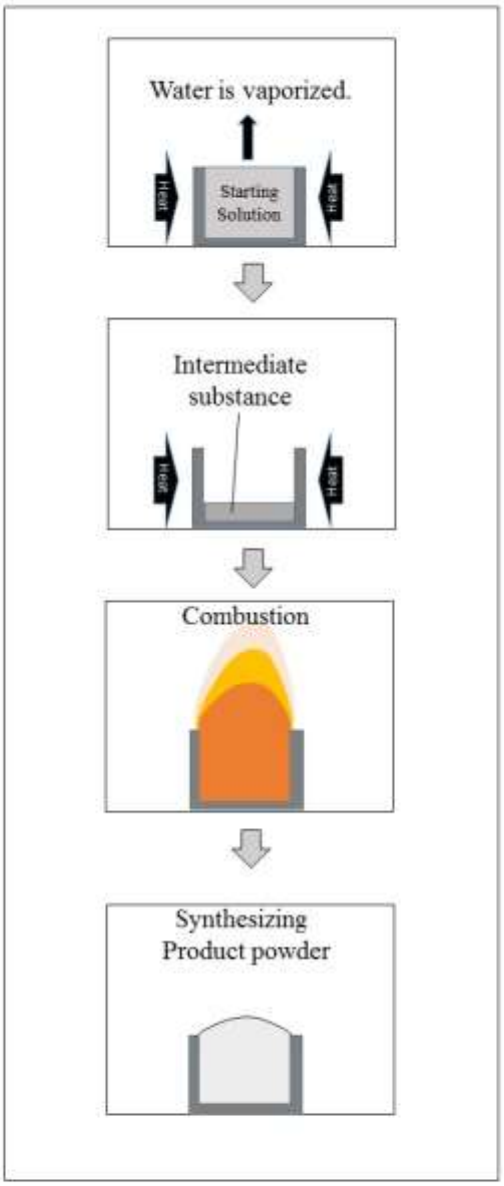


**Figure 1.8 Schematic illustration of solution combustion synthesis method**

**Table 1.8 Products of solution combustion synthesis**

| **Compounds** | **Products** |
|---|---|
| **Mono-oxides** | $Al_2O_3$[4, 31-33], $CeO_2$[34, 35], $ZrO_2$[35], $Fe_2O_3$[36], $Gd_2O_3$[37, 38], $Y_2O_3$[39-42], $MnO_2$[43], $Cr_2O_3$[44], ZnO[45-50], CuO[51] |
| **Complex oxides** | $SrAl_2O_4$[18], $CaAl_2O_4$[52-55], $MgAl_2O_4$[56-63], $LiMn_2O_4$[64-65], $LiCoO_2$[66-67], $LiAlO_2$[68], $YCoO_3$[69], $BiVO_4$[70,71], $LaAlO_3$[72], $Y_3Al_5O_{12}$[73-75] |

The reaction of these methods includes the oxidation-reduction reaction between nitrates and organic fuels such as urea [$CO(NH_2)_2$], glycine [$NH_2(CH_2)COOH$], and carbohydrazide [$CO(N_2H_3)_2$]. Starting solution of nitrates and fuels were heated in a furnace, in a microwave, or on a hot plate, then the combustion reaction occurs after evaporation of solvent and fine oxide particles are obtained.

To control the distribution and particle sizes of products, it is important to make clear the process of solution combustion synthesis. Not only mono oxide particles, but complex oxide particles can be synthesized by solution combustion synthesis.

$SrAl_2O_4$ which is a well-known host matrix of long-lasting phosphor is notable materials. Physical properties of $SrAl_2O_4$ will be discussed in Chapter 2.

The combustion reaction of $SrAl_2O_4$ is shown in the Equation (1.14),

$$Sr(NO_3)_2+2Al(NO_3)_3\cdot 9H_2O+ 20m/3\ CO(NH_2)_2+10(m\text{-}1)\ O_2$$
$$\rightarrow SrAl_2O_4+20m/3\ CO_2+(40m+54)/3\ H_2O+(20m+12)/3\ N_2 \qquad (1.14)$$

Where, "*m*" is a stoichiometric fuel ratio.

In order to apply the solution combustion synthesis to synthesize functional materials, it is necessary to make clear and control the process of solution combustion synthesis precisely. Furnace temperature, the kind of fuels, fuel ratio, heating time can be controlled as parameters in solution combustion synthesis experiments. The characteristics of solution combustion reactions, such as reducing power and generated gas amount, can be controlled by the selection of fuel, such as urea [$CO(NH_2)_2$], glycine [$NH_2(CH_2)COOH$], and carbohydrazide [$CO(N_2H_3)_2$].

Necessary conditions to select organic fuels of solution combustion synthesis are follows; water soluble, oxidizer compatible, high reducing power, and including highly reactive functional group such as amino group. Because urea is compatible with aluminum nitrate in solution, urea is suitable fuels of solution combustion synthesis of alumina.

Temperature profiles during self-propagating high-temperature synthesis process and solution combustion synthesis process were already shown in Figure 1.5.
In the case of SHS, in general, the combustion front passed in one direction, therefore combustion synthesis process can be controlled through research of the reaction propagation process. However, in the case of SCS, because of almost simultaneous combustion in the whole volume, it is difficult to control reaction propagation process. Therefore, in the case of SCS, the combustion synthesis process can be controlled by changing pre-heating circumstance and fuel condition.

Synthesizing high-temperature phase (β-phase) is also the unique characteristic of combustion synthesis technology. Because of the rapid cooling process after the combustion reaction, β-phase can be preserved. This characteristic of preserving β-phase can also be seen combustion synthesis of the gas-included system

such as combustion synthesis of $Si_3N_4$ [76, 77].

Nowadays, aluminates got a lot of attention as a host matrix of long-lasting phosphors [78]. $SrAl_2O_4$ doped with rare earth ions has a characteristic of long-lasting luminescence. It was reported that luminescence efficiency of β-$SrAl_2O_4$ doped with $Eu^{2+}$ and $Dy^{3+}$ is higher than that of α-$SrAl_2O_4$ [79]. Strontium aluminates can be synthesized by SCS [18], however the report of synthesizing β-phase products by SCS is few. Therefore, SCS of synthesizing β-phase is a notable theme in the research field of combustion synthesis.

Therefore the influence of pre-heating circumstance of SCS into phases of products will be discussed in Chapter 3, and solution combustion synthesis process will be discussed in Chapter 4.

## 1.3 The purpose of this work

Generally, the combustion synthesis process consists in two processes, the reaction propagation process and structure formation process. The reaction propagation process is that the chemical reaction occurs in a successive zone resulting in combustion wave propagation. The structure formation process is that recrystallization and structure formation proceed at the zone behind the passing combustion wave. In the case of SHS which combustion wave propagates in one direction, the combustion wave propagation process is an important factor to clarify combustion synthesis process. However, in the case of SCS, the combustion reaction initiates in whole volume almost simultaneously, and combustion wave propagates in any direction. Therefore, propagation is not a key factor to clarify SCS process. To

clarify the SCS process, the structure formation process is an important factor. However, there are few reports about the structure formation process of SCS. Indeed, in the case of SCS of complex oxides, the combustion synthesis process has not been cleared.

Therefore, the main theme of this work is "To clarify the structure formation process of solution combustion synthesis of strontium aluminates".

To clarify this theme, following research was described in this thesis.

(1) In order to make clear how starting materials react, the influence of starting conditions such as pre-heating temperature and fuel ratio on phase composition of the final products including α-phase and β-phase was investigated.

(2) In order to clarify the solution combustion synthesis process in time series, the evolution of synthesized substances during the process of solution combustion synthesis was clarified by using the method of arrested samples.

The results of these two themes would be of help to elucidate the structure formation process and how to synthesize β-$SrAl_2O_4$ by SCS. Some results revealed in this work [80, 81] have been recently referred at the report published in physical chemistry chemical physics [82], where the present data relating to β-$SrAl_2O_4$ solution combustion synthesis are mainly concerned.

The construction of this thesis is as follows:

**Chapter 1**

This chapter shows the outline of combustion synthesis and the purpose of this work.

**Chapter 2**

This chapter shows thermodynamic analysis of solution combustion synthesis of $SrAl_2O_4$. In this chapter, the results of thermal analysis and thermochemical calculation are discussed. It will be shown that the adiabatic temperature of the system is higher than transition points of all starting materials and lower than a transition point of products.

**Chapter 3**

This chapter shows the influence of the starting conditions of the solution combustion synthesis of $SrAl_2O_4$ on products. In order to control phase composition included α-$SrAl_2O_4$ and β-$SrAl_2O_4$ of products, starting conditions such as fuel ratio and furnace temperature were changed.

**Chapter 4**

The solution combustion synthesis process of strontium aluminates was studied. This process has still been unclear. In this work, the arrested sample method is investigated to clarify the whole process of solution combustion synthesis of strontium aluminates, and the process of solution combustion synthesis of $SrAl_2O_4$ is proposed. This process might apply to synthesizing β-phase by SCS many kinds of complex oxides.

**Chapter 5**

This chapter gives combustion synthesis of ZnS as a related process to strontium aluminates solution combustion synthesis. In the case of solution combustion synthesis of strontium aluminates, the heat of reaction is relatively low, and the combustion reaction will initiate with increasing combustion temperature by changing urea ratio and furnace temperature. On the other hand, in the process of combustion synthesis of ZnS, a combustion wave front can propagate directionally which is similar to the process of SHS. However, gas phases are produced behind the combustion wave, because the adiabatic temperature of the system is higher than the decomposition temperature of products. Behind the combustion wave, the temperature of sample decrease to below the decomposition temperature of ZnS, resulting in crystallizing β-ZnS. In this chapter, the influence of heat of reaction in the process of combustion synthesis will be discussed.

**Chapter 6**

Finally, the conclusion of this work is presented in Chapter 6.

# Chapter 2
# Thermochemical study for solution combustion synthesis of $SrAl_2O_4$

## 2.1 Introduction

Thermodynamics calculation is important for combustion synthesis because it suggests that the combustion reaction occurs or not and estimates the maximum temperature during combustion synthesis process. In this chapter, thermodynamics calculation of solution combustion synthesis (SCS) of $SrAl_2O_4$ is introduced. $SrAl_2O_4$ is selected in this work because it is unique optic complex oxides. It is known that $SrAl_2O_4$ nano oxides can be synthesized by SCS [18], however, control of phase composition and particle sizes has not been achieved yet, therefore in this work, $SrAl_2O_4$ was selected as target of research.

## 2.2 Strontium aluminates

Nano phosphors are important materials due to their chemically and thermally stable characteristics [24]. For example, ZnS has been used host matrix of phosphors for several decades [83-87]. $Y_2O_3$ is a well-known matrix of phosphors which has higher stability [42, 88], $Y_3Al_5O_{12}$ (YAG) is known as a host of lasers and for a phosphor [89], and $SrAl_2O_4$ is also a host matrix of phosphors [78]. To apply phosphors to devices, fine nano particles are needed for high resolutions. Moreover, it

is reported that nano particles phosphors have unique luminescent properties, like blue shift etc. However, when nano phosphors are synthesized by typical solid state reaction method, additional process such as grinding is needed, resulting in surface defect is formed.

Long lasting phosphors have been widely applied in the real world such as the dial plate of a watch, sign of emergency exit, etc. Historically speaking, ZnS doped radioactive materials such as Pm-147 were widely used as long-lasting phosphors, however, sulfides are chemically unstable and endurable materials. Moreover, radioactive materials are harmful to our health and difficult to dispose.

In 1996, new long lasting phosphors of strontium aluminates were invented [78]. Because of chemically stable and non-toxic properties of oxides, nowadays this phosphor is widely used in the real world. Table 2.1 [90] shows major long lasting phosphors of aluminates.

**Table 2.1 Long-lasting phosphor of aluminates [90]**

| **Host materials** | **Dopants** | **Luminescent wavelength [nm]** | **Afterglow duration [h]** |
|---|---|---|---|
| **$CaAl_2O_4$** | $Eu^{2+}$, $Dy^{3+}$ | 440 | 5 |
| **$BaAl_2O_4$** | $Eu^{2+}$, $Nd^{3+}$ | 500 | 2 |
| **$SrAl_2O_4$** | $Eu^{2+}$, $Dy^{3+}$ | 520 | 30 |
| **$SrAl_4O_7$** | $Eu^{2+}$, $Dy^{3+}$ | 480 | 3 |
| **$Sr_3Al_2O_6$** | $Eu^{2+}$, $Dy^{3+}$ | 510 | 1 |

In the literature, the host matrix of $SrAl_2O_4$ shows extremely long afterglow

duration time. In the crystal structure of $SrAl_2O_4$, $Eu^{2+}$ ions role luminescent center and this luminescence is caused by the transition between the $4f^6 5d^1$ and $4f_7$ electron configurations [91]. Ion radius of $Eu^{2+}$ is almost same as $Sr^{2+}$, therefore when $Eu^{2+}$ ions are doped, $Sr^{2+}$ ions would be displaced to $Eu^{2+}$ ions. $Dy^{3+}$ ions would be an important function of long afterglow duration. $Dy^{3+}$ ions are also doped into $Sr^{2+}$ sites. $Dy^{3+}$ ions would trap electrons, and emit electron slowly by thermal luminescence, resulting in long afterglow duration [90]. Distance between $Eu^{2+}$ and $Dy^{3+}$ in the matrix would affect luminescent and afterglow properties of phosphors. It was reported that $SrAl_2O_4$ has two phases [92, 93], monoclinic structure (low temperature phase, α-phase) and hexagonal structure (high temperature phase, β-phase). It was reported that the transition temperature from monoclinic to hexagonal structure is around 920K [92]. These two structures are shown in Figures 2.1 and 2.2.

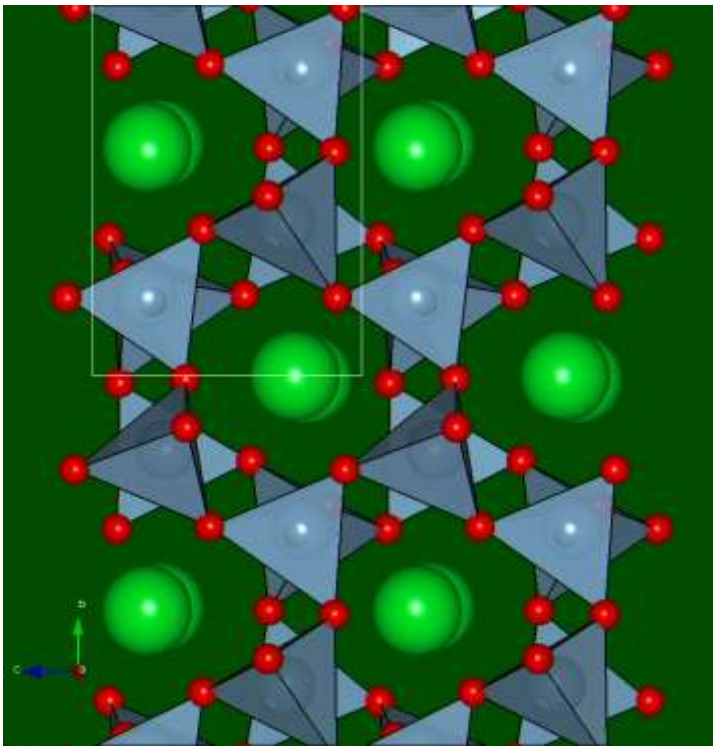

**Figure 2.1 Monoclinic structure of $SrAl_2O_4$ (α-$SrAl_2O_4$)**

**(Blue tetrahedrons: $AlO_4^{5-}$, Green balls: $Sr^{2+}$) [94, 95]**

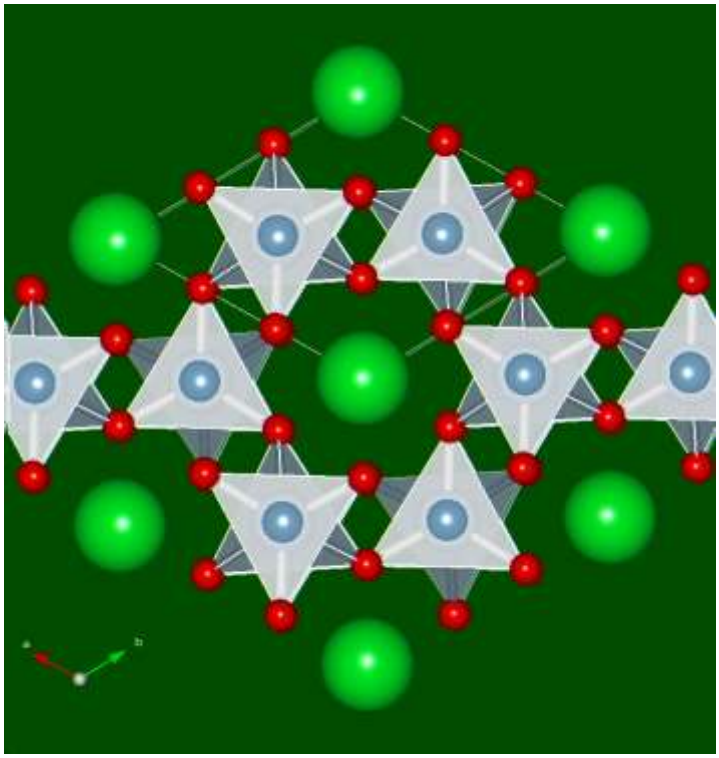

**Figure 2.2 Hexagonal structure of $SrAl_2O_4$ ($\beta$-$SrAl_2O_4$)**

**(Blue tetrahedrons: $AlO4^{5-}$, Green balls: $Sr^{2+}$) [93, 95]**

In Figures 2.1 and 2.2, pyramid-like structure is $AlO_4^{5-}$, and green sphere is $Sr^{2+}$ ions. The difference between $\alpha$-$SrAl_2O_4$ and $\beta$-$SrAl_2O_4$ is arrangements of $AlO_4^{5-}$ structure. In the case of $\alpha$-$SrAl_2O_4$, $AlO_4^{5-}$ makes distorted arrangement, on the other hands, $\beta$-$SrAl_2O_4$ makes symmetric arrangement.

Crystal parameters of these two phases are shown in Table 2.2 [92, 94]. It is reported that the emission wavelengths of $\alpha$-$SrAl_2O_4$, Eu, Dy and $\beta$-$SrAl_2O_4$, Eu, Dy are both 520 nm, however $\beta$-$SrAl_2O_4$, Eu, Dy shows stronger intensity than $\alpha$-$SrAl_2O_4$.

**Table 2.2 Crystal parameters of α-$SrAl_2O_4$ and β-$SrAl_2O_4$ [92, 94]**

| Structure | Crystal structure type | Lattice parameters | | | |
|---|---|---|---|---|---|
| | | a [nm] | b [nm] | c [nm] | β [nm] |
| α-$SrAl_2O_4$ | Monoclinic | 0.844 | 0.882 | 0.516 | 93.4 |
| β-$SrAl_2O_4$ | Hexagonal | 0.514 | 0.514 | 0.846 | - |

To synthesize $SrAl_2O_4$, usually solid-state reaction method, sol-gel method, spray dry method, and co-preparation method are used. These methods are shown in Table 2.3.

**Table 2.3 Synthesis methods of strontium aluminates**

| Methods | Process time | Heating temperature | Phase | Products Morphology | References |
|---|---|---|---|---|---|
| **Solution combustion synthesis** | ~10min | 873 K~ | α, β | Nano particles | [80, 81] |
| **Spray dry** | 2 h | 1600 K | amorphous | Particles in μm order | [96] |
| **Solid state reaction** | 7 h | 1600 K~ | α | Bulk | [78] |
| **Sol-gel** | 30 h | 360~390 K | α | Nano particles | [97] |
| **Coprecipitation method** | 24 h | 400 K~ | α | Bulk | [98] |

In the case of solid-state reaction method, to obtain homogeneous and well-crystalline products, high temperature circumstances, many steps and a long

process time are necessary. Moreover, because of these conditions, it is difficult to synthesize nanoparticles without any other step like grinding resulting in surface defects. The sol-gel method can be synthesized well crystalline method, however, it need too long time. The spray dry method can be synthesized in few seconds, however, as-prepared samples are amorphous phase.

On the other hands, in solution combustion synthesis, starting solution would react within a short interval (several minutes) and in a low temperature (873 K~) [80, 81]. Moreover, the solution combustion synthesis method can be synthesized β-phase containing products because of large temperature gradients during combustion synthesis process. In the case of solution combustion synthesis method, it is reported that $SrAl_2O_4$ nanoparticles shows blue shift (from 520 nm to 512 nm) [99].

Strontium aluminates exist in many phases (Figure 2.3) [100, 101]. In this phase diagram, SA means $SrO+Al_2O_3$ ($SrAl_2O_4$), $SA_2$ means $SrO+2Al_2O_3$ ($SrAl_4O_7$) and $S_3A$ means $3SrO+Al_2O_3$ ($Sr_3Al_2O_6$). Among these phases, $SrAl_2O_4$ which is well known as a host matrix of phosphors is intensively investigated.

$SrAl_2O_4$ powders doped with rare-earth ions ($Eu^{2+}$, $Dy^{3+}$, etc.) are well-known long-lasting phosphors [78]. In general, their luminescent intensity and afterglow lifetime would be controlled with the relationship between the Sr-positions in the $SrAl_2O_4$ matrix doped with rare-earth ions. It was reported that $SrAl_2O_4$ can be synthesized by solution combustion synthesis technology [99]. Solution combustion synthesis would be one of suitable methods to synthesize nano particles of high-temperature phase because of high heat of reaction and large temperature gradients during combustion synthesis process.

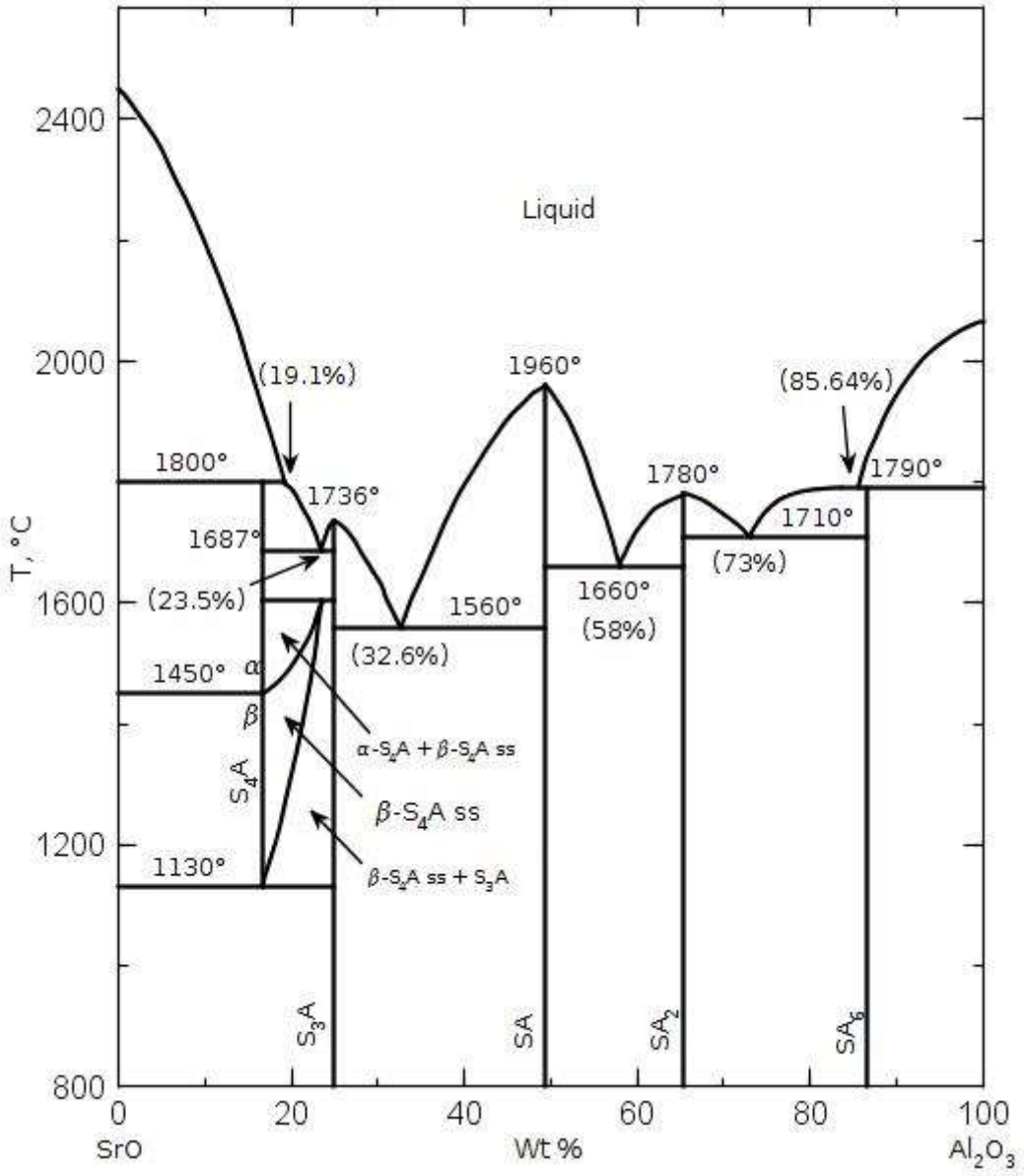


**Figure 2.3 The phase diagram of $SrO$-$Al_2O_3$ systems**

**(F. Ganits et al, (1979) [100], and The American Ceramic Society**

**and The National Institute of Standards and Technology (2016) [101])**

## 2.3 Thermochemical calculation of solution combustion synthesis of $SrAl_2O_4$

As shown in Section 1.2, when using the urea as the fuel, the solution combustion reaction of $SrAl_2O_4$ would be much milder compared with other fuels. Thermochemical data in this chapter are taken from references [5, 102]. These data are shown in Table 2.4. In Table 2.4, "$C_p$" is a heat capacity ("T" is the temperature), "$\Delta H_{298}$" is an enthalpy of formation at 298 K, "$\Delta H_t$" is an enthalpy of transition, and "$T_t$" is the phase transition point.

Urea is often used in solution combustion synthesis of alumina-related systems. The reaction of solution combustion synthesis of $SrAl_2O_4$ using urea, $CO(NH_2)_2$ is shown in the following the Equation (2.1),

$$Sr(NO_3)_2+2Al(NO_3)_3\cdot 9H_2O+20/3\ CO(NH_2)_2 \rightarrow SrAl_2O_4+20/3\ CO_2+94/3\ H_2O+32/3\ N_2 \quad (2.1)$$

Heat of reaction at 298K for the Equation (2.1) was calculated as $\Delta H_{298K}$= - 3100 kJ/mol, and the adiabatic temperature was calculated to be 1090 K. As the similar calculated process of Carbohydrazide ($CO(N_2H_3)_2$) and glycine ($NH_2(CH_2)COOH$), the heats of reaction were calculated $\Delta H_{298K}$=-5300 kJ/mol and $\Delta H_{298K}$=-3211 kJ/mol, respectively. These results are shown in Table 2.5.

**Table 2.4 Thermochemical properties of materials related in combustion synthesis of strontium aluminates**

| Substances | $C_p$[J·mol$^{-1}$·K$^{-1}$] | $\Delta H_{298}$ [kJ·mol$^{-1}$] | $\Delta H_t$ [kJ·mol$^{-1}$] | $T_t$ [K] | References |
|---|---|---|---|---|---|
| α-$SrAl_2O_4$ | 177.19+4.94·10$^{-3}$·T-5.3·10$^6$·T$^{-2}$ | -2338.9 | - | 2063 | [102] |
| β-$SrAl_2O_4$ | 146.11+29.29·10$^{-3}$·T | -2234.8 | 4.1 | ~920 | [92, 102] |
| $Sr(NO_3)_2$ | 149.87 | -978.22 | - | - | [5] |
| $Al(NO_3)_3$·9$H_2O$ | 433.0 | -3757.1 | - | - | [5] |
| SrO | 45.0 | -592.0 | 81 | 2693 | [5] |
| $Al_2O_3$ | 117.49+10.38·10$^{-3}$·T-3.71·10$^6$·T$^{-2}$ | -1675 | 111.4 | 2327 | [102] |
| $CO(NH_2)_2$ | 93.1 | -333.1 | 15.1 | 406 | [5] |
| $CO_2$ | 51.13+4.37·10$^{-3}$·T-1.47·10$^6$·T$^{-2}$ | -393.5 | - | - | [102] |
| $H_2O$ (l) | 20.36+109.2·10$^{-3}$·T-2.03·10$^6$·T$^{-2}$ | -285.8 | 2259 | 373 | [102] |
| $H_2O$ (g) | 34.38+7.84·10$^{-3}$·T-0.42·10$^6$·T$^{-2}$ | -241.8 | - | - | [102] |
| $N_2$ | 30.42+2.54·10$^{-3}$·T-0.24·10$^6$·T$^{-2}$ | 0 | - | - | [102] |
| $NO_2$ | 34.53+24.67·10$^{-3}$·T-0.42·10$^6$·T$^{-2}$-6.87·10$^6$·T$^2$ | 33.1 | - | - | [102] |

**Table 2.4 Thermochemical properties of materials related in combustion synthesis of strontium aluminates (Continued)**

| Substances | $Cp^0$[J·mol$^{-1}$·K$^{-1}$] | $\Delta H_{298}$ [kJ·mol$^{-1}$] | $\Delta H_t$ [kJ·mol$^{-1}$] | $T_t$ [K] | References |
|---|---|---|---|---|---|
| NO | $29.41+3.85\cdot10^{-3}\cdot T-0.06\cdot10^{6}\cdot T^{-2}$ | 91.29 | - | - | [102] |
| $O_2$ | $29.15+6.48\cdot10^{-3}\cdot T-0.18\cdot10^{6}\cdot T^{-2}-1.02\cdot10^{6}\cdot T^{2}$ | 0 | - | - | [102] |

**Table 2.5 Influence of the kind of fuels on the heats of reaction**

| Fuels | Formula | Heat of reaction (298 K) |
|---|---|---|
| Urea | $CO(NH_2)_2$ | -3100kJ/mol |
| Carbohydrazide | $CO(N_2H_3)_2$ | -5300kJ/mol |
| Glycine | $NH_2(CH_2)COOH$ | -3211kJ/mol |

To gain some excess of heat, the ratio of urea can be added to the Equation (2.1), which is shown in the Equation (2.2).

$$Sr(NO_3)_2+2Al(NO_3)_3\cdot9H_2O+20m/3\ CO(NH_2)_2+10(m\text{-}1)\ O_2 \rightarrow SrAl_2O_4+20m/3\ CO_2+(40m+54)/3\ H_2O+(20m+12)/3\ N_2 \quad (2.2)$$

The value of "*m*" is a urea ratio of stoichiometric amount.

In the case of m=1.5 and 2.0, heat of formation was calculated $\Delta H_{298K}$=-5240 kJ/mol and $\Delta H_{298K}$=-7310 kJ/mol, respectively (Table 2.6).

Adiabatic combustion temperatures are calculated from the following Equations (2.3), (2.4), and (2.5) [103].

$$-\Delta H_0 = \int_{T_0}^{T_{ad}} Cp(s)dT \quad (T_{ad}<T_t) \tag{2.3}$$

$$-\Delta H_0 = \int_{T_0}^{T_{ad}} Cp(s)dT + \nu\ \Delta H_t \quad (T_{ad}=T_t) \tag{2.4}$$

$$-\Delta H_0 = \int_{T_0}^{T_t} Cp(s)dT + \nu\ \Delta H_t + \int_{T_t}^{T} Cp(s)dT \ (T_{ad}>T_t) \tag{2.5}$$

Where, "$C_p$" is the heat capacity of product, "$T_t$" is phase transition point of product, "$\Delta H_t$" is heat of transition, "$\Delta H_0$" is heat of reaction, "$T_{ad}$" is adiabatic combustion temperature, and "$T_o$" is the normal temperature.

Heats of reaction and adiabatic combustion temperatures with each ratio are shown in Table 2.6. With an increase urea ratio, heat of formation and adiabatic combustion temperature increase.

**Table 2.6 Influence of urea ratio on the heat of reaction and adiabatic combustion temperature**

| Urea ratio | Heat of reaction (298 K) [kJ/mol] | Adiabatic temperature [K] |
|---|---|---|
| 1.0 | -3100 | 1090 |
| 1.5 | -5240 | 1300 |
| 2.0 | -7310 | 1410 |

Calculated adiabatic temperature of each pre-heating temperature of $SrAl_2O_4$ and combustion temperature are shown in Table 2.7. Combustion temperatures were measured by type S thermocouples (Pt, Pt-10%Rh, diameter: 0.5mm), and Data from thermocouple were collected by data logger (logging distance: 25 ms). In every case, maximum temperatures are lower than adiabatic combustion temperatures because of the large amount of gases released during combustion synthesis process.

**Table 2.7 Adiabatic temperature and maximum temperature of each furnace temperature**

| Furnace Temperature [K] | Adiabatic Temperature [K] | Maximum Temperature measured by type S thermocouple [K] |
|---|---|---|
| 873 | 1354 | 1293 |
| 1073 | 1543 | 1281 |
| 1273 | 1735 | 1415 |

# 2.4 Experimental

For making clear decomposition of the starting materials, starting samples were measured by thermogravimetry (TG) and differential thermal analysis (DTA) in order to investigate decomposition of starting samples. The experiments were carried out by changing temperatures from 373K to 1073K, with a heating rate of 5K/min.

As shown in Table 2.8, six samples were selected; the present combustion synthesis samples, $Al(NO_3)_3 \cdot 9H_2O$ with $CO(NH_2)_2$, $Sr(NO_3)_2$ with $CO(NH_2)_2$, $Al(NO_3)_3 \cdot 9H_2O$, $Sr(NO_3)_2$ and $CO(NH_2)_2$.

**Table 2.8 Samples of TG/DTA measurements**

| Sample No. | Contents | Heating rate [K/min.] | Weight [mg] |
|---|---|---|---|
| 1 | $2Al(NO_3)_3 \cdot 9H_2O+Sr(NO_3)_2+20/3 \cdot CO(NH_2)_2$ (the present combustion synthesis samples) | 5 | 30 |
| 2 | $Al(NO_3)_3 \cdot 9H_2O + 5CO(NH_2)_2$ | 5 | 30 |
| 3 | $Sr(NO_3)_2+25/6 \cdot CO(NH_2)_2$ | 5 | 30 |
| 4 | $Al(NO_3)_3 \cdot 9H_2O$ | 5 | 30 |
| 5 | $Sr(NO_3)_2$ | 5 | 30 |
| 6 | $CO(NH_2)_2$ | 5 | 30 |

# 2.5 Results and discussion

The results of TG/DTA analysis of starting materials are shown in Figures 2.4, 2.5 and 2.6, and phase transition data of nitrates in literature [104-106] are shown in Figure 2.7. $Sr(NO_3)_2$ decomposes into SrO around 900 K [104], and $Al(NO_3)_3 \cdot 9H_2O$ decomposes around 400 K [105]. In literature [105], decomposition of $Al(NO_3)_3 \cdot 9H_2O$ has several steps, however, these steps cannot be identified in this work, because of the high heating rate. The purpose of this work is to clarify the process of combustion synthesis which has high temperature gradients, therefore a heating rate is selected in high heating rate (5 K/s). All starting samples decompose

with the endothermic heat.

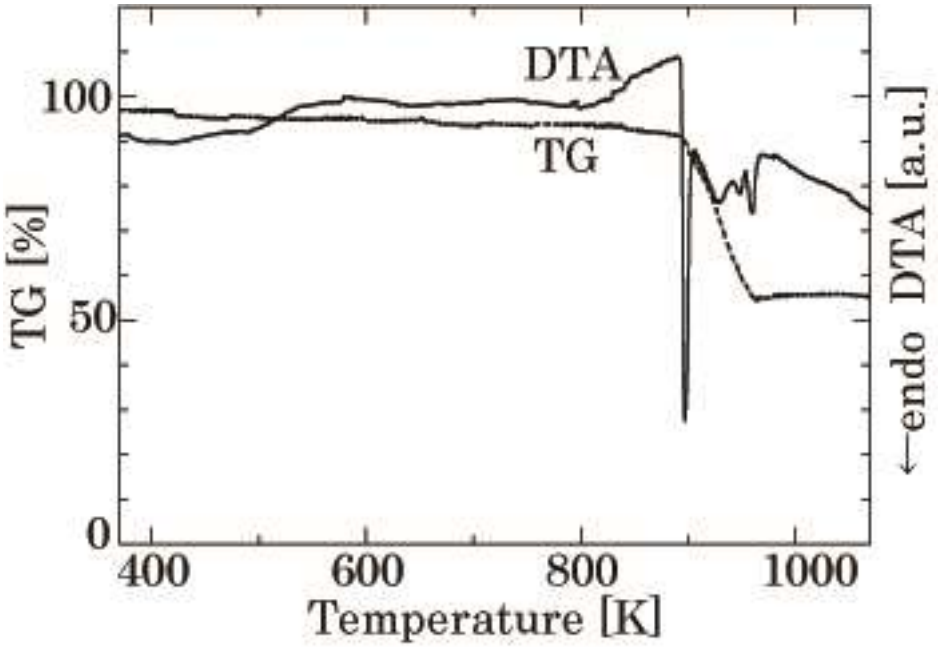


**Figure 2.4 TG/DTA data of $Sr(NO_3)_2$**

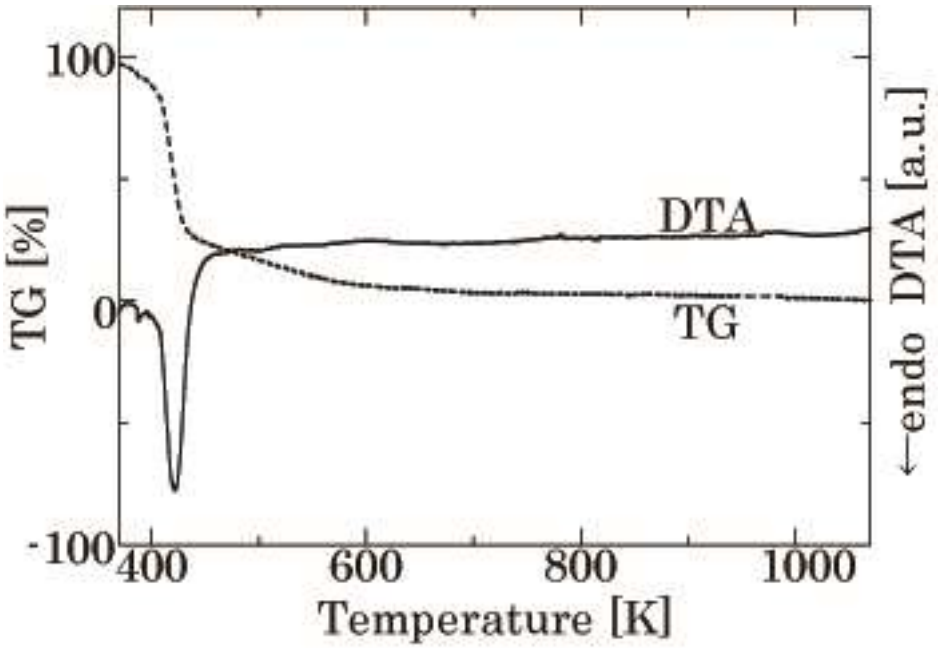


**Figure 2.5 TG/DTA data of $Al(NO_3)_3 \cdot 9H_2O$**

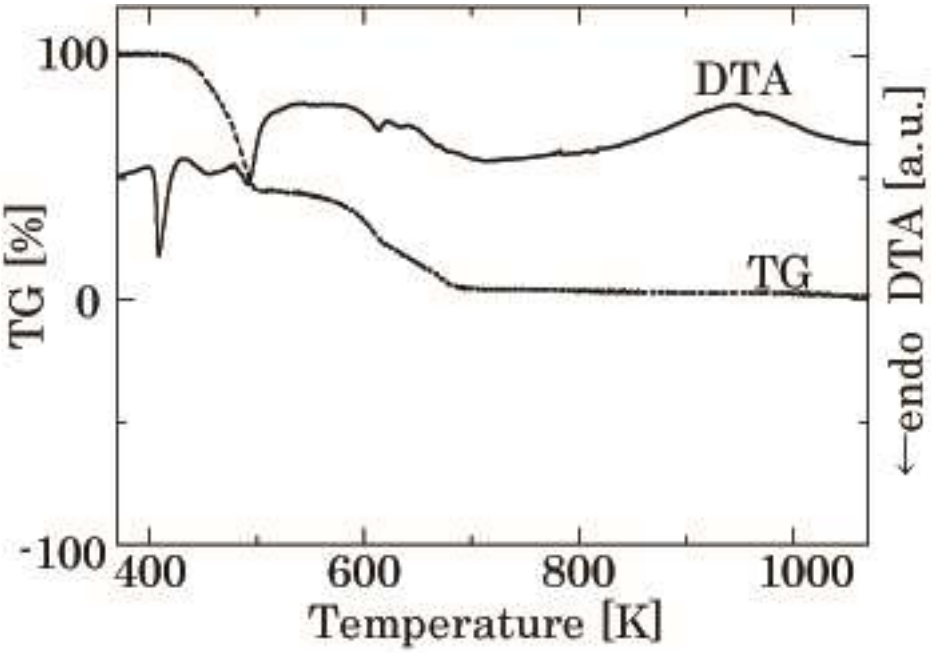


**Figure 2.6 TG/DTA data of $CO(NH_2)_2$**

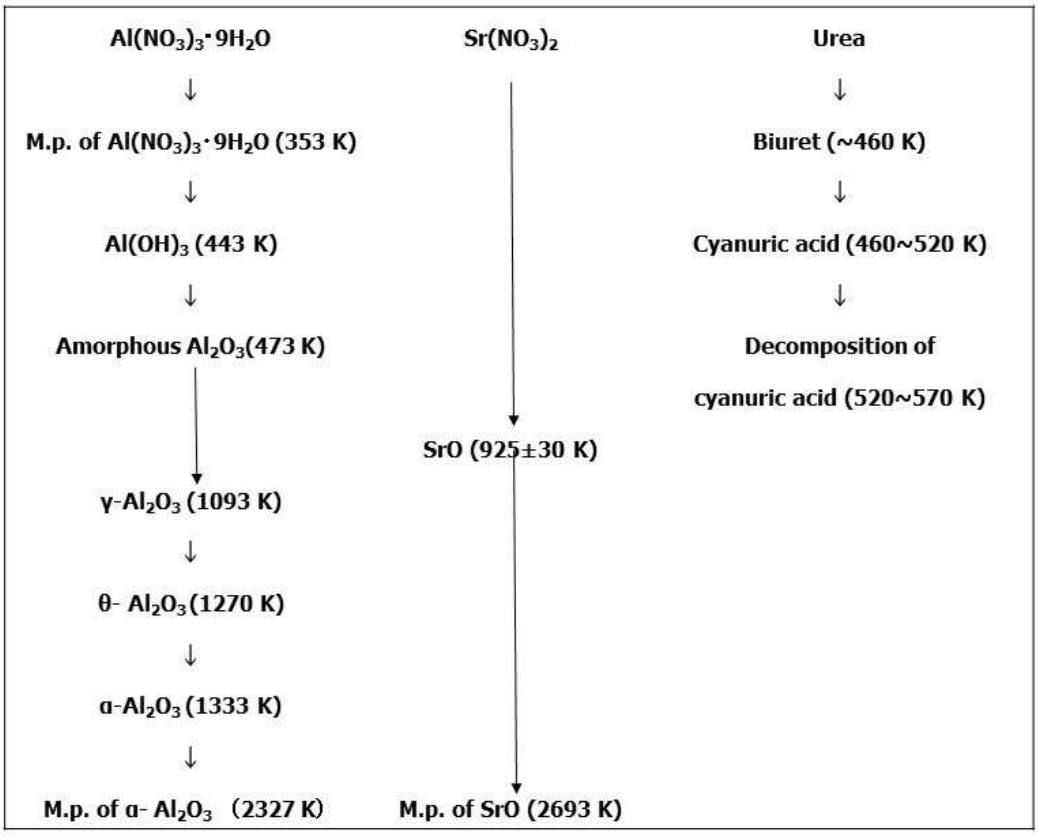


**Figure 2.7 Thermal decomposition of aluminum and strontium nitrates in the literature [104-106]**

**"M.p." is a melting point.**

The typical results of samples mixed with all starting materials (Sample No.1) of TG/DTA curves are shown in Figure 2.8. According to the DTA curve, it is observed that an endothermic peak at 350 K which is equal to the melting point of $Al(NO_3)_3 \cdot 9H_2O$, an exothermic peak around 400K, and an endothermic peak at around 900 K.

From the TG curves shown in Figure 2.8, the weight loss relating to the DTA peak around 400 K was 75 % calculated by the TG curve between 298 K and 530 K. This weight loss corresponds to the combustion of $CO(NH_2)_2$ and decomposition of

$Al(NO_3)_3 \cdot 9H_2O$ into $Al_2O_3$. The DTA peak around 400K was observed only in the case of $Al(NO_3)_3 \cdot 9H_2O$, $Sr(NO_3)_2$ and $CO(NH_2)_2$ (Sample No.1 in Table 2.8) , and $Al(NO_3)_3 \cdot 9H_2O$, $CO(NH_2)_2$ (Sample No.2 in Table 2.8). The weight loss in the TG curve at around 900 K corresponds to the decomposition of $Sr(NO_3)_2$ to SrO [104].

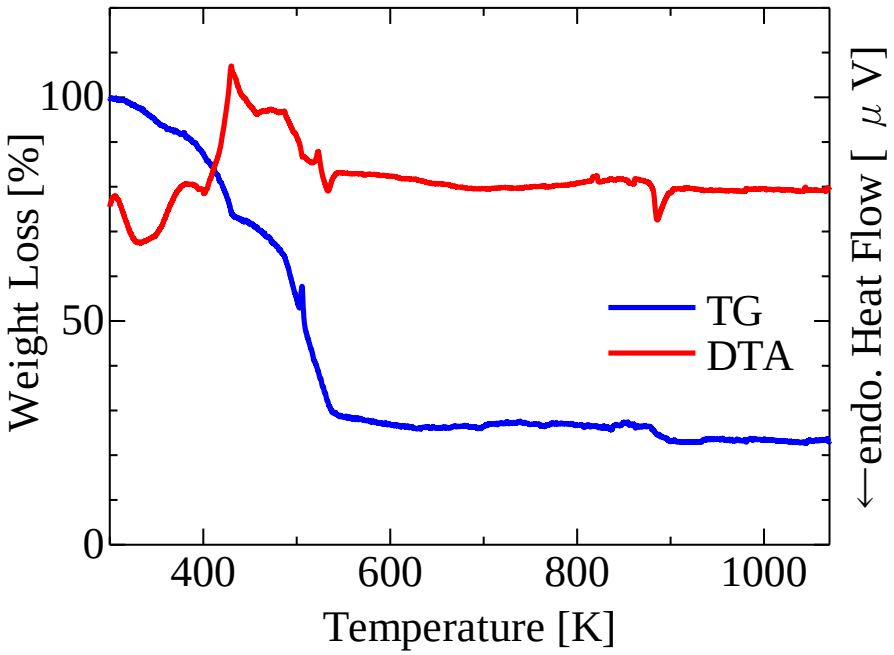


**Figure 2.8 TG/DTA curves of starting materials**

The decomposition reaction around 400 K was proposed as follows [99, 100].

$$Al(NO_3)_3 \cdot 9H_2O \rightarrow 1/2\ Al_2O_3 + 3\ NO_2 + 3/2\ O_2 + 3/2\ N_2 + 9H_2O$$

$$\Delta H_{400\ K} = 533.1\ \text{kJ/mol} \qquad (2.6)$$

Taking into consideration of decomposition of $NO_2$, the following reaction is possible.

$$Al(NO_3)_3 \cdot 9H_2O \rightarrow 1/2\ Al_2O_3 + 15/4\ O_2 + 3/2\ N_2 + 9H_2O$$

$$\Delta H_{400\ K} = 627.9\ kJ/mol \quad (2.7)$$

The combustion reaction between $CO(NH_2)_2$ and $O_2$ at 400 K is shown in the Equation (2.8).

$$CO(NH_2)_2 + 1.5O_2 \rightarrow CO_2 + 2H_2O + N_2$$

$$\Delta H_{400\ K} = -544.9\ kJ/mol \quad (2.8)$$

According to the Equation of (2.7) and (2.8), the reaction between $Al(NO_3)_3 \cdot 9H_2O$ and $CO(NH_2)_2$ is shown in the Equation (2.9).

$$Al(NO_3)_3 \cdot 9H_2O + 5CO(NH_2)_2 \rightarrow 0.5\ Al_2O_3 + 5CO_2 + 6.5N_2 + 19H_2O$$

$$\Delta H_{400\ K} = -1830\ kJ/mol \quad (2.9)$$

The endothermic peak around 900 K is related to the thermal decomposition of $Sr(NO_3)_2$. The decomposition reaction was proposed as follows [106].

$$Sr(NO_3)_2 \rightarrow SrO + 2NO_2 + 1/2\ O_2$$

$$\Delta H_{900\ K} = 35.7\ kJ/mol \quad (2.10)$$

The possible thermal decomposition reaction of $Sr(NO_3)_2$ in consideration of decomposition of $NO_2$ is as follows.

$$Sr(NO_3)_2 \rightarrow SrO + N_2 + 5/2\ O_2$$

$$\Delta H_{900\ K} = 113\ kJ/mol \qquad (2.11)$$

The heat of this endothermic peak at 900 K calculated from the endothermic peak area of DTA curve is about 142 kJ/mol which would not correspond to the result of the Equation (2.11). Therefore, another endothermic reaction might occur at 900 K. The possible endothermic reaction is expressed in the Equation (2.12).

$$SrO + Al_2O_3 \rightarrow SrAl_2O_4$$

$$\Delta H_{900\ K} = 24.5\ kJ/mol \qquad (2.12)$$

The total amount of the decomposition heat in the Equation (2.11) and reaction heat in the Equation (2.12) is 137.5 kJ/mol, which is nearly equal to heat calculated from the DTA peak area. Therefore, at around 900 K, thermal decomposition of $Sr(NO_3)_2$ and the reaction between SrO and $Al_2O_3$ would occur.

In the case of combustion synthesis of $TiB_2$ in Section 1.1, the adiabatic temperature of the system is equal to melting point of $TiB_2$, and higher than melting point of Ti and B, resulting in synthesis of β-$TiB_2$.

In the case of SCS of $SrAl_2O_4$, the adiabatic temperature of systems with all conditions in this work is lower than melting point of $SrAl_2O_4$ (2063 K) [102], and higher than decomposition temperatures of all starting materials. Therefore, it is necessary to control pre-heating temperature and urea ratio properly. The relationship between starting condition which is urea ratio and pre-heating temperature and the composition of combustion products will be discussed in Chapter 3.

## 2.6 Summary

In this chapter, the important parameter of the adiabatic temperature and heat of formation is discussed.

In the case of solution synthesis of the $SrAl_2O_4$ system, the reaction temperature difference between aluminum nitrate and strontium nitrate is more than 400 K, and adiabatic temperature is a little larger than the reaction temperature of strontium nitrate (around 900 K). Therefore, solution combustion synthesis can be performed with pre-heating support by heating devices such as furnace, hot plate and microwave.

# Chapter 3
# Influence of fuel ratio and pre-heating temperature on solution combustion synthesized strontium aluminates

## 3.1 Introduction

$SrAl_2O_4$ powders are one of typical candidates useful for establishing inorganic fluorescent materials doped with rare-earth ions such as $Eu^{2+}$, $Dy^{3+}$ which has mainly been synthesized by solid-phase reactions [78]. In general, its luminescent intensity and afterglow lifetime are controlled with the relationship between the Sr-positions in the $SrAl_2O_4$ matrix and the doped $Eu^{2+}$, and with the distributions of rare-earth ions in the matrix, respectively.

In this chapter, influences of fuel ratio and pre-heating temperature on the characteristics of the products were investigated.

The typical temperature change during combustion synthesis reaction is shown in Figure 3.1. The temperature increased from 373 K to more than 1000 K in a few seconds, and the maximum temperature was almost the same independent of urea amounts and furnace temperatures.

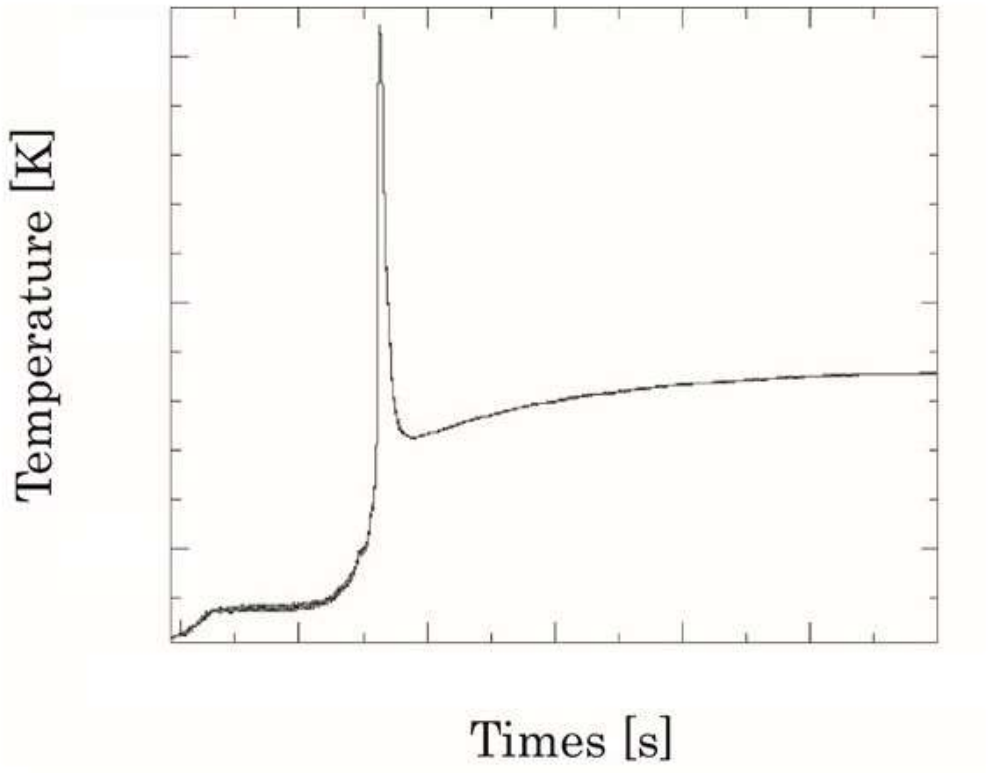


**Figure 3.1 Temperature of a sample during combustion synthesis**

In this work, urea was used as a fuel, its combustion reaction propagates much milder compared with other fuels. To gain some excess of heat, the ratio of urea can be added to the Equation (3.1).

$$Sr(NO_3)_2+2Al(NO_3)_3\cdot 9H_2O+ 20m/3\ CO(NH_2)_2+10(m\text{-}1)\ O_2$$

$$\rightarrow SrAl_2O_4+20m/3\ CO_2+(40m+54)/3\ H_2O+(20m+12)/3\ N_2 \quad (3.1)$$

The value ”*m*” is a urea ratio of stoichiometric amount.

In the present work, the phase composition of products by solution combustion synthesis were studied as varying pre-heating temperature and urea ratio from 1.0 to 2.0 as the above value of “*m*” in order to vary calculated adiabatic

temperature.

The adiabatic temperature at 298 K of the system is little higher than the decomposition temperature of $Sr(NO_3)_2$, therefore, to proceed combustion synthesis, it is important to increase the combustion temperature to react $Sr(NO_3)_2$ by an increase urea ratio and pre-heating temperature. And, phase-phase-transition point from α-$SrAl_2O_4$ to β- $SrAl_2O_4$ is also similar to the adiabatic temperature of the system. Therefore, the relationship between structure of products and combustion temperature is an important factor to synthesize β-phase.

# 3.2 Experimental

## 3.2.1 Solution combustion synthesis method

Schematic illustration of experimental setup is shown in Figure 3.2. The present process of solution combustion synthesis has been performed by the following steps; (1) preparing the sample by mixed with urea, $Sr(NO_3)_2$, $Al(NO_3)_3 \cdot 9H_2O$ and water, (2) combustion synthesis processing with an electric furnace, and (3) analyzing the product.

In the step (1), the amounts of $Sr(NO_3)_2$ and $Al(NO_3)_3 \cdot 9H_2O$ were 0.020mol (4.232g) and 0.040mol (15.005g), respectively. $CO(NH_2)_2$ ratios were measured by following the value of "*m*" which is the urea ratio in the Equation (2.2) as 0.133mol (8.007g, *m*=1.0), 0.200mol (12.001g, *m*=1.5), and 0.267mol (16.015g, *m*=2.0). These elements were mixed to 60ml of distilled water, and the solution was used as the

starting samples.

In the step (2), these starting solutions were put into alumina holders with a capacity of 7ml. The combustion holders were put in an electrical furnace for 10 minutes to perform the combustion synthesis process in the atmospheric condition (Figure 3.2). The furnace temperature was varied for 11 conditions (373K to 1273K). The combustion reaction started within 3 minutes. The temperature changes of the samples were measured by inserting a thermocouple (type S) to the sample solution.

In the step (3), the products were analyzed by x-ray diffraction (XRD) with radiation of CuKα (λ=1.5406 angstroms), and scanning electron microscopy (SEM). The obtained XRD data were mainly investigated by focusing to each lattice plane.

Combustion temperatures were measured by type-S thermocouples (Pt, Pt-10%Rh, diameter: 0.5mm), and data from thermocouple were collected by a data logger (Interval: 25 milliseconds). Thermocouple was contacted the inner bottom of the sample holder.

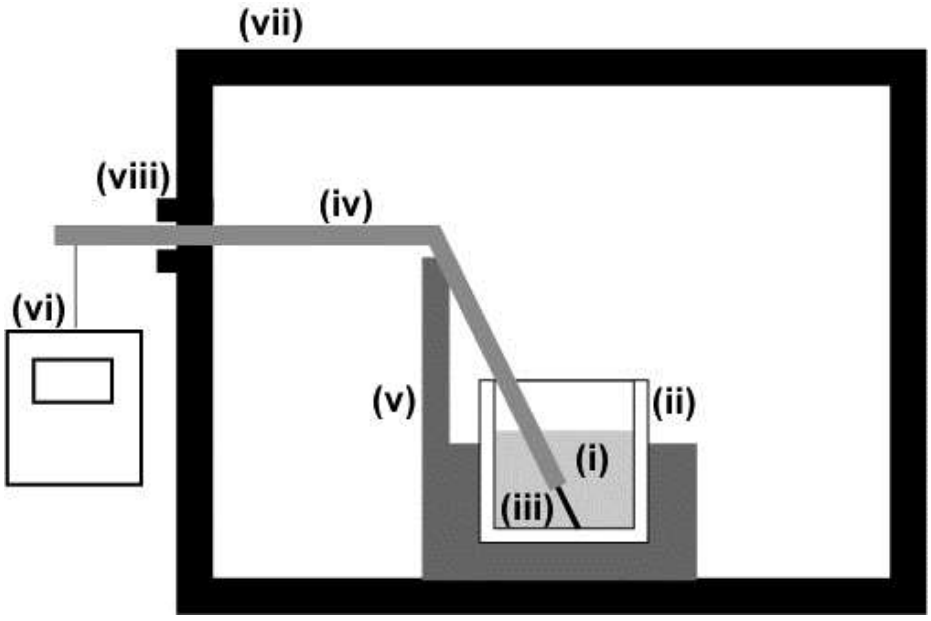


**Figure 3.2 Schematic illustration of apparatus: (i) Combustion reaction solution, (ii) Alumina crucible, (iii) Thermocouple (type S), (iv) Alumina protection tube, (v) spacer, (vi) Data logger, (vii) Electric furnace, and (viii) Observation window.**

## 3.2.2 Analysis method of composition ratio between α-$SrAl_2O_4$ and β-$SrAl_2O_4$

The XRD patterns of products are shown in Figure 3.3. At the furnace temperatures below 773 K, only Sr $(NO_3)_2$ was identified, and $Al_2O_3$ was not observed. Since $Al(NO_3)_3 \cdot 9H_2O$ decomposed into $Al_2O_3$ in an amorphous phase (Figure 2.7 in Chapter 2, pp. 44), the evidence could not be observed in the present XRD data. It suggested that the main synthesis reaction was not attained below 773 K. At the

temperatures above 873 K, the peaks of monoclinic-$SrAl_2O_4$ (α-SA), hexagonal-$SrAl_2O_4$ (β-SA), $Sr_3Al_2O_6$ ($S_3A$), and $SrAl_4O_7$ ($SA_2$) were identified. The peaks of the present combustion synthesized samples, SrO and $Al_2O_3$ were not observed. The phase diagram of SrO-$Al_2O_3$ systems has already been shown in Figure 2.3 in Chapter 2 (pp. 35). $SA_2$ is in $Al_2O_3$ rich region, and $S_3A$ is in the so rich region. These results indicate that the combustion synthesis reaction can be performed above 873 K of the furnace temperature, which means that the present solution combustion synthesis is initiated at least more than 873 K as the furnace temperature.

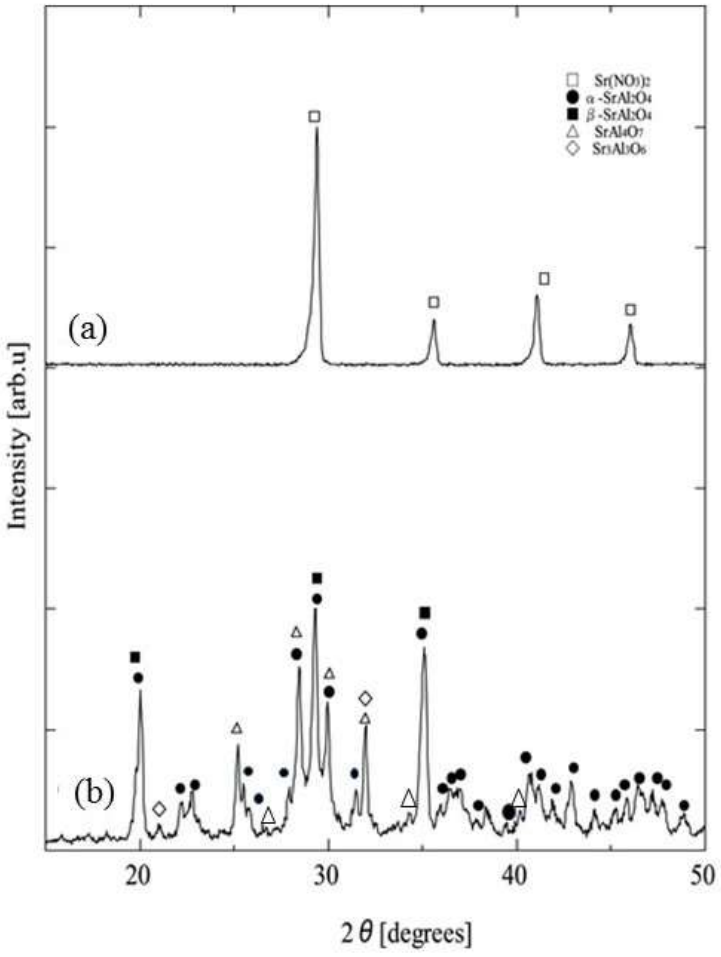


**Figure 3.3. XRD patterns of combustion synthesized materials**

**(a) 773 K, (b) 873 K**

As shown in Figure 3.3, the peaks of α-SA, β-SA, $S_3A$ and $SA_2$ were overlapped and identification was difficult, therefore, the composition ratios were calculated from simultaneous equations of several peak heights. In this work, four peaks in Figure 3.4 were used to calculate the composition ratio. X-ray diffraction data are shown in Table 3.1. In this work, diffraction angles of four samples (α-SA, β-SA, $S_3A$ and $SA_2$) are similar, therefore the composition ratio is calculated to use peak intensity instead of peak integral intensity.

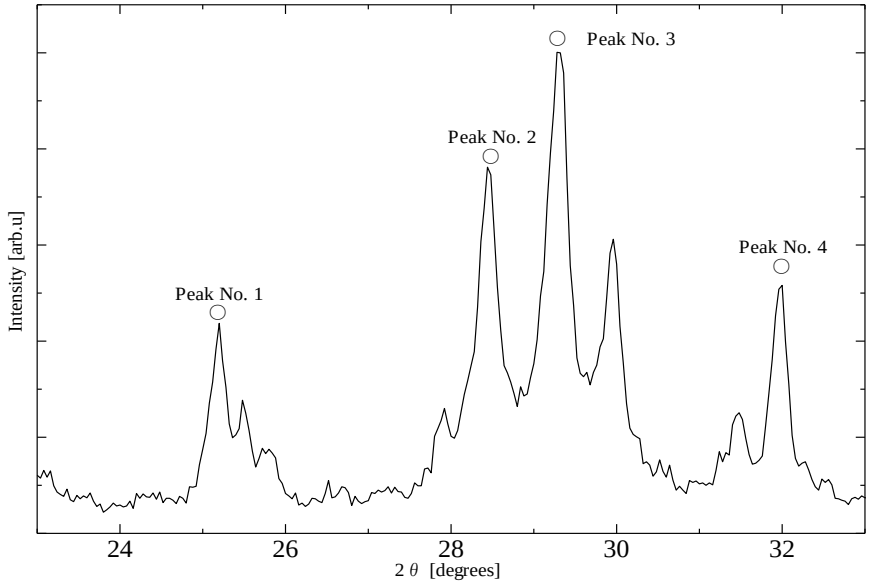


**Figure 3.4 XRD peaks used for calculation of composition ratio**

**(Composition ratio is calculated from peak No.1-4, and values in brackets are peak intensity [arb.u])**

**Table 3.1 X-ray diffraction data of strontium aluminates**

| Peak No. | | 1 | 2 | 3 | 4 | References |
|---|---|---|---|---|---|---|
| Relative intensity (Diffraction angles [2θ]) | **α-$SrAl_2O_4$ (α-SA)** **(PDF#00-034-0379)** | | **100** (28.385) | **91** (29.274) | | [94] |
| | **β-$SrAl_2O_4$ (β-SA)** **(PDF#00-031-1336)** | | | **100** (29.061) | | [92] |
| | **$Sr_3Al_2O_6$ ($S_3A$)** **(PDF#00-024-1187)** | | | | **100** (31.948) | [107] |
| | **$SrAl_4O_7$ ($SA_2$)** **(PDF#00-30-1276)** | **60** (24.991) | **80** (28.307) | **80** (28.965) | **40** (32.052) | [108] |

The relation between peak intensity and the composition ratio given by H.P. Klug and L.E. Alexander is shown in the Equation (3.2) [109].

$$I_J = \frac{K_J x_J}{\rho_J \left[ x_J (\mu_J - \mu_m) + \mu_m \right]} \tag{3.2}$$

Where, "$I_J$" is the peak intensity of component *"J"* , "$x_J$" is the composition ratio (weight ratio) of component *"J"*, "$\rho_J$" is the density of component *"J"*, "$\mu_J$" is the mass absorption coefficient of component *"J"*, "$\mu_m$" is the mass absorption coefficient of matrix, and "$K_J$" is the constant which depends on the component and apparatus.

The mass absorption coefficients and atomic weights of the elements are shown in Table 3.2 [5].

**Table 3.2 Values of the mass absorption coefficients for CuKα lines and atomic weights [5]**

| Elements | Mass absorption coefficient [$cm^2g^{-1}$] | Atomic weights |
|---|---|---|
| **Strontium** | 90.0 | 87.6 |
| **Aluminum** | 49.6 | 27.0 |
| **Oxygen** | 12.9 | 16.0 |

The mass absorption coefficient can be calculated from the sum of the multiplication of the mass absorption coefficients and the composition ratio of the constituent element [110] which is shown in the Equation (3.3),

$$\mu_c = \sum_{a=1}^{N} f_a \mu_a \tag{3.3}$$

Where, "$\mu_c$" is the mass absorption coefficient of the compound, "$\mu_a$" is the mass absorption coefficient of constituent element, and "$f_a$" is the mass fraction of the constituent element. The value of the mass absorption coefficients of strontium aluminates can be calculated from the Equation (3.3) and the value of Table 3.2. These calculated values are shown in Table 3.3.

**Table 3.3 Mass absorption coefficient of strontium aluminates for CuKα lines**

| Compounds | Mass absorption coefficient [$cm^2g^{-1}$] |
|---|---|
| **α-$SrAl_2O_4$ (α-SA)** | 55.4 |
| **β-$SrAl_2O_4$ (β-SA)** | 55.4 |
| **$SrAl_4O_7$ ($SA_2$)** | 47.7 |
| **$Sr_3Al_2O_6$ ($S_3A$)** | 60.2 |

The mass absorption coefficient of matrix is shown in the Equation (3.4) [109].

$$\mu_m = \sum_{L=1}^{N} f_L \mu_L \tag{3.4}$$

Where, "$f_L$" is the mass fraction of constituent phase, and "$\mu_c$" is the mass fraction of constituent phase.

Since main components of combustion synthesized materials would be α-SA and β-SA and amounts of $SA_2$ and $S_3A$ is relatively small, the mass absorption coefficient of the matrix which is expressed as the Equation (3.4) is similar to that of α-SA and β-SA. In addition, the mass absorption coefficients of α-SA, β-SA, $SA_2$ and $S_3A$ in Table 3.3 are similar, therefore, in this work, the composition ratios of α-SA and β-SA were calculated on the assumption that the mass absorption coefficient of the matrix is equal to that of all components which is expressed as the Equation (3.5).

$$\mu_m \approx \mu_j \tag{3.5}$$

According to the Equations (3.2) and (3.5), the following Equation (3.6) is calculated.

$$I_j = \frac{K_J x_J}{\mu_m} \tag{3.6}$$

This equation means peak intensity of component *"J"* is proposal to the composition ratio of component *"J"*, therefore in this work, the composition ratios of each component will be calculated on that assumption.

The values of RIR (Reference Intensity Ratio), which is also known as "$I/I_c$" are shown in Table 3.4. This value means the ratio of the peak intensity of the strongest line between analyte and corundum ($\alpha$-$Al_2O_3$) as the standard substance when corundum and analyte are mixed into the weight ratio of 50:50. The values of RIR of $\alpha$-$SrAl_2O_4$, $\beta$-$SrAl_2O_4$, and $SrAl_4O_7$ were not described in JCDPS/ICDD cards in Table 3.1, therefore, in this work, these values of RIR were referred from the data of the other JCPDS/ICDD cards. In Table 3.4, RIR of $\alpha$-$SrAl_2O_4$, $\beta$-$SrAl_2O_4$, and $SrAl_4O_7$ were chosen in JCPDS /ICDD cards which are same crystal systems and space groups, and similar lattice constants and diffraction angles of the strongest peaks to the data in Table 3.1.

**Table 3.4 Reference intensity ratios of strontium aluminates on JCPDS/ICDD cards**

| Phase | Structure | Reference Intensity Ratio ($I/I_c$) | References |
|---|---|---|---|
| **$\alpha$-$SrAl_2O_4$ ($\alpha$-SA)** | Monoclinic | 1.52 | [111] |
| **$\beta$-$SrAl_2O_4$ ($\beta$-SA)** | Hexagonal | 3.74 | [112] |
| **$Sr_3Al_2O_6$ ($S_3A$)** | Cubic | 5.20 | [107] |
| **$SrAl_4O_7$ ($SA_2$)** | Orthorhombic | 2.97 | [113] |

To calculate the composition ratio by using the reference intensity ratio (RIR), following calculation method was proposed [114-116]. The peak intensities of phase α, phase β and corundum (α-$Al_2O_3$) are shown in Equation (3.7), (3.8) and (3.9), respectively. Where, lowercase subscripts α, β, and c mean phase α, phase β, and corundum (α-$Al_2O_3$), respectively.

$$I_\alpha = \frac{K_\alpha x_\alpha}{\mu_m} \tag{3.7}$$

$$I_\beta = \frac{K_\beta x_\beta}{\mu_m} \tag{3.8}$$

$$I_c = \frac{K_c x_c}{\mu_m} \tag{3.9}$$

Peak intensity ratios between phase α and phase β, corundum (α-$Al_2O_3$) and phase α, and corundum (α-$Al_2O_3$) and phase β are shown in Equation (3.10), (3.11) and (3.12), respectively.

$$\frac{I_\beta}{I_\alpha} = \frac{K_\alpha x_\alpha}{K_\beta x_\beta} \tag{3.10}$$

$$\frac{I_\alpha}{I_c} = \frac{K_\alpha x_\alpha}{K_c x_c} \tag{3.11}$$

$$\frac{I_\beta}{I_c} = \frac{K_\beta x_\beta}{K_c x_c} \tag{3.12}$$

Equation (3.13) is calculated from Equations (3.11) and (3.12).

$$\frac{I_\alpha / I_c}{I_\alpha / I_c} = \frac{K_\alpha x_\alpha}{K_\beta x_\beta} \tag{3.13}$$

Compared with the Equations (3.10) and (3.13), the relationship between peak intensity and composition ratio used the value of RIR ($I/I_c$) is shown in the Equation (3.14).

$$\frac{I_\alpha}{I_\beta} = \frac{I_\alpha / I_c}{I_\beta / I_c} \times \frac{x_\alpha}{x_\beta} \tag{3.14}$$

The composition ratio of β-SA, $SA_2$ and $S_3A$ to α-SA were calculated by following method. In this section, the characters of *"$I_1$", "$I_2$", "$I_3$",* and *"$I_4$"* represent peak intensity of the peaks No.1, No.2, No.3, and No.4 in Figure 3.4, respectively. Intensity of these four peaks varies as the experimental conditions (furnace temperatures and urea ratios). Characters of *"$I_\alpha$"*, "$I_\beta$", "$I_{SA2}$" and "$I_{S3A}$" mean the peak intensity of α-SA, β-SA, $SA_2$, and $S_3A$, respectively.

The Equation (3.15) is come from peaks intensity of peaks No.1 and No.2 in Figure 3.4, and the values of relative peak intensity in Table 3.1.

$$I_1 : I_2 = [\frac{60}{100} I_{SA2}] : [\frac{100}{100} I_\alpha + \frac{80}{100} I_{SA2}] \tag{3.15}$$

Therefore,

$$I_{SA2} = \frac{1.0I_1}{0.60I_2 - 0.80I_1} I_\alpha \tag{3.16}$$

The Equation (3.17) derives from peaks No.2 and No.3,

$$I_2 : I_3 = [\frac{100}{100} I_\alpha + \frac{80}{100} I_{SA2}] : [\frac{91}{100} I_\alpha + \frac{100}{100} I_\beta + \frac{80}{100} I_{SA2}] \tag{3.17}$$

The Equation (3.18) is calculated from the Equation (3.16) and (3.17).

$$I_\beta = \frac{-0.072I_1 - 0.546I_2 + 0.60I_3}{0.60I_2 - 0.80I_1} I_\alpha \tag{3.18}$$

The Equation (3.19) derives from peaks No.2 and No.4.

$$I_2 : I_4 = [\frac{100}{100} I_\alpha + \frac{80}{100} I_{SA2}] : [\frac{100}{100} I_{S3A} + \frac{40}{100} I_{SA2}] \tag{3.19}$$

Therefore, the Equation (3.20) is come from the Equations (3.16) and (3.19).

$$I_{S3A} = \frac{-0.40I_1 + 0.60I_4}{0.60I_2 - 0.80I_1} I_\alpha \tag{3.20}$$

Therefore, the ratios of β-SA, $SA_2$, and $S_3A$ to α-SA which are shown in the Equation (3.21) are expressed as the Equations (3.16), (3.18) and (3.20).

$$I_\alpha : I_\beta : I_{SA2} : I_{S3A}$$
$$= I_\alpha : \frac{-0.072I_1 - 0.546I_2 + 0.60I_3}{0.60I_2 - 0.80I_1} I_\alpha : \frac{1.0I_1}{0.60I_2 - 0.80I_1} I_\alpha : \frac{-0.40I_2 + 0.60I_4}{0.60I_2 - 0.80I_1} I_\alpha$$

(3. 21)

In this chapter, composition ratios of synthesized strontium aluminates shown in Figure 3.5 and 3.6 are calculated as the Equation (3.21) used values in Table 3.1.

# 3.3 Results and discussion

The composition ratios of the products varied by furnace temperature and urea ratio are shown in Figures 3.5 and 3.6.

As furnace temperature increases from 873 K to 1273 K shown in Figure 3.5, α-SA existed over the whole temperature range, and the ratio of β-SA became maximum at 1073 K. In addition, $S_3A$ and $SA_2$ existed. As furnace temperature increases the ratio of $S_3A$ increased and the ratio of $SA_2$ decreased. These results can show that a part of Sr $(NO_3)_2$ does not react and the ratio of SrO is insufficient at low temperatures. With the increase of furnace temperatures, $Sr(NO_3)_2$ is decomposed into SrO, because the reaction temperature between $Sr(NO_3)_2$ and $CO(NH_2)_2$ would be around 900 K.

Each ratio of product component with the relation of $CO(NH_2)_2$ amount is shown in Figure 3.6. The ratio of α-SA and β-SA was maximum and the ratio of $S_3A$

and $SA_2$ was minimum at 1.5 times at $CO(NH_2)_2$ stoichiometric amount. At the stoichiometric ratio of $CO(NH_2)_2$, a part of $CO(NH_2)_2$ would be evaporated and the reaction system was in the state of insufficient of $CO(NH_2)_2$, because the decomposition temperature of $CO(NH_2)_2$ has been reported to be ranged between 408K and 570K [106]. When 1.5 times the stoichiometric ratio of urea, the ratio of nitrates and fuel was considered to be close to theoretical ratio, and when 2.0 times the stoichiometric ratio of $CO(NH_2)_2$, the ratio of fuel might be too excess.

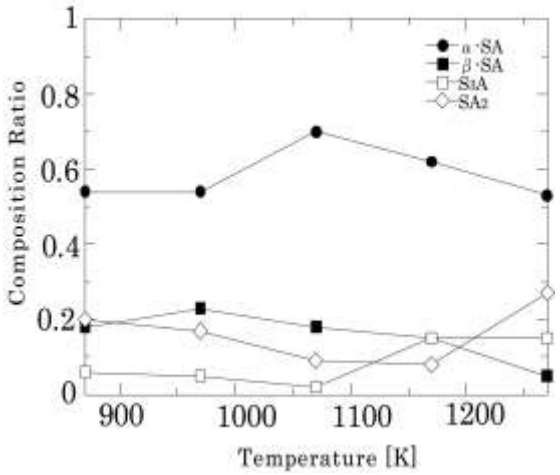


**Figure 3.5 Composition ratio to total amount of samples at each furnace temperature (urea ratio of stoichiometric amount: 1.5)**

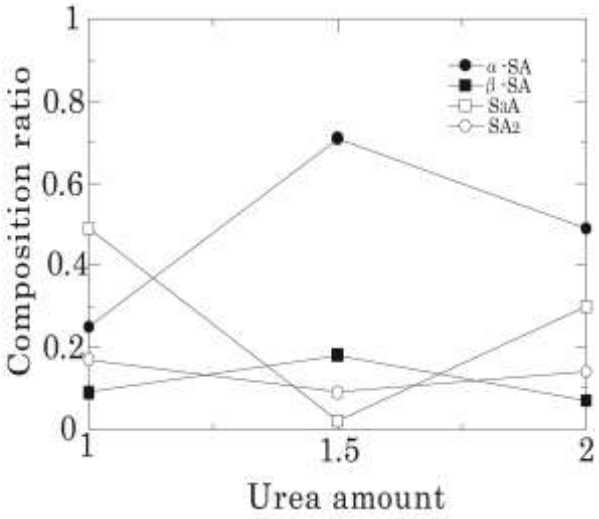


**Figure 3.6 Composition ratio to total amount of samples at excess urea ratio of stoichiometric amount (furnace temperature: 1073K)**

The SEM images are shown in Figure 3.7. Particle sizes became fine as temperature increased. It is also suggested that the reactivity of samples should be improved as increasing furnace temperature.

When the combustion temperature by increasing furnace temperature and urea ratio is higher than the decomposition temperature of strontium nitrate, combustion synthesis is conducted.

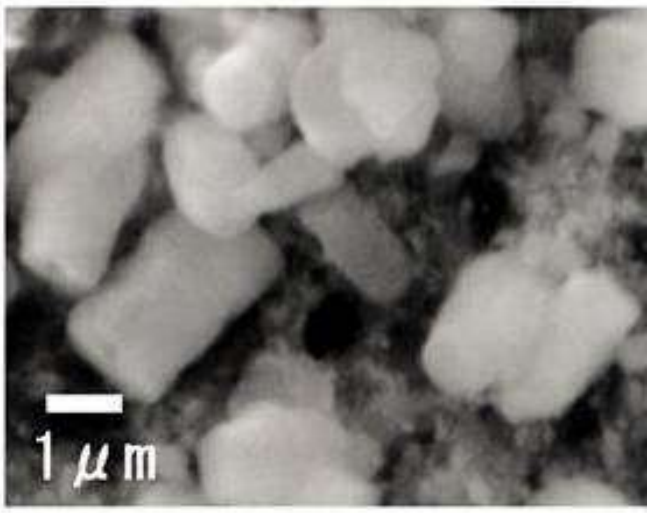


(a) 873 K

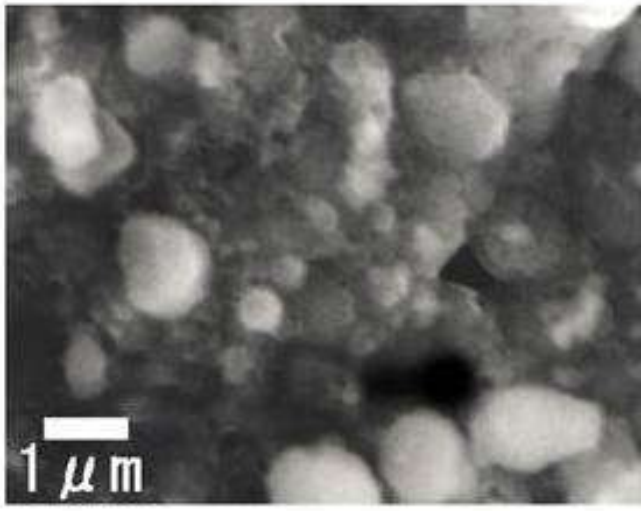


(b) 1073 K

**Figure 3.7 SEM images of samples**

## 3.4 Summary

The composition of strontium aluminate products by the present solution combustion synthesis has been studied by changing furnace temperatures and urea amount in order to varying calculated adiabatic temperature.

The present conditions were: the range of furnace temperature between 373 K and 1273 K, and the urea amounts 1.0, 1.5, and 2.0. Combustion synthesis reactions occurred above 873 K. With increasing furnace temperature from 873 K to 1273 K, β-$SrAl_2O_4$ existed in the whole temperature range, and the ratio of α-$SrAl_2O_4$ became maximum at 1073 K. In addition, little amount of $Sr_3Al_2O_6$ and $SrAl_4O_7$ existed.

With the increasing urea amount from stoichiometric amount, the ratio of α-$SrAl_2O_4$ and that of β-$SrAl_2O_4$ became maximum and those of $Sr_3Al_2O_6$ and $SrAl_4O_7$ became minimum at 1.5 times of the stoichiometric urea amount.

Phase composition of strontium aluminates is confirmed to be controlled with changing combustion synthesis conditions such as furnace temperature and urea ratio.

# Chapter 4
# Investigation of arrested samples of solution combustion synthesis process of strontium aluminates

## 4.1 Introduction

In this chapter, solution combustion synthesis (SCS) of complex oxides was investigated. In this chapter, as well as in the previous chapter, $SrAl_2O_4$ powders which are well-known long-lasting phosphor matrix were used as target materials.

In the previous Chapter 3, it was indicated that the SCS reaction of $SrAl_2O_4$ includes two step process; the reaction between $Al(NO_3)_3 \cdot 9H_2O$ and $CO(NH_2)_2$, and the reaction among $Sr(NO_3)_2$, $Al(NO_3)_3 \cdot 9H_2O$ and $CO(NH_2)_2$ simultaneously. It is known that $Al(NO_3)_3 \cdot 9H_2O$ decomposes into amorphous $Al_2O_3$ at around 400 K [105], and $Sr(NO_3)_2$ into SrO at around 900 K [104]. Regardless of the fact that the difference between the decomposition temperature of $Al(NO_3)_3 \cdot 9H_2O$ and that of $Sr(NO_3)_2$ is more than 400 K, these two reactions are supposed to occur almost simultaneously because of the rapid temperature rise during the SCS process, however these processes have not been confirmed directly under the conditions of SCS yet. Moreover a rapid cooling phenomenon after the SCS reaction was also observed in the Chapter 3, however the effects of this cooling phenomenon on the characteristics of products, such as phase distribution and particle sizes have not been clear. In the present chapter, to complete the entire picture of the SCS process of $SrAl_2O_4$ synthesis, the SCS reaction was arrested in determined intervals of time, and arrested samples were investigated from the points of view of phase composition, element distribution and particle size.

A typical temperature profile during the SCS process of $SrAl_2O_4$ synthesis is shown in Figure 4.1. After evaporation of $H_2O$, the SCS process of $SrAl_2O_4$ proceeded from the stage (1) to stage (4) as follows.

**Stage (1):** After evaporation of $H_2O$, the temperature finished increased gradually from the boiling point of $H_2O$ (about 373 K) to the temperature of about 920 K where the combustion reaction started. The sample became white moist and viscous substance because of dehydration of aluminum hydrates.

**Stage (2):** After the combustion started, the temperature increased rapidly to more than 1200 K, which was the maximum temperature in this SCS process, with the evolution of large amounts of gases such as $CO_2$, $H_2O$, and $N_2$. The combustion reaction occurred and white watery powders were obtained in this stage.

**Stage (3):** The cooling phenomenon occurred after combustion finished. White dry powders were also obtained at this stage. The temperature of sample decreased rapidly to less than 1000 K which was lower than the temperature of the furnace (1073 K) within several seconds, and evolution of gases still continued. Cooling rates were calculated from the maximum temperature and lowest temperature. In this work, combustion temperatures were measured by type S thermocouples (Pt, Pt-10%Rh, diameter: 0.5mm) and data were collected by a data logger (interval: 25 ms), however calculated cooling rates were unstable, because combustion phenomenon occurs whole volume of samples and combustion temperature of each point of samples is variable. Calculated cooling rates were varied from 15 K/s to 59 K/s. The mean cooling rate in this work is 35 K/s.

**Stage (4):** A gradual temperature increasing phenomenon occurred after the cooling phenomenon. Evolution of large amounts of gases had already finished at this stage. The temperature of the sample slowly increased to the temperature of the furnace. The sample represented also white dry powders.

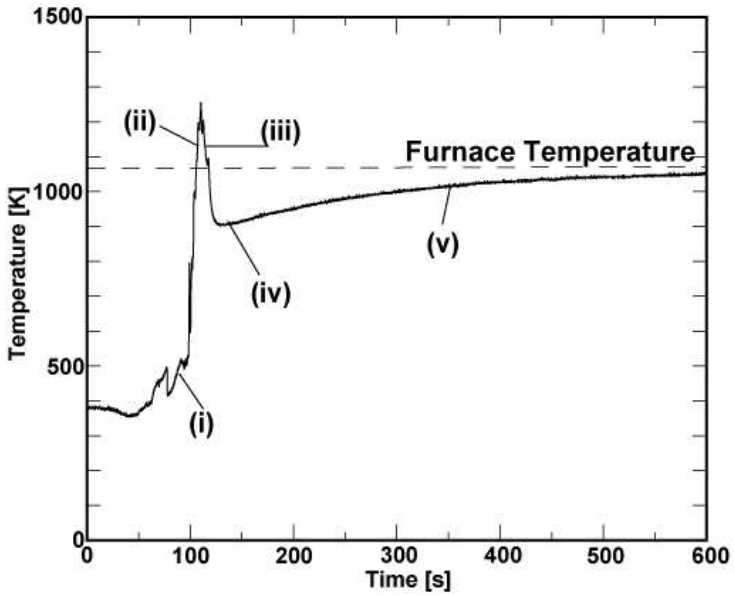


**Figure 4.1 Typical temperature profile of**

**solution combustion synthesis process of $SrAl_2O_4$ synthesis:**

**(i) sample (a), (ii) sample (b), (iii) sample (c), (iv) sample (d), and (v) sample (e).**

## 4.2 Experimental

Schematic illustration of the apparatus is already shown in Figure 3.2 in Chapter 3 (pp.53). Starting substances were the powders of $Sr(NO_3)_2$, $Al(NO_3)_3 \cdot 9H_2O$ and $CO(NH_2)_2$. These powders were mixed in proportion according to the Equation (3.1) in Chapter 3.

These powders were dissolved in distilled water. Then, starting solutions were put into a furnace. Preheating temperature was 1073 K, and urea ratio ($m$) was 1.5. According to the results of Chapter 3, these conditions would be suitable for synthesizing $SrAl_2O_4$ because of proper balances between the amounts of $Sr(NO_3)_2$, $Al(NO_3)_3 \cdot 9H_2O$ and $CO(NH_2)_2$ considering decomposition of starting substances. The temperature of the sample was measured by type S thermocouples (Pt, Pt-10%Rh, diameter: 0.5mm), and temperature data were logged by a data logger (interval: 25 milliseconds). To clarify the SCS process of $SrAl_2O_4$ synthesis, five arrested samples were investigated; sample (a): the sample taken after evaporation of $H_2O$ finished (before combustion started), sample (b): the sample obtained at 5 seconds after combustion started, sample (c): the sample obtained at 10 seconds after combustion started, sample (d): the sample obtained at 60 seconds after combustion started, and sample (e): the sample 4btained at 240 seconds after combustion started. Each sample was obtained by the arrest of the combustion reaction at fixed points of time. The arrest was achieved by taking a crucible with sample out of a furnace, and covering the crucible with an alumina plate in order to stop the combustion reaction, and cooling it down in the air. The obtained samples were measured by x-ray diffraction (XRD) (Rigaku, Rint-2000), field-emission scanning electron microscopy and energy dispersive spectroscopy (FE-SEM and EDS, Hitachi High-tech, S-4800), and scanning

electron spectroscopy and energy dispersive spectroscopy (SEM and EDS, JEOL, JSM-6610LA).

In Table 4.1, the obtained timings of samples from (a) to (e) are related to the stages from (1) to (4) in Figure 4.1. Sample (a) was the sample at the point of stage (1) which was gradual temperature increasing stage before combustion started. Sample (b) was the sample at the point of stage (2) where the combustion reaction continued. Sample (c) was the arrested sample during rapid cooling phenomenon in stage (3). Sample (d) was the sample at the point of minimum temperature after combustion reaction which is the around boundary between stages (3) and (4). Sample (e) was the samples at the point of stage (4) after cooling phenomenon finished.

**Table 4.1 Each arrested sample in relation to each stage in the solution combustion synthesis process.**

| **Samples** | **Stage** | **Temperature of samples** |
|---|---|---|
| (a) | Stage (1) | 480 K |
| (b) | Stage (2) | 1180 K |
| (c) | Stage (3) | 1150 K |
| (d) | Around the boundary between stage (3) and stage (4) | 910 K |
| (3) | Stage (4) | 1020 K |

In the Chapter 3, it was measured that the reaction temperature between $Al(NO_3)_3 \bullet 9H_2O$ and $CO(NH_2)_2$ was around 400 K, and $Sr(NO_3)_2$ reacted about 900 K. The temperature of the stage (1) would correspond to the reaction temperature of

$Al(NO_3)_3 \cdot 9H_2O$, and $CO(NH_2)_2$ and the temperature of the stage (2) would correspond to the decomposition temperature of $Sr(NO_3)_2$ (about 900 K).

# 4.3 Results and discussion

## 4.3.1 XRD patterns of arrested samples

To make clear the SCS process precisely, samples of each stage were analyzed. XRD patterns of each sample are shown in Figure 4.2. In the pattern of sample (a) (stage (1)), peaks of $Al(OH)_3$, urea-nitrate related substances ($CH_4N_2O \cdot HNO_3$ and $C_2H_5N_3O_2 \cdot H_2O$), and $Sr(NO_3)_2$ were observed. The sample (a) is the mixture of the of $Al(OH)_3$, biuret, and urea-nitrate. Decomposition of $Al(NO_3)_3 \cdot 9H_2O$ has already shown in Figure.2.7 in Chapter 2 (pp. 44). For sample (b) (stage (2)), in addition to the peaks of intermediate substances same as the sample (a), peaks of $SrAl_2O_4$ were observed. For samples (c)-(e) (stage (3)-(4)), only the peaks of strontium aluminates were observed. In addition to the peaks of $SrAl_2O_4$ (main phase), the peaks of $SrAl_4O_7$ and $Sr_3Al_2O_6$ were observed. These results suggest that during the stage (1), $Al(NO_3)_3 \cdot 9H_2O$ and $CO(NH_2)_2$ reacted, however $Sr(NO_3)_2$ had not reacted yet, and that during the stage (2), $Sr(NO_3)_2$ also reacted with $Al(NO_3)_3 \cdot 9H_2O$ and $CO(NH_2)_2$, which was the combustion reaction. Then, after the combustion reaction completed (stage (3), (4)), only strontium aluminates were obtained, and starting substances or intermediate substances were not remained in the product.

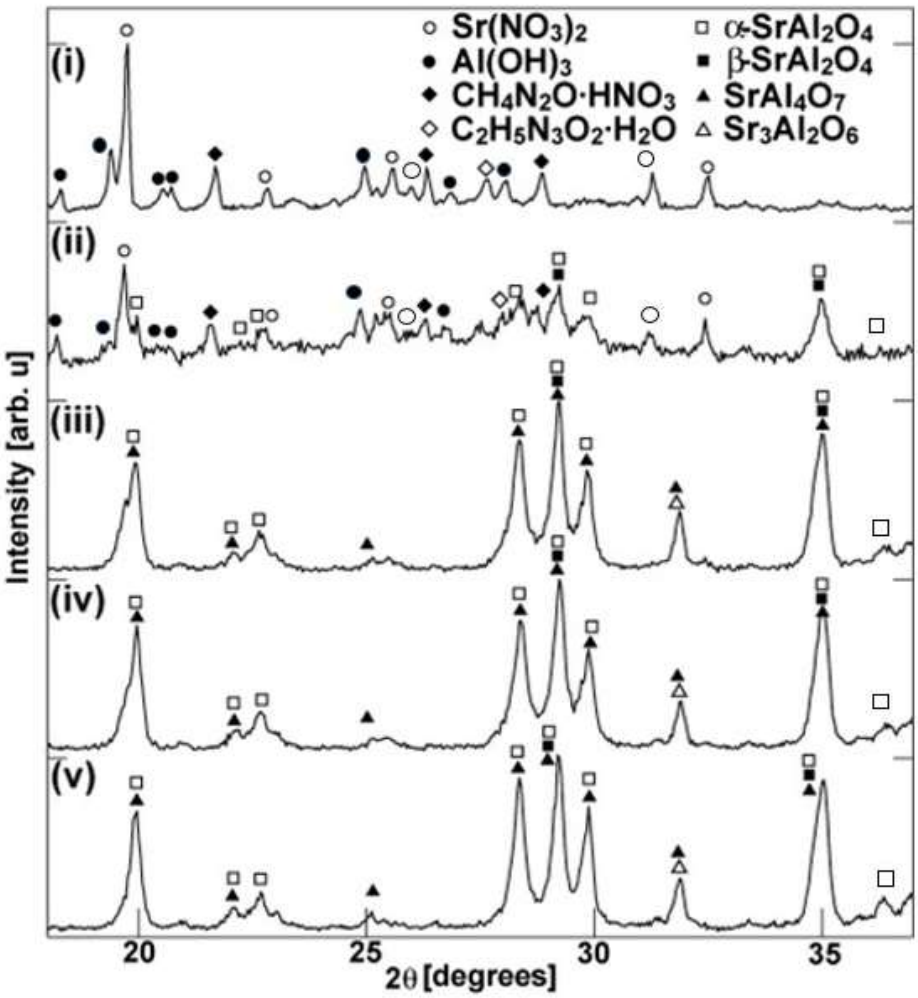


**Figure 4.2 XRD patterns of each sample**

**(i) sample (a), (ii) sample (b), (iii) sample (c), (iv) sample (d), and (v) sample (e).**

## 4.3.2 Particle sizes and element distribution

The SEM and EDS mapping images of the samples are shown in Figure 4.3. It can be seen that in case of the sample (a) (stage (1)), the element of aluminum distributed globally, however, the element of strontium distributed locally. At the sample (b) (stage (2)), both the elements of aluminum and strontium distributed, however, some shadows of strontium containing particles were seen on the mapping image of aluminum. The images of the sample (c) (stage (3)) shows that both the elements of aluminum and strontium distributed uniformly, and there were no shadows of strontium containing particles on the mapping image of aluminum. These results indicate that the SCS process of $SrAl_2O_4$ synthesis proceeded as follows; stage (1): $Al(NO_3)_3 \bullet 9H_2O$ and $CO(NH_2)_2$ reacted, and $Al(OH)_3$ and urea-nitrate related substances ($CH_4N_2O \bullet HNO_3$ and $C_2H_5N_3O_2 \bullet H_2O$) were formed, however $Sr(NO_3)_2$ had not reacted yet in this stage, stage (2): the combustion reaction among all starting substances were occurred and $SrAl_2O_4$ were synthesized, however unreacted $Sr(NO_3)_2$ and intermediate substances were still remained, and stages (3-4): all starting and intermediate substances reacted completely, and strontium aluminates were obtained. In addition to the phase of $SrAl_2O_4$ (main phase), little amounts of $SrAl_4O_7$ and $Sr_3Al_2O_6$ can be seen in the products.

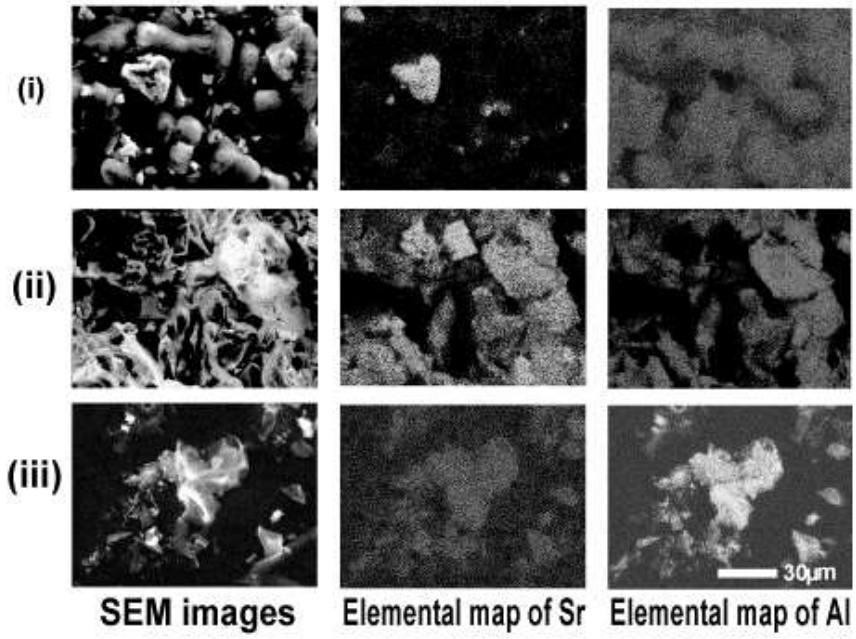


**Figure 4.3 SEM and EDS mapping images of the each sample**

**(i) sample (a), (ii) sample (b), and (iii) sample (c).**

FE-SEM and EDS mapping images of the sample (c) (stage (3)) are shown in Figure 4.4. The elements of strontium and aluminum are distributed in the nanometer range after the combustion reaction. This result can be explained by one of the characteristics of the SCS process. Starting substances which have a large reaction temperature, such as $Sr(NO_3)_2$ (around 900 K) and $Al(NO_3)_3 \bullet 9H_2O$ (around 400 K), can react because of high combustion temperature during the SCS process (more than 1200 K).

The molar ratio of Al/Sr in arrested samples as a function of time after initiation of combustion is shown in Figure 4.5. These data were estimated from EDS peaks. EDS measurements were performed by FE-SEM and EDS within sub-micron range. After combustion completed, the ratio would be gradually close to the value of "2", which means that the composition of strontium aluminates is close to $SrAl_2O_4$ in

sub-micron range. For the sample (c), the width of error bar was narrow, however the width of error bars became wider after the cooling phenomenon completed (samples (d) and (e)). It suggests that during stages (3), the sample of non-equilibrium phases was obtained because of large temperature gradients during SCS process, then after cooling phenomenon completed (stage (4)), the sample was heated in a furnace gradually and the composition of sample reached slowly the phase of $SrAl_2O_4$ which is theoretical ratio in the initial conditions of the present work. Just after rapid cooling phenomenon, the temperature distribution inside the furnace and sample would not be under uniform conditions, therefore the phase composition of the sample might become slightly non-uniform within a short time heating by the furnace (several minutes). In this work, besides the main phase of $SrAl_2O_4$, little amounts of $SrAl_4O_7$, and $Sr_3Al_2O_6$ were obtained in the products.

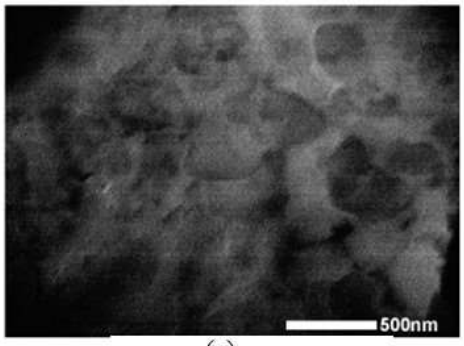


(a)

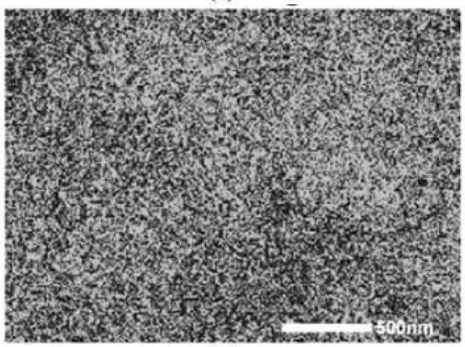


(b)

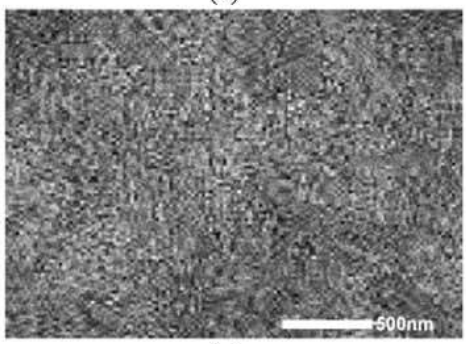


(c)

**Figure 4.4 FE-SEM and EDS images of the sample at the point of stage (3) (Sample (c)).**

**(a) SEM images**

**(b) Sr**

**(c) Al**

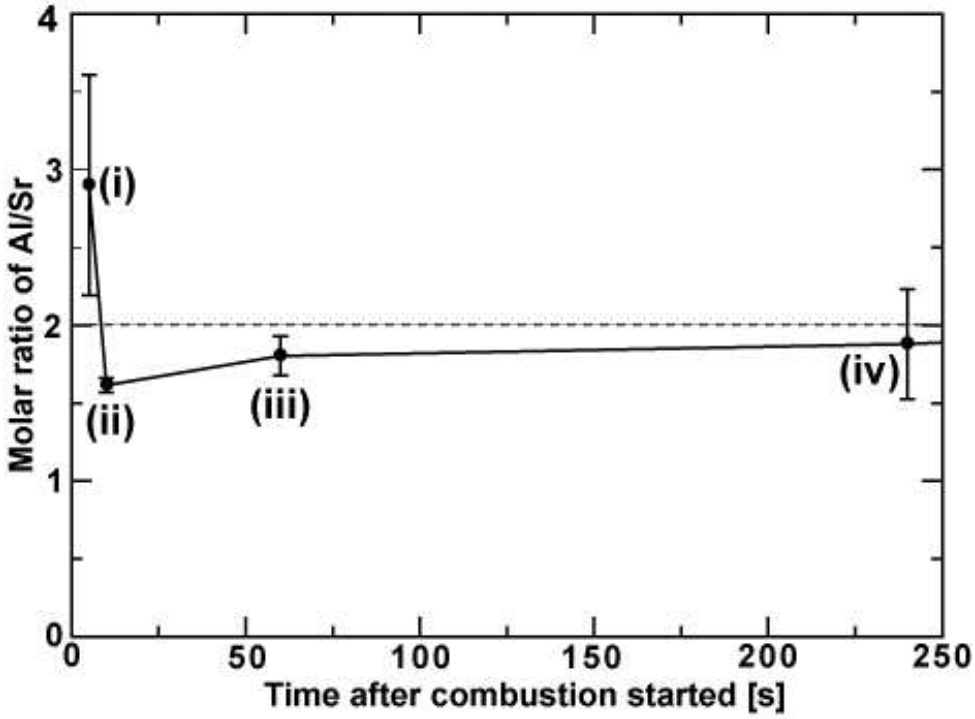


**Figure 4.5 Molar ratio of Al/Sr in each sample as a function of time after initiation of combustion:**
**(i) sample (b), (ii) sample (c), (iii) sample (d), and (iv) sample (e).**

FE-SEM images of samples are shown in Figure 4.6. Many nuclei were seen on the surface of large particles in the sample (b). For the sample (c), the particles in size of 20-30 nm were observed. For the both samples (d) and (e), the particles in size of 50 nm were observed. It was suggested that during the stage (2), nuclei were formed in combustion reaction, and these nuclei grow during the stage (3) which is a rapid cooling phenomenon. Then, at the end of the stage (3), the particles in size of about 50 nm were formed. During the stage (4), particle sizes did not change meaningfully. This rapid cooling phenomenon is one of the unique characteristics of SCS. In the case of SHS, the combustion reaction initiates by local heating, and then the combustion wave would proceed in one direction, therefore after the combustion

wave passed, the temperature of products would decrease gradually because of the heat of reaction provided by the reaction zone. On the other hand, in the cases of SCS, the combustion reaction initiates by global heating, and the combustion reaction would occur in the whole sample almost simultaneously, then after combustion reaction finished almost simultaneously in the entire sample, then the temperature would decrease rapidly without heat provided by the combustion reaction. Moreover, large amounts of gases such as $CO_2$, $H_2O$ and $N_2$ which were evolved in the SCS process would absorb the part of the heat of reaction, and assist cooling phenomenon during stage (3). As a result, 50 nm nano particles were obtained in the SCS process of $SrAl_2O_4$ synthesis.

According to the results obtained in the present work, an entire image of the SCS process of $SrAl_2O_4$ synthesis was summarized as follows. After evaporation of $H_2O$, the reaction between $Al(NO_3)_3 \bullet 9H_2O$ and $CO(NH_2)_2$ occurred and intermediate substances such as $Al(OH)_3$, urea-nitrate related substances ($CH_4N_2O \bullet HNO_3$ and $C_2H_5N_3O_2 \bullet H_2O$) were synthesized, however $Sr(NO_3)_2$ had not reacted yet (stage (1)), then during in the stage (2), in addition to $Al(NO_3)_3 \bullet 9H_2O$ and $CO(NH_2)_2$ , $Sr(NO_3)_2$ also reacted and the combustion reaction started with rapid temperature increase to maximum temperature (more than 1000 K). $SrAl_2O_4$ was synthesized during this stage, however intermediate substances and unreacted $Sr(NO_3)_2$ were still remained. Starting substances which has large reaction temperature difference between $Al(NO_3)_3 \bullet 9H_2O$ (around 400 K) and $Sr(NO_3)_2$ (about around 900 K) can react under such a high temperature conditions of SCS process. After combustion finished, a rapid cooling phenomenon occurred (Stage (3)). Besides the phase of $SrAl_2O_4$, little amounts of $SrAl_4O_7$ and $Sr_3Al_2O_6$ were synthesized. Nuclei of strontium aluminates did not grow larger (20-50nm) in this stage (3) because of this cooling phenomenon.

In the stage (4), the particle sizes did not change significantly, and nano particles of $SrAl_2O_4$ were obtained (~50 nm).

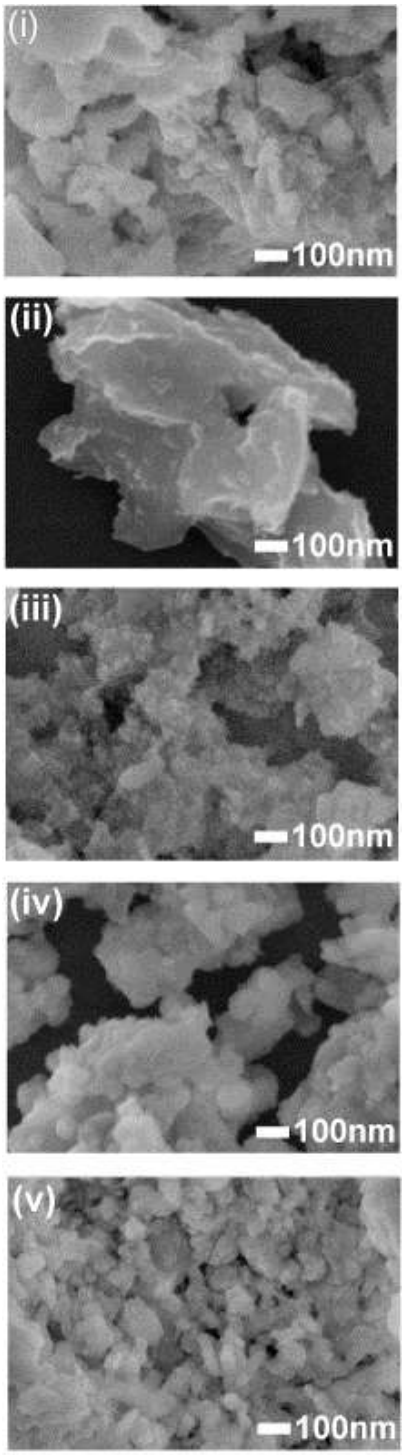


**Figure 4.6 FE-SEM images of each sample**

**(i) sample (a), (ii) sample (b), (iii) sample (c), (iv) sample (d), and (v) sample (e).**

# 4.4 Solution combustion synthesis process of $SrAl_2O_4$

According to this work, the model of solution combustion synthesis reaction process can be expressed as follows;

**Stage (1)**

After water completely evaporated, $Al(NO_3)_3 \cdot 9H_2O$ which has a low reaction temperature reacts with fuel decomposed materials, and temperature of samples increases gradually to the decomposition temperature of $Sr(NO_3)_2$ which has a high reaction temperature. The possible reaction of stage (1) can be expressed as an Equation (4.1)

.

$$Al(NO_3)_3 \cdot 9H_2O + 5CO(NH_2)_2 \rightarrow 0.5\ Al_2O_3 + \text{Gaseous products } (N_2, H_2O \text{ and } CO_2) \quad (4.1)$$

**Stage (2)**

The temperature of the sample increases slowly to the decomposition temperature of metal nitrate, which has a high reaction temperature, and then the combustion reaction of both nitrates and fuels occurred. It is possible that two types of main reaction as follows.

$$Sr(NO_3)_2 + 5/3 \cdot CO(NH_2)_2 \rightarrow SrO + \text{Gaseous products } (N_2, H_2O \text{ and } CO_2) \quad (4.2)$$

$$SrO + Al_2O_3 \rightarrow SrAl_2O_4 \quad (4.3)$$

**Stage (3)**

The temperature of the sample is decreased rapidly to below the furnace temperature because large amounts of gaseous products which produced in the combustion process remove heat from reaction samples. Phase composition of the product would be conserved, and the particles of strontium aluminates cannot grow in this stage.

**Stage (4)**

After cooling stage, the temperature of the sample increases gradually to furnace temperature. Phase composition of samples would not change dramatically in this stage.

The solution combustion reaction can be divided into these four stages. In these four stages, there are two important reaction stages which are related to nitrates, which have low reaction temperature nitrates (stage (2)) and with nitrates which have high reaction temperature nitrates (stage (3)). More noteworthy is the cooling stage (Stage (3)). This rapid cooling phenomenon is unique characteristics of solution combustion synthesis. According to this phenomenon, nanoparticles included β-phase are synthesized.

Schematic illustration of solution combustion synthesis of strontium aluminates is shown in Figure 4.7.

In stage (1), after evaporation of $H_2O$, mixture of nitrates and decomposed fuel are obtained. In stage (2), the main combustion reaction is occurred and all fuels and nitrate ions are reacted, and nuclei of fine nano oxide particles are formed. Then, in stage (3), which is a rapid cooling stage, crystal growth is prohibited by emitting large

amount of gas. These drastically rapid heating and cooling phenomena are distinctive characteristics of solution combustion synthesis process, resulting in forming fine oxide particles in stage (4).

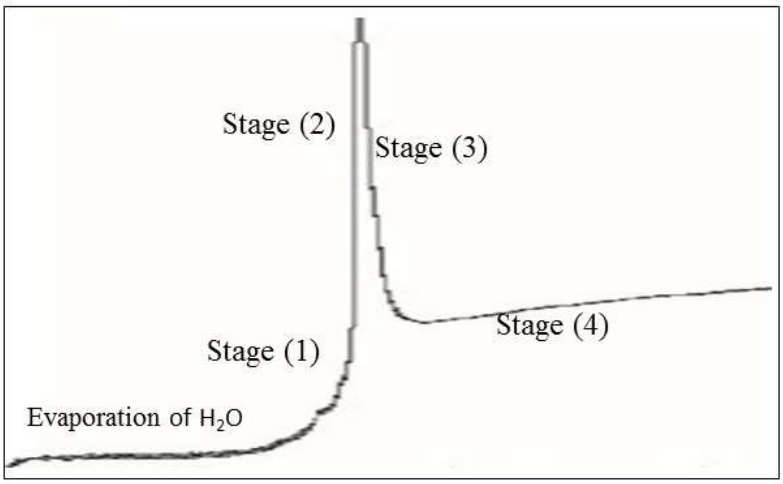


**Figure 4.7 Schematic illustration of solution combustion synthesis of strontium aluminates**

**Stage (1): Formation of $Al(OH)_3$ and urea related materials**

**Stage (2): Formation of Strontium aluminates (Combustion reaction)**

**Stage (3): Preserving β-phase (Cooling process)**

**Stage (4): Gradually heating stage**

# 4.5 Summary

In order to elucidate the entire picture of the SCS process of $SrAl_2O_4$ synthesis, the arrested samples obtained through SCS were investigated. It was shown that $Al(NO_3)_3 \cdot 9H_2O$ and $CO(NH_2)_2$ reacted after evaporation of $H_2O$, and intermediate substances such as $Al(OH)_3$ and urea-nitrate related substances were synthesized, however $Sr(NO_3)_2$ had not reacted yet. Then, in addition to the reaction between $Al(NO_3)_3 \cdot 9H_2O$ and $CO(NH_2)_2$, $Sr(NO_3)_2$ with high decomposition temperature (around 900 K) also reacted and combustion reaction started. In this stage, $SrAl_2O_4$ were synthesized, however starting and intermediate substances were still remained. The temperature increased rapidly to more than 1000 K which is the maximum temperature in the present work. The reaction temperature difference between $Al(NO_3)_3 \cdot 9H_2O$ (around 400 K) and $Sr(NO_3)_2$ (around 900 K) is more than 400 K. Starting substances which have the large temperature difference can react under high temperature conditions during the SCS process. After the combustion reaction completed, the rapid cooling phenomenon can be seen. Besides the phase of $SrAl_2O_4$ (main phase), small quantities of $SrAl_4O_7$ and $Sr_3Al_2O_6$ were synthesized during this cooling stage. Strontium aluminates particles did not grow larger according to this cooling phenomenon with evaporation of large amounts of gases. As a result, fine nano strontium aluminates particles (~50 nm) can be obtained in the SCS process.

In the case of SCS of $SrAl_2O_4$, the combustion temperature is lower than melting point of $SrAl_2O_4$, however, higher than transition points of all starting materials, resulting in the formation of both $\alpha$-$SrAl_2O_4$, and $\beta$-$SrAl_2O_4$.

In the case of combustion synthesis of $TiB_2$, the combustion temperature is equal to melting point of Ti, B, and $TiB_2$, therefore, intermediate substance is once

melted and recrystallized, resulting in formation of only β-$TiB_2$. In the case of combustion synthesis of ZnS, the combustion temperature is higher than the decomposition temperature of ZnS, resulting in formation of β-ZnS.

It is concluded when combustion temperature is higher than or equal to transition points of products, it tends to synthesize pure high-temperature phase, and when combustion temperature is lower than the transition point of products, high-temperature phase is partially synthesized.

In terms of the reaction of solution combustion synthesis of $SrAl_2O_4$, there are two step main reactions. Initially, metal nitrate which has a low reaction temperature reacts with organic fuels, and releases the heat of reaction. Then, the temperature of the sample increases by heat of reaction, and metal nitrate which has high decomposition temperature starts to react. The reaction between the metal nitrate which has a low reaction temperature and fuels are ignition of this main reaction, therefore, in the case of solution combustion synthesis of complex oxides, fuels can be selected as high reactivity of the nitrate of low reaction temperature.

In terms of change of particle size shows prohibit of particle sizes of products. Large amount of gases evolved during the process would take much of heat out from the system, and prohibit particle growth. In the case of solution combustion synthesis of $SrAl_2O_4$ in this work, nano oxide particles whose diameters are about 50 nm are obtained. When fuels amounts increase, larger amounts of gases are released, therefore particle sizes can be controlled with organic fuel ratio.

# Chapter 5
# ZnS combustion synthesis as a related process to strontium aluminates solution combustion synthesis for making clear the influence of the heat of reaction on structure formation

## 5.1 Introduction

As was mentioned in Section 1.3, combustion synthesis mainly consists of two processes; the reaction propagation process and structure formation process. After the reaction initiates, the reaction propagates self-sustainingly with the aid of the generation of exothermic heat of reaction in the front of the reaction zone. In the reaction zone, the reaction products are affected by large gradients of heating and cooling processes following heat generation and release in the microscopic range. Through these processes, the final products of combustion synthesis become fine in size and uniform in composition.

An adiabatic temperature is one of an important factor to comprehend the combustion synthesis process. In this section, combustion synthesis of $TiB_2$, ZnS, and $SrAl_2O_4$ will be discussed. The relationship between adiabatic temperatures of systems and transition temperature of combustion synthesized products are shown in Figure 5.1.

In the section 1.1.1, combustion synthesis of $TiB_2$ was described as a typical example of self-propagating high-temperature-synthesis (SHS). In the case of combustion synthesis of $TiB_2$, the adiabatic temperature is equal to the melting point of

products and higher than the melting point of all starting materials, therefore, the product would not evaporate in the combustion process. This fact means that the combustion wave propagates in one direction without the influence of evaporation of products and starting materials. The heat of evaporation of products and that of starting materials draw heat from samples, resulting in unstable combustion wave propagation.

In the case of solution combustion synthesis (SCS) of $SrAl_2O_4$ which is shown in Chapters 2, 3 and 4, the adiabatic temperature of the system is 1090 K. This adiabatic temperature is less than the decomposition temperature of $SrAl_2O_4$ (2063 K) [102], which means that it is difficult to propagate the combustion wave spontaneously. Therefore, in this case, in order to initiate the combustion synthesis reaction, global heating is needed. In addition, this adiabatic temperature is higher than the decomposition temperature of starting materials of $Al(NO_3)_3 \cdot 9H_2O$ (around 400 K), and urea (below 570 K), however, little higher than that of $Sr(NO_3)_2$ (around 900 K). Therefore, in order to initiate the combustion reaction, it is important to increase the combustion temperature by controlling furnace temperature and urea (fuel) ratio in order to react $Sr(NO_3)_2$.

In the case of combustion synthesis of ZnS which will be described precisely in this chapter, the adiabatic temperature of the system (2200 K) is higher than the decomposition temperature of ZnS (1655 K) and boiling temperature of all starting materials. Therefore, the combustion wave might propagate spontaneously with the aid of the large heat of reaction, however, after the combustion wave passed, ZnS is once decomposed, resulting in gas included structure formation process.

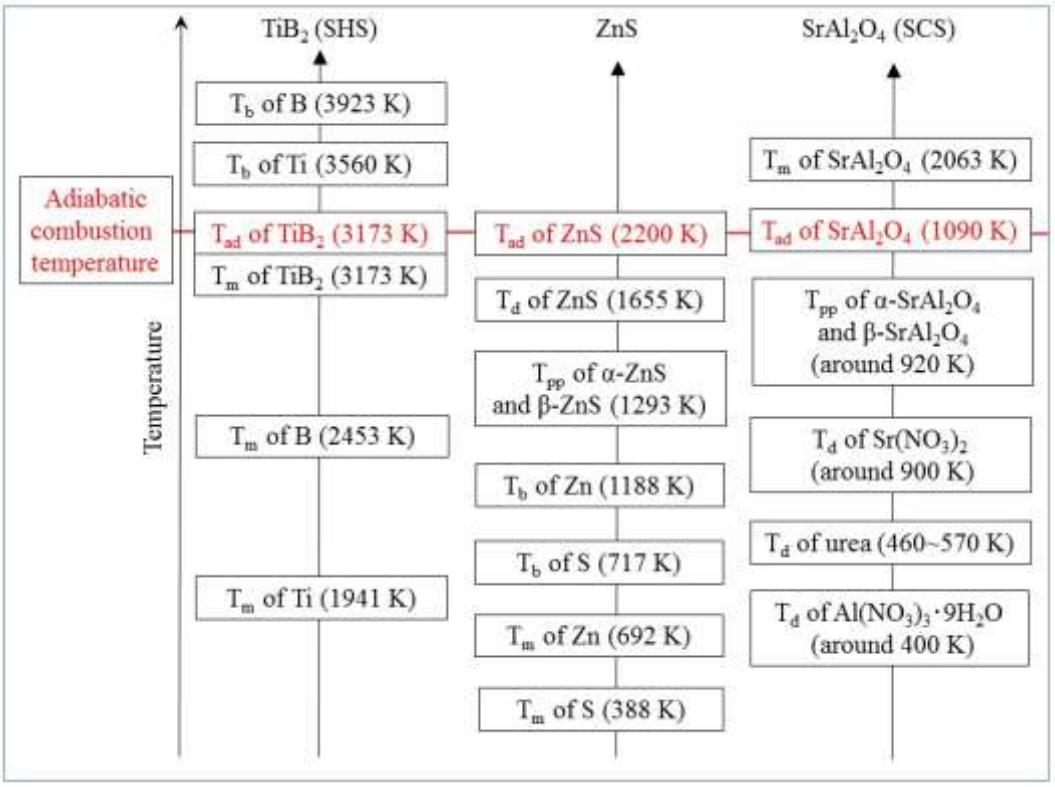


**Figure 5.1 Relationship between adiabatic temperatures of systems and transition points of starting materials and products [5, 102, 104-106].**

**"$T_m$" is a melting point, "$T_b$" is a boiling point, "$T_d$" is a decomposition temperature, "$T_{pp}$" is phase-phase transition point, and "$T_{ad}$" is the adiabatic temperature of the system.**

# 5.2 Zinc sulfide

ZnS is known as one of the important photoelectric semiconductors because of its direct-type wide band gap (3.7 eV) [117]. Luminescence properties of

Mn-mixed ZnS, such as photoluminescence (PL) and electroluminescence (EL), have been studied to apply photoelectric devices, e.g. display panel and lasers [118-120], for many years. In 1994, it was found that Mn-mixed ZnS nano particles show unique characteristics, e.g. increase of band gap, high quantum efficiency and shortening of decay time [83-86]. Mn-mixed ZnS nano particles commonly are obtained by applying sol-gel methods which take several days [121]. Since combustion synthesis can provide the products in a short time, it should be applied to the production of fine ZnS. To attain fine phase distribution and formation of fine particles is also one of the characteristics of combustion synthesis, therefore, it would be appropriate for synthesizing ZnS fine particles.

Zinc sulfide has two possible types of crystal structure [117]; α-ZnS (zincblende structure) and β-ZnS (wurtzite structure). Zincblende structure is a cubic type shown in Figure 5.2 and wurtzite structure is a hexagonal type shown in Figure 5.3. Physical properties of α-ZnS and β-ZnS are shown in Table 5.1 [87]. The solid-solid transition temperature is 1293 K [102]. Melting point of zinc sulfide is 1975 K at 500 MPa [102], and heat of formation of zinc sulfide is 203 kJ/mol at 298 K [102]. The melting point of zinc sulfide depends weakly on the pressure. At atmospheric pressure, zinc sulfide does not melt at all, since its decomposition temperature (1655 K) is considerably lower than its melting point. Physical properties of these two types of crystalline are not so different. In the present work, it is expected to obtain β-ZnS because of characteristics of combustion synthesis.

Most of combustion synthesis experiments on ZnS have been carried out under high pressures [15, 16, 122-124], in order to suppress evaporation of starting materials, however it seems not to be easy to control their synthesis conditions. If the amount of sulfur can be properly controlled, the combustion synthesis process results in

obtaining proper products. Therefore, the experiments under atmospheric pressure were attempted in the present work.

There are some reports about combustion synthesis of the gas included reaction system like combustion synthesis of ZnS in this work. For example, as is shown in Section 1.2, it was reported about combustion synthesis of solid silicon and nitrogen gas [76, 77]. β-$Si_3N_4$ fine particles were obtained in these experiments. $Si_3N_4$ has a low decomposition temperature, therefore synthesized $Si_3N_4$ sublimates, and forms β-$Si_3N_4$ fine particles in the process of alternation between decomposition and crystallization.

Therefore, in this chapter, combustion synthesis of zinc sulfide of the gas included system will be discussed. In the case of combustion synthesis of zinc sulfide, the starting powder compact is a condensed system, however, in combustion synthesis process, gaseous substances would be generated. These gaseous substances would affect structure formation of products.

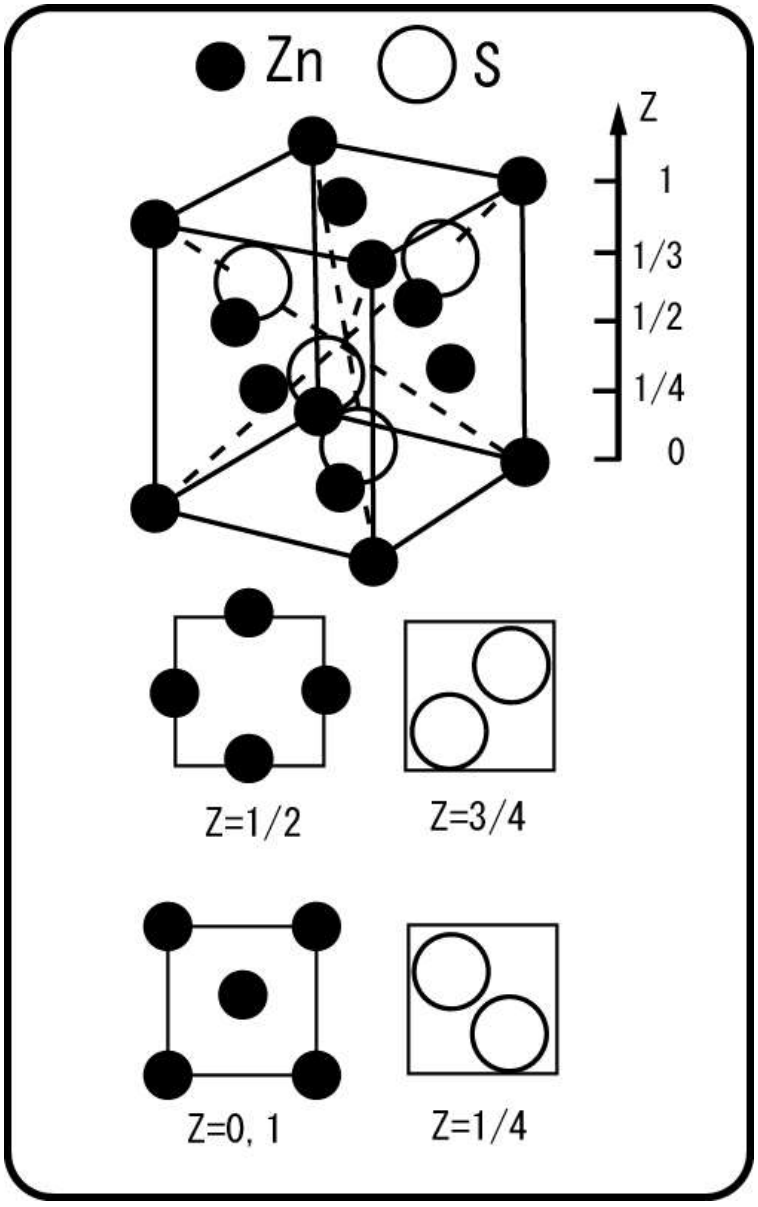


**Figure 5.2 Zinc blende structure of ZnS [5]**

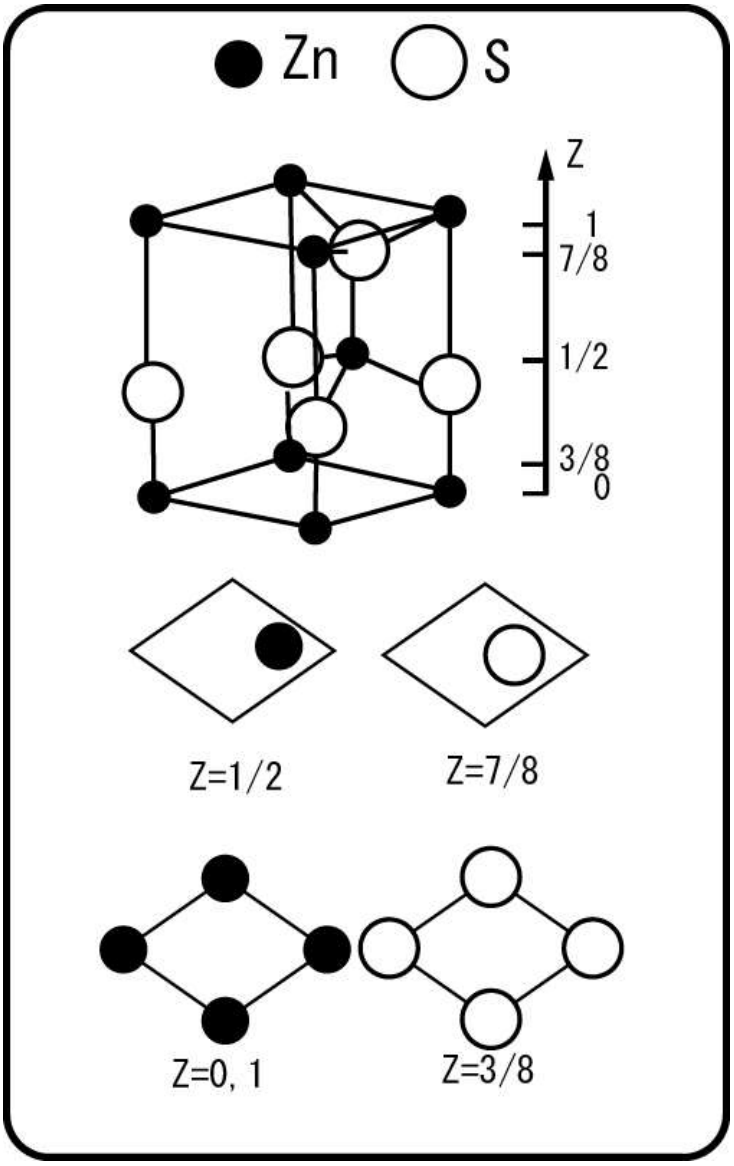


**Figure 5.3 Wurtzite structure of ZnS [5]**

**Table 5.1 Crystal parameters of α-ZnS and β-ZnS [117]**

| Structure | Crystal structure type | Lattice parameters [Angstrom] | | Band Gap [eV] |
|---|---|---|---|---|
| | | a | b | |
| **α-ZnS** | Zinc blend | 5.4109 | — | 3.6 |
| **β-ZnS** | Wurtzite | 3.811 | 9.348 | 3.7 |

# 5.3 Experimental

Zinc, sulfur, and manganese powders were selected as starting materials. The specifications of starting materials are shown in Table 5.2. These powders were mixed in a ratio following the expression (5.1),

$$(1-x)\mathrm{Zn} + x\mathrm{Mn} + \mathrm{S} \rightarrow \mathrm{Zn}_{1-x}\mathrm{Mn}_x\mathrm{S} \qquad (5.1)$$

Where, $x$ is the manganese ratio (6 values of x were selected in the present work, i.e. $x$=0, 0.01, 0.02, 0.03, 0.04, 0.05).

These powders were mixed in agate mortar. Because of a low boiling temperature of sulfur (717 K) [102], the extra addition of sulfur was treated with 10% in consideration of sulfur vaporizing. Then, the powder mixture was pressed into a cylindrical shape of 70 % packing density. The powder compacts were shaped in

15 mm$^{\varphi}$×10 mm$^{h}$. The image of a powder compact is shown in Figure 5.4.

A schematic illustration of the apparatus is shown in Figure 5.5. The experiments were carried out under argon of atmospheric pressure and room temperature. The powder compacts were initiated by electrical heating of a tungsten filament. Since it was expected that synthesized materials sublimate, the starting samples were placed in the vessel made of a quartz tube and stainless plates to collect synthesized powder.

Synthesized materials were measured by X-ray diffraction (XRD), Scanning electron microscope (SEM), and PL measurements.

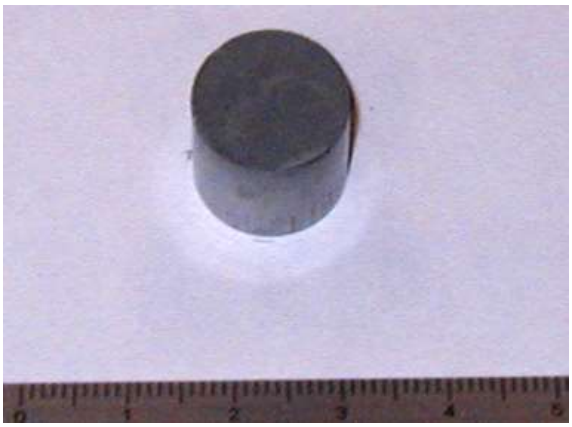

**Figure 5.4 Image of powder compact**

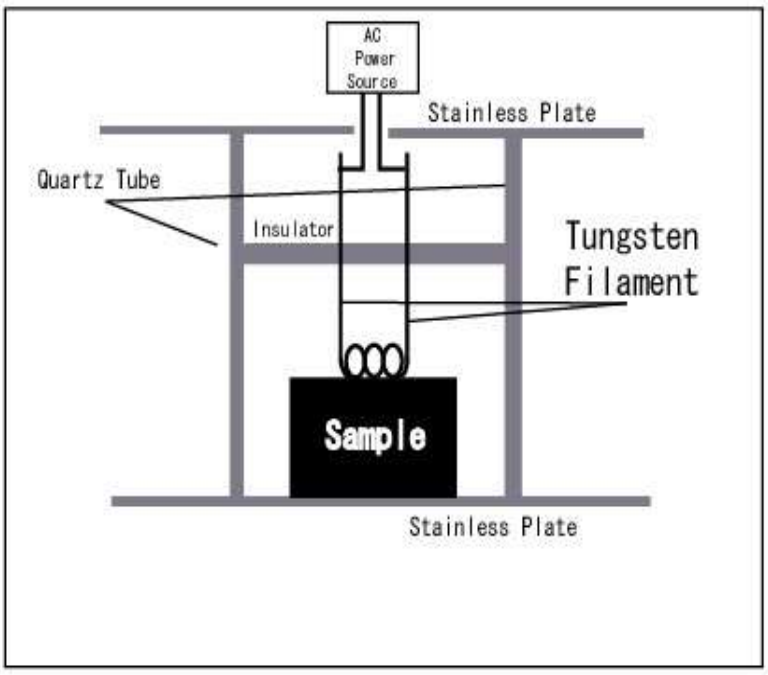


**Figure 5.5 Schematic illustration of apparatus**

**Table 5.2 Specification of starting materials**

| | **Particle sizes [μm]** | **Purity [%]** |
|---|---|---|
| **Zinc** | ~85 | 97.2 |
| **Sulfur** | ~85 | 98.0 |
| **Manganese** | ~85 | 99.99 |

## 5.4 Results and discussion

### 5.4.1 Phase composition of products

The images of synthesized materials are shown in Figure 5.6, because of decomposition of synthesized materials, not showing the shape of starting powder compacts. The powdery product was remained whole chamber.

Although it was not clearly measured the reaction propagation rate precisely, it is observed that light-emitting face propagated from the top of the sample to the bottom of the sample within a few seconds, therefore, a reaction propagation rate was estimated several millimeters per second.

XRD patterns of synthesized ZnS:Mn are shown in Figure 5.7. The XRD patterns were identified as β-ZnS (high temperature phase), which is wurtzite (Table 5.1, Figure 5.2). SEM images of the synthesized ZnS:Mn are shown in Figure 5.8. Particles of 1-10 μm in size were observed. These particle sizes are less than that of starting powders (80 μm). It was not observed that the dependence of XRD patterns and particle sizes in SEM images on the manganese ratio in the range from x=0 to x=0. 05. Moreover, the place dependability in apparatus would not be confirmed by XRD measurements, since synthesized zinc sulfide could once sublimate and decompose after combustion synthesis reaction. These results might be explained of the processes of gas phase combustion synthesis.

Adiabatic temperatures are calculated from the following Equation (5.2) [103].

$$\Delta H = \int_{298}^{T_t} C_p(s)dT + \int_{T_t}^{T_{ad}} C_p(g)dT + \Delta \mathrm{H_t} \quad (5.2)$$

(*"$\Delta H$"* is an enthalpy of formation at 298 K, *"$T_{ad}$"* is calculated adiabatic temperature, *"$C_p$"* is the specific heat of products, *"$T_t$"* is the transition temperature of products, and *"$\Delta H_t$"* is transition heat of products)

Using thermochemical data in the literature (Table 5.3) [102], calculated adiabatic temperature of this system is 2200 K. In Table 5.3, "$C_{p298\ K}$" is a heat capacity at 298 K, "$\Delta H_{298}$" is an enthalpy of formation at 298 K," $T_t$" is transition temperature, and "$\Delta H_t$" is an enthalpy of transition.

**Table 5.3 Thermochemical properties of ZnS, Zn, and S [102]**

| **Substances** | **$C_{p298\ K}$[J·mol$^{-1}$·K$^{-1}$]** | **$\Delta H_{298}$ [kJ·mol$^{-1}$]** |
|---|---|---|
| **α-ZnS(s)** | 49.46+4.44·10$^{-3}$·T-0.44·10$^{6}$·T$^{-2}$ | -139.8 |
| **β-ZnS(s)** | 49.25+5.27·10$^{-3}$·T-0.49·10$^{6}$·T$^{-2}$ | -205 |
| **S (s)** | 14.8+24.08·10$^{-3}$·T-24.08·10$^{6}$·T$^{-2}$ | 0 |
| **Zn(s)** | 21.33+11.65·10$^{-3}$·T-0.05·10$^{6}$·T$^{-2}$ | 0 |

Once the reaction initiates, the temperature of reaction zone would rapidly increase to the decomposition temperature of zinc sulfide (1655 K), because the decomposition temperature of zinc sulfide is lower than the adiabatic temperature of combustion (2200 K). Synthesized solid zinc sulfide would be sublimated, and would come to coexistent states with vapor sulfur and vapor zinc [125]. Vapor zinc and sulfur would be rapidly cooled under argon atmosphere. Then, zinc which has a higher melting point (1188 K) [102] would become liquid phase, and liquid zinc particles are formed. Liquid zinc particles would react with vapor sulfur, resulting in recrystallization and generation of β-ZnS fine particles. Phase transition of zinc and sulfur is shown in Table 5.4, and structure formation model of β-ZnS is shown in Figure 5.9.

**Table 5.4 Phase transition of zinc and sulfur [102]**

| | **Zinc** | **Sulfur** |
|---|---|---|
| **Melting point [K]** | 692 | 388 |
| **Boiling point [K]** | 1188 | 717 |

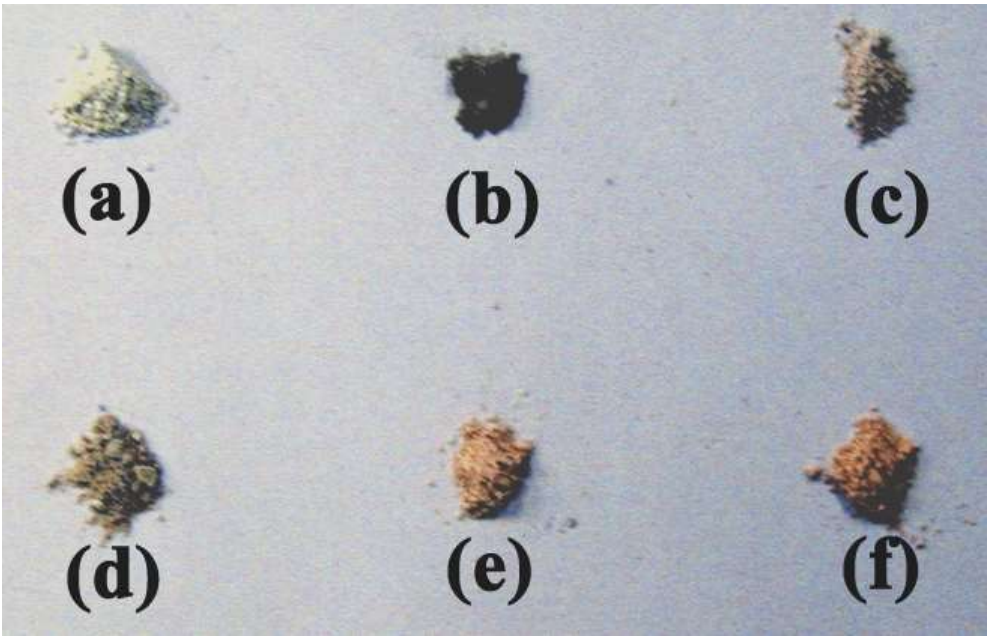


**Figure 5.6 Images of synthesized materials**

**(a)- (f): x=0.01α (α=0,1,2,3,4,5)**

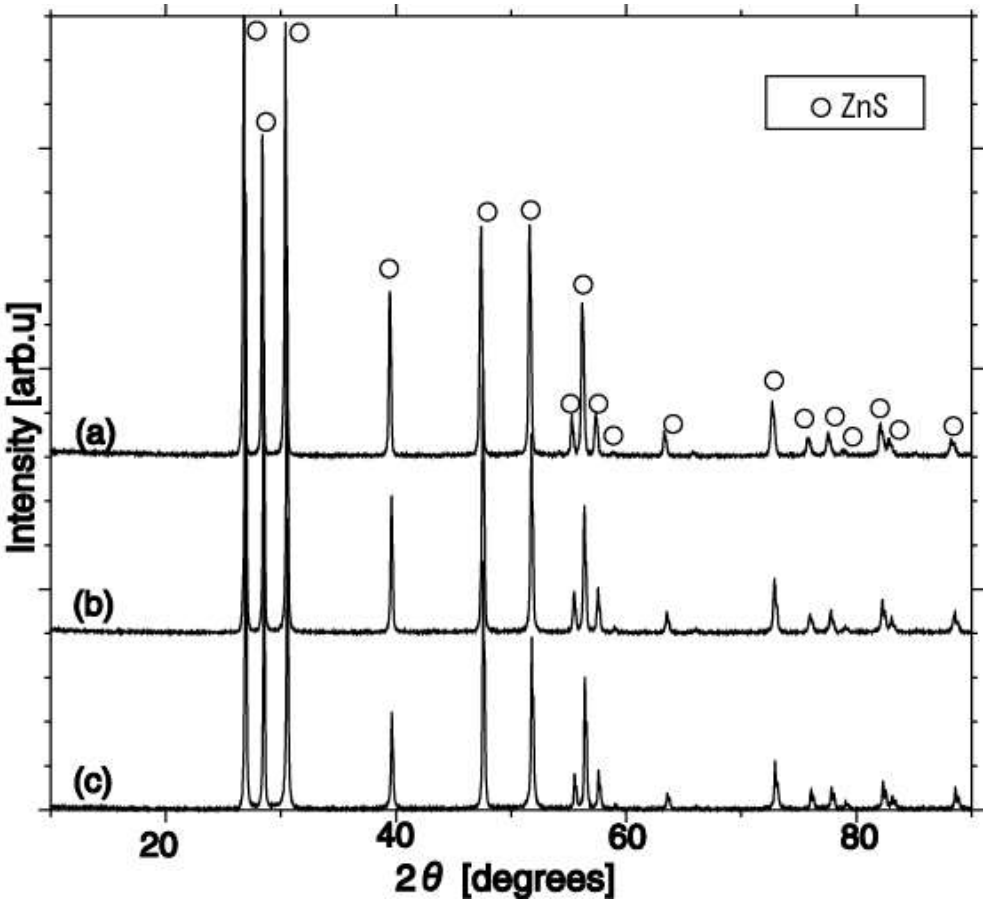


**Figure 5.7 XRD patterns of synthesized $Zn_{1-x}Mn_xS$ with varying manganese ratio**

**(a): x=0, (b): x=0.03, (c): x=0.05**

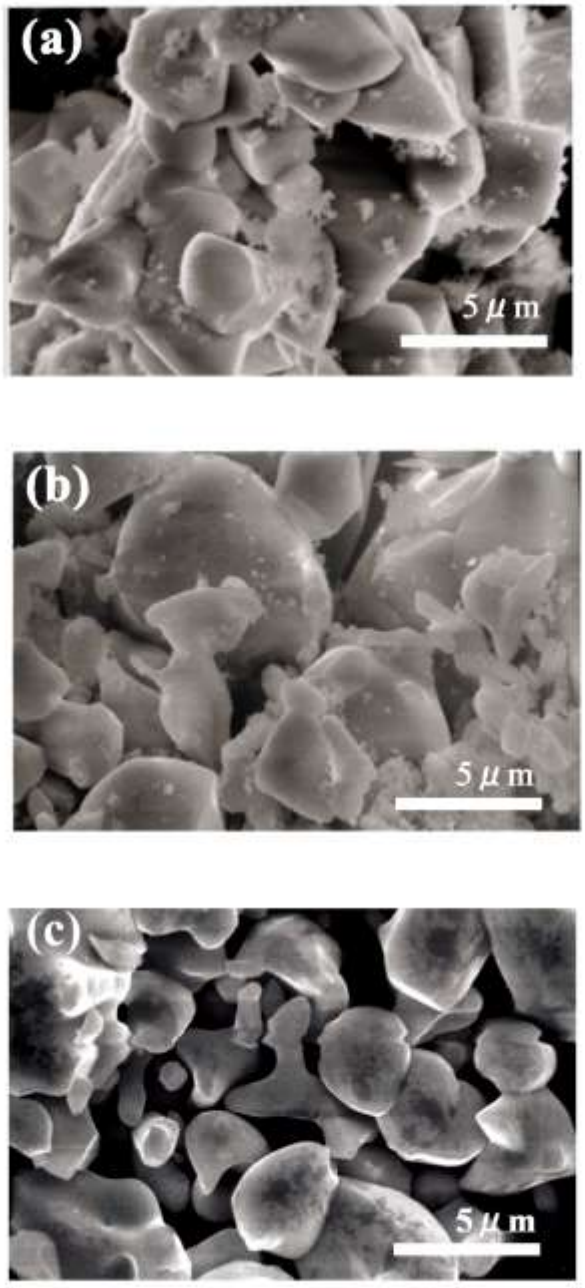


**Figure 5.8 SEM images of synthesized $Zn_{1-x}Mn_xS$ particles of 1-10 μm in size with varying manganese ratio**

**(a): x=0, (b): x=0.03, (c): x=0.05**

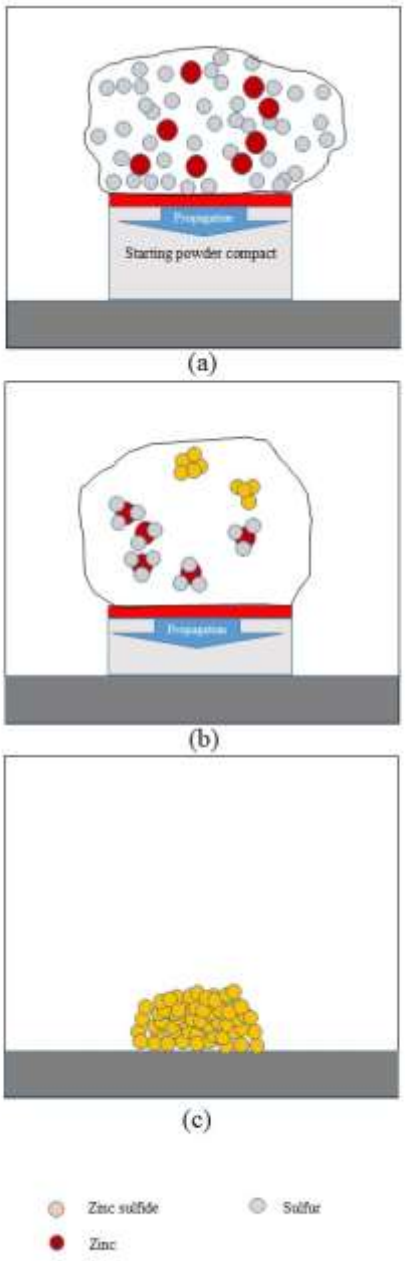


**Figure 5.9 Structure formation process of combustion synthesis of ZnS**

**(a) Combustion wave propagation and gasification of ZnS**

**(b) Reaction of Zn and S**

**(c) Product powder is synthesized**

## 5.4.2 Photoluminescence properties of products

PL spectra are shown in Figure 5.10. It was observed that the peaks at 480 nm shifted to the peaks at 580 nm with the increase of the manganese ratio in starting materials. To increase manganese ratio, the peak of 480 nm becomes smaller, and the peak of 580 nm become larger.

The peaks at 480nm are self-activated (SA) emission relating to a vacancy of zinc sites and impurities near that site in the structure of zinc sulfide [126]. There are many types of SA emission is studied, e.g. $Cl^{-}$, $Al^{3+}$. SA emission is donor-acceptor pear emission. In the case of $Cl^{-}$ ions as impurities, the vacancy of $Zn^{2+}$sites and proximal $Cl^{-}$ ions form acceptor, and second close position of $Cl^{-}$ ion is the donor.

The peaks at 580 nm are related to ions of Mn [127]. These peaks can be observed not only zinc sulfide matrix, but also any other matrix, e.g. CdS, CdTe, and ZnSe. This type of luminescence emission dues to the internal transition within 3d-shell of Mn on a regular metal site ($Zn^{2+}$site in present work). The peaks at 580 nm are related to $3d^5$ orbital transition of $Mn^{2+}$ ions.

Ion radius of manganese is close to that of zinc, therefore, $Mn^{2+}$ ions would penetrate vacancies of $Zn^{2+}$ ions.

Supposing vacancies of $Zn^{2+}$ ions exist uniformly, these results of the PL spectra suggest that $Mn^{2+}$ ions are distributed uniformly into the vacancies of $Zn^{2+}$ ions as increasing the manganese ratio in starting materials. These results of uniform distribution of manganese compounds could be explained by the characteristics of combustion synthesis technology. That is, the combustion synthesis technology was expected that the manganese components could distribute uniformly and finely into the

synthesized zinc sulfide matrix, and that composition in the starting materials could be conserved in the synthesized materials due to the high propagation rate (~5 mm/s) and the large temperature gradient in the combustion synthesis reaction. Therefore, the combustion synthesis technology which has the characteristic of uniform distribution would be suitable for synthesis of ZnS:Mn fine luminescent particles.

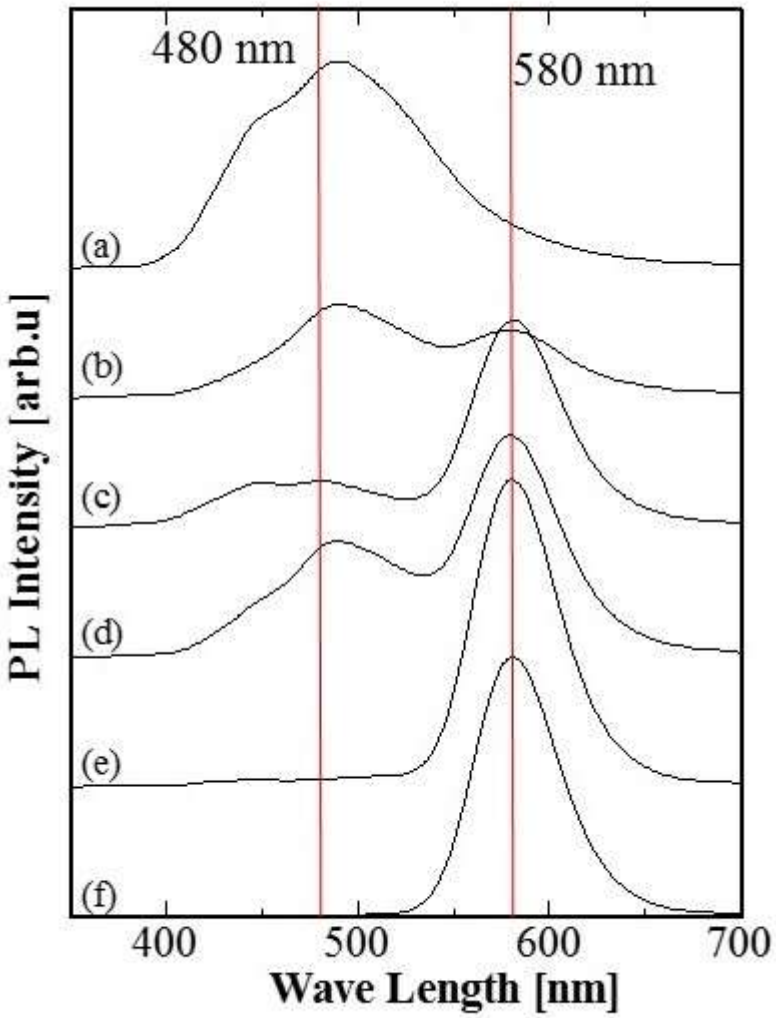


**Figure 5.10 PL spectra of synthesized $Zn_{1-x}Mn_xS$**

**(a) -(f): x=0.01α (α=0,1,2,3,4,5)**

## 5.5 Summary

ZnS combustion synthesis as a related process to strontium aluminates solution combustion synthesis was discussed. The heat of reaction affects the process of structure formation. In the case of solution combustion synthesis of strontium aluminates shown in Chapter 2, 3, and 4, the combustion reaction initiated with increasing combustion temperature by changing urea ratio and furnace temperature, because the adiabatic temperature of the system is similar to the decomposition temperature of $Sr(NO_3)_2$ which is the reaction starting temperature.

In this chapter, combustion synthesis of the compounds of ZnS:Mn was attempted with varying manganese ratio in the starting powder compacts (manganese ratio:0 ~ 0.05). From XRD patterns, the obtained compounds were identified as β-ZnS. The other peaks were not observed. Microscopy revealed that the combustion synthesized particles had 1-10 μm in size. Generation of β-ZnS fine particles could be explained by the high propagation rate and the cooling rate during gas phase combustion synthesis process.

PL properties could be controlled with varying manganese ratio in starting materials. It was observed that the photoluminescence peak at 480 nm shifted to the peak at 580 nm with increasing manganese ratio.

These results would be a proof that manganese components distributed uniformly into the combustion synthesized materials. These results of uniform distribution could be explained of the characteristic of combustion synthesis. Therefore, combustion synthesis of gas-included systems, which has a large cooling rate, can be synthesized as uniform and fine particles of high-temperature phase. In the process of solution combustion synthesis, large amounts of gases are evaporated. These gases caused rapid cooling phenomena. These cooling phenomena in the solution

combustion synthesis process would affect the composition and morphology of products, resulting in fine nano oxide particles would be synthesized.

In this work, the combustion wave propagates directionally which is similar to SHS process. The heat of reaction from a reaction zone would propagate to unreacted starting materials constantly. However, after the combustion wave passed, all starting materials are decomposed and ZnS is once decomposed because of the heat of reaction from the reaction zone, therefore gas included combustion occurred.

It is a notable fact that the products of combustion synthesis of ZnS in atmospheric pressure is all β-phase. In the case of combustion synthesis of ZnS in pressure vessel in order to suppress gasification. Both α-phase and β-phase are synthesized.

# Chapter 6
# General conclusion

In this work, structural formation of $SrAl_2O_4$ by solution combustion synthesis has been discussed. In Chapter 1, general background and the purpose of this work are presented. The purpose of this thesis is to clarify structure formation of strontium aluminates under conditions of high temperature gradients existing during combustion reaction. High-temperature phase can be synthesized under this rapid cooling process in solution combustion synthesis.

In Chapter 2, thermodynamics calculation of solution combustion synthesis of $SrAl_2O_4$ is presented. Thermodynamics calculation is important for combustion synthesis because it suggests that the combustion reaction occurs or not and estimates the maximum temperature during combustion synthesis process.

In Chapter 3, influences of fuel ratio and furnace temperature in the process of solution combustion synthesis on the characteristics of the products were investigated. As a result, it is realized that the phase composition of strontium aluminates is confirmed to be controlled with changing combustion synthesis conditions such as furnace temperature and urea ratio. β-$SrAl_2O_4$ can be synthesized by SCS method. It was found that solution combustion of $SrAl_2O_4$ would proceed when combustion temperature is increased with controlled starting conditions such as fuel ratio and furnace temperature in order to react all starting materials.

In Chapter 4, the model of the solution combustion synthesis process of $SrAl_2O_4$ synthesis is proposed. It is found that in the case of solution combustion synthesis of $SrAl_2O_4$, fuels can be selected as high reactivity with the nitrate of low reaction temperature, and found that particle growth is prohibited by the evolution of the large amount of gases during the solution combustion synthesis process. This

phenomena means particle sizes can be controlled with amounts of gas evolution during combustion synthesis. Gases amounts can be controlled by organic fuel ratio.

In Chapter 5, combustion synthesis of ZnS as a related process to strontium aluminates solution combustion synthesis was discussed. The structure formation process of combustion synthesis is effected by the heat of formation. In the case of solution combustion synthesis of strontium aluminates, the heat of reaction of system is not so high and the adiabatic temperature of the system is similar to the decomposition temperature of $Sr(NO_3)_2$ which is the reaction starting temperature. Therefore, in order to initiate the reaction, it is necessary to increase the combustion temperature by changing urea ratio and furnace temperature. On the other hand, in the case of combustion synthesis of ZnS, the combustion temperature is higher than all boiling points of starting materials and decomposition temperature of ZnS. Therefore, all starting materials and products are once gasified and recrystallized. In this case, the combustion wave propagates in one direction with the aid of the large heat of formation, however, behind the passing combustion wave, ZnS is once decomposed and re-crystallized, resulting in formation of β-ZnS, because the adiabatic temperature of the system is higher than the decomposition temperature of ZnS.

Finally, in this chapter (Chapter 6), general conclusion of this work is presented. Conclusions made in this work can be summarized as follows;

・β-$SrAl_2O_4$ can be synthesized by increasing combustion temperature by changing conditions such as furnace temperature and urea ratio.

・Solution combustion synthesis model of $SrAl_2O_4$ was developed. Two step main reaction model and cooling phenomena are discussed in this model.

・Particle sizes would be determined by cooling phenomena during solution combustion synthesis of $SrAl_2O_4$.

In this work, it is confirmed that the condition of solution combustion synthesis which has large temperature gradients and rapid combustion propagation affects the structural formation of products, resulting in synthesizing β-$SrAl_2O_4$.

In the case of combustion synthesis of $TiB_2$, the combustion temperature is equal to melting point of $TiB_2$, resulting in synthesis of β-$TiB_2$. In the case of combustion synthesis of ZnS, the combustion temperature is higher than the boiling points of Zn and S, and higher than the decomposition temperature of ZnS. Therefore, all starting substances and products are once gasified and recrystallized, resulting in formation of β-ZnS. On the other word, in the case of combustion synthesis of $SrAl_2O_4$, adiabatic temperature of the system at 298 K is higher than decomposition temperatures of all starting materials, lower than the decomposition temperature of $SrAl_2O_4$, and little higher than the phase-phase-transition point of α-$SrAl_2O_4$ and β-$SrAl_2O_4$. Therefore, in order to increase the ratio of β-$SrAl_2O_4$, it is important to increase combustion temperatures by controlling urea ratio and furnace temperature.

It is concluded that when combustion temperature is higher than the boiling point, sublimation point or decomposition temperature of product, and the product is once vaporized, it tends to be synthesized high-temperature phase. However, the combustion temperature is less than those transition points of the product, the product is not vaporized in the synthesis process, and high-temperature phase is partially synthesized. Therefore, to increase combustion temperatures by controlling furnace temperature and fuel ratio is the important factor to increase the ratio of high-temperature phase.

Structure formation of strontium aluminates by solution combustion synthesis is clarified in this work. This work would connect to the study on the relation between structure formation of α-phase and β-phase and luminescent properties of strontium

aluminates doped with europium and dysprosium ions.

# References

[1] A.G. Merzhanov, “History and recent developments in SHS,” *Ceram. Inter*., vol. 21, pp. 371–379, 1995.

[2] A.G.Merzhanov, “Fundamentals, achievements, and perspectives for development of solid-flame combustion,” *Rus. Chem. Bull.*, vol.46, no. 1, pp.1–27, 1997.

[3] A.G. Merzhanov, V.M Shkiro, and I.P. Borovinskaya, USSR Patent No.255221, 1971, U.S. Patent No. 3726643, 1973, Japan Patent No. S57-1098839, 1982.

[4] J. J. Kingsley and K. C. Patil, “A novel combustion process for the synthesis of fine particle α-alumina and related oxide materials,” *Mater. Lett*., vol. 6, no. 11-12, pp. 27–432, 1988.

[5] J. A. Dean, *Lange's handbook of chemistry 15 ed.*, McGraw-hill, 1999.

[6] Nensyougousei kenkyukai, *The chemistry of combustion synthesis*, pp.33-38, TIC, Co. ltd., 1992 (In Japanese).

[7] Y. Momoi, M. Imai, T. Yano, and O. Odawara, “Combustion synthesis of Ti-Al-B Composites,” *Chem. Soc. J*., vol.10 po.1443-1447, 1991.

[8] K. C. Patil, S. T. Aruna, and S. Ekambaram, “Combustion synthesis,” *Curr. Opin. Solid State Mater. Sci.*, vol. 2, pp. 159–165, 1997.

[9] K. C. Patil, S. T. Aruna, and T. Mimani, “Combustion synthesis: an update,” *Curr. Opin. Solid State Mater. Sci*., vol. 6, no. 6, pp. 507–512, 2002.

[10] Nensyougousei kenkyukai, *The chemistry of combustion synthesis*, pp.43, TIC, Co. ltd., 1992 (In Japanese).

[11] A.S.Mukasyan, “Combustion synthesis of nitrides: mechanistic studies,” *Proc. Combust. Inst.*, vol. 30, no. 2, pp. 2529–2535, 2005.

[12] J.B. Holt and D.D. Kingman, “Combustion synthesis of transition metal nitrides,” *Mater. Sci. Res*., vol. 17, pp 167-175, 1984.

[13] O. Odawara, T. Narita, and W. Hua, “Combustion synthesis of TiN with liquid nitrogen,” *J.Com.Chem. J.*, vol. 10, pp. 1461‑1463, 1991 (In Japanese).

[14] M. Shibuya, J. Despres, and O. Odawara, “Combustion nitridation of titanium wires in liquid nitrogen,” *Mater. Res. Bull*., vol. 32, no. 10, pp. 1341–1347, 1997.

[15] S. V. Kozitsky, V. P. Pisarsky and D. D. Polishchuck, “Chemical Composition and Some Properties of Zinc Sulfide Synthesized in Combustion Wave,” *Izv. Acad. Nauk SSSR Neorganicheskie Materialy*, vol. 26, no.12, pp.2472-2475, 1990.

[16] S. Goroshin, J. H.S. Lee, and D. L.Frost, “Combustion synthesis of ZnS in microgravity,” *25th Symp. Combust.*, pp. 1651–1657, 1994.

[17] O. Odawara and Y Kaieda, “A new process for ceramic synthesis-SHS process,” *Trans. national res. Inst. metals*, vol.30, No.2, pp.18-24, 1988.

[18] J.J Kingsley, K. M. Suresh, and K. C. Patil, “Combustion synthesis of fine-particle metal aluminates,” *J. Mater. Sci*., vol. 25, no. 2, pp. 1305–1312, 1990.

[19] A. Varma and A. Mukasyan, “Combustion synthesis of advanced materials: Fundamentals and applications,” *Korean J. Chem. Eng*., vol. 21, no. 2, pp. 527–536, 2004.

[20] O. Odawara, “Ceramics synthesis of combustion synthesis,” *Eng. Mater.*, vol.37, no.8, pp.43-48, 1989 (In Japanese).

[21] A.G. Merzhanov, “Combustion processes that synthesize materials,” *J. Mater. Process. Technol.*, vol. 56, pp. 222–241, 1996.

[22] A. G. Merzhanov, “Fundamentals, achievements, and perspectives for development of solid-flame combustion,” *Russ. Chem. Bull*., vol. 46, no. 1, pp. 1–27, Jan. 1997.

[23] K. C. Patil, “Advanced ceramics: Combustion synthesis and properties,” *Bull. Mater. Sci*., vol. 16, no. 6, pp. 533–541, 1993.

[24] K. C. Patil, M. S. Hegde, T. Rattan, and S. T. Aruna, *Chemistry of nanocrystalline oxide materials-Combustion synthesis, properties and applications*, New Jersey: World Scientific, 2008.

[25]T. Mimani and K. C. Patil, "Solution combustion synthesis of nanoscale oxides and their composites," *Mater. Phys. Mech.*, vol. 4, pp. 134–137, 2001.

[26] A. S. Mukasyan and P. Dinka, "Novel approaches to solution-combustion synthesis of nanomaterials," *Int. J. Self-Propagating High-Temperature Synth.*, vol. 16, no. 1, pp. 23–35, 2007.

[27] A. S. Mukasyan, P. Epstein, and P. Dinka, "Solution combustion synthesis of nanomaterials," *Proc. Combust. Inst.*, vol. 31, no. 2, pp. 1789–1795, 2007.

[28] A. Kumar, E. Wolf, and A. Mukasyan, "Solution combustion synthesis of metal nanopowders: Copper and copper/nickel alloys," *AIChE J.*, vol. 57, no. 12, pp. 473–3479, 2011.

[29] P. Dinka and A. Mukasyan, "Solution Combustion Synthesis of Nano Materials," *NSTI-Nanotech*, vol. 1, pp. 456–459, 2006.

[30] A. K. Tyagi, "Combustion synthesis: a soft-chemical route for functional nano-ceramics," *Barc Newsl.*, vol. 285, pp. 39–48, 2007.

[31] V. D. Zhuravlev, V. G. Bamburov, A. R. BEletov, L. A. Perelyaeva, I. V. Baklanova, O. V. Sivtova, V. G. VAsil'ev, E. V. Vladimirova, V. G. Shevchenko, and I. G. Grigorov, "Solution combustion synthesis of $\alpha$-$Al_2O_3$ using urea," *Ceram. Int.*, vol. 39, pp. 1379–1384, 2013.

[32] L. Pathak, T. Singh, S. Das, A. Verma, and P. Ramachandrarao, "Effect of pH on the combustion synthesis of nano-crystalline alumina powder," *Mater. Lett.*, vol. 57, no. 2, pp. 380–385, 2002.

[33] R. Ianoş, I. Lazău and C. Păcurariu, “The influence of combustion synthesis conditions on the α-$Al_2O_3$ powder preparation,” *J. Mater, Sci*., vol. 44, pp. 1016–1023, 2009.

[34] W. Chen, F. Li, J. Yu, and L. Liu, “A facile and novel route to high surface area ceria-based nanopowders by salt-assisted solution combustion synthesis,” *Mater. Sci. Eng. B*, vol. 133, no. 1–3, pp. 151–156, 2006.

[35] S. T. Aruna and K. C. Patil, “Combustion synthesis and properties of nanostructured ceria-zirconia solid solutions,” *Nanostructured Mater.*, vol. 10, no. 6, pp. 955–964, 1998.

[36] M. Jayalakshmi and K. Balasubramanian, “Solution combustion synthesis of $Fe_2O_3$/C, $Fe_2O_3$-$SnO_2$/C, $Fe_2O_3$-ZnO/C composites and their electrochemical characterization in non-aqueous electrolyte for supercapacitor application,” *Int. J. Electrochem. Sci.*, vol. 4, pp. 878–886, 2009.

[37] L. G. Jacobsohn, S. C. Tornga, B. L. Bennett, R. E. Muenchausen, O. Ugurlu, T.-K. Tseng, J. Choi, and P. H. Holloway, “Annealing effects on the photoluminescence yield of $Gd_2O_3$:Eu nanoparticles produced by solution combustion synthesis,” *Radiat. Meas.*, vol. 45, no. 3–6, pp. 611–614, Mar. 2010.

[38] L. G. Jacobsohn, B. L. Bennett, R. E. Muenchausen, S. C. Tornga, J. D. Thompson, O. Ugurlu, D. W. Cooke, and a. L. Lima Sharma, “Multifunction $Gd_2O_3$:Eu nanocrystals produced by solution combustion synthesis: structural, luminescent, and magnetic characterization,” *J. Appl. Phys.*, vol. 103, no. 10, pp. 104303(6 pages), 2008.

[39] G. Tessari, M. Bettinelli, A. Speghini, D. Ajo, G. Pozza, L. E. Depero, B. Allieri, and L. Sangaletti, “Synthesis and optical properties of nanosized powders: lanthanide-doped $Y_2O_3$,” *Appl. Surf. Sci.*, vol. 144–145, no. 1–4, pp. 686–689, 1999.

[40] L. G. Jacobsohn, R. Wang, P. Crozier, B. L. Bennett, and R. E. Muenchausen, "Electron energy-loss spectroscopy investigation of dopant homogeneity in Tb-doped $Y_2O_3$ nanoparticles prepared by solution combustion synthesis," *Opt. Mater. (Amst).*, vol. 34, no. 4, pp. 671–674, 2012.

[41] T. Ye, Z. Guiwen, Z. Weiping, and X. Shangda, "Combustion synthesis and photoluminescence of nanocrystalline $Y_2O_3$: Eu phosphors," *Mater. Res. Bull.*, vol. 32, no. 5, pp. 501–506, 1997.

[42] T. Takeda, D. Koshiba, and S. Kikkawa, "Gel combustion synthesis and luminescence properties of $Y_2O_3$: Eu," *J. Ceram. Soc.*, vol. 929, pp. 927–929, 2004.

[43] P. Yu, X. Zhang, Y. Chen, and Y. Ma, "Solution-combustion synthesis of ε-$MnO_2$ for supercapacitors," *Mater. Lett.*, vol. 64, no. 1, pp. 61–64, 2010.

[44] M. D. Lima, R. Bonadimann, M. J. de Andrade, J. C. Toniolo, and C. P. Bergmann, "Nanocrystalline $Cr_2O_3$ and amorphous $CrO_3$ produced by solution combustion synthesis," *J. Eur. Ceram. Soc.*, vol. 26, no. 7, pp. 1213–1220, 2006.

[45] C.C. Hwang and T.Y. Wu, "Synthesis and characterization of nanocrystalline ZnO powders by a novel combustion synthesis method," *Mater. Sci. Eng. B*, vol. 111, no. 2–3, pp. 197–206, 2004.

[46] C.S. Lin, C.C. Hwang, W.H. Lee, and W.Y. Tong, "Preparation of zinc oxide (ZnO) powders with different types of morphology by a combustion synthesis method," *Mater. Sci. Eng. B*, vol. 140, no. 1–2, pp. 31–37, 2007.

[47] C.C. Hwang, C.S. Lin, G.P. Wang, C.H. Peng, and S.L. Chung, "A self-propagating high-temperature synthesis method for synthesis of zinc oxide powder," *J. Alloys Compd.*, vol. 467, no. 1–2, pp. 514–523, 2009.

[48] V. Sousa, A. Segadaes, M. Morelli, and R. Kiminami, “Combustion synthesized ZnO powders for varistor ceramics,” *Int. J. Inorg. Mater.*, vol. 1, no. 3–4, pp. 235–241, 1999.

[49] M. Jayalakshmi, “Single step solution combustion synthesis of ZnO/carbon composite and its electrochemical characterization for supercapacitor application,” *Int. J. Electrochem. Sci.*, vol. 3, pp. 96–103, 2008.

[50] A. J. Reddy, M. K. Kokila, H. Nagabhushana, R. P. S. Chakradhar, C. Shivakumara, J. L. Rao, and B. M. Nagabhushana, “Structural, optical and EPR studies on ZnO:Cu nanopowders prepared via low temperature solution combustion synthesis,” *J. Alloys Compd.*, vol. 509, no. 17, pp. 5349–5355, 2011.

[51] L. D. Jadhav, S. P. Patil, A. U. Chavan, A. P. Jamale, and V. R. Puri, “Solution combustion synthesis of Cu nanoparticles : a role of oxidant-to-fuel ratio,” *Eng. Technol.*, vol. 6, pp. 812 –815, 2011.

[52] D.A. Fumo, M.R. Morelli, and A.M. Segadaes, “Combustion synthesis of calcium aluminates,” *Mater. Res. Bull.*, vol. 31, no. 10, pp. 1243–1255, 1996.

[53] C. Zhao and D. Chen, “Synthesis of $CaAl_2O_4$:Eu,Nd long persistent phosphor by combustion processes and its optical properties,” *Mater. Lett.*, vol. 61, no. 17, pp. 3673–3675, Jul. 2007.

[54] B. Zhang, C. Zhao, and D. Chen, “Synthesis of the long-persistence phosphor $CaAl_2O_4:Eu^{2+}$, $Dy^{3+}$, $Nd^{3+}$ by combustion method and its luminescent properties,” *Lumin.*, vol. 25, no. 1, pp. 25–9, 2010.

[55] M. A. Rodríguez, C. L. Aguilar, and M. A. Aghayan, “Solution combustion synthesis and sintering behavior of $CaAl_2O_4$,” *Ceram. Int.*, vol. 38, no. 1, pp. 395–399, 2012.

[56] S. B. Bhaduri and K. A. Prisbrey, “Auto ignition synthesis of nanocrystalline $MgAl_2O_4$ and related nanocomposites,” *J. Mater. Res.*, vol. 14, no. 9, pp. 3571–3580, 1999.

[57] I. Ganesh, B. Srinivas, R. Johnson, B. P. Saha, and Y. R. Mahajan, “Microwave assisted solid state reaction synthesis of $MgAl_2O_4$ spinel powders,” *J. Eur. Ceram. Soc.*, vol. 24, no. 2, pp. 201–207, Jan. 2004.

[58] C. Păcurariu, I. Lazău, Z. Ecsedi, R. Lazău, P. Barvinschi, G. Mărginean, C. Pacurariu, I. Lazau, R. Lazau, and G. Marginean, “New synthesis methods of $MgAl_2O_4$ spinel,” *J. Eur. Ceram. Soc.*, vol. 27, no. 2–3, pp. 707–710, 2007.

[59] R. Ianoş and I. Lazău, “Application of new organic fuels in the direct $MgAl_2O_4$ combustion synthesis,” *Eur. J. Inorg. Chem.*, pp. 931–938, 2008.

[60] R. Ianoş¸I. Lazău, C. Păcurariu, and P. Barvinschi, “Solution combustion synthesis of $MgAl_2O_4$ using fuel mixtures,” *Mater. Res. Bull.*, vol. 3, no. 12, pp. 3408–3415, Dec. 2008.

[61] K. Prabhakaran, D. S. Patil, R. Dayal, N. M. Gokhale, and S. C. Sharma, “Synthesis of nanocrystalline magnesium aluminate ($MgAl_2O_4$) spinel powder by the urea–formaldehyde polymer gel combustion route,” *Mater. Res. Bull.*, vol. 44, no. 3, pp. 13–618, Mar. 2009.

[62] F. Li, Y. Zhao, Y. Liu, Y. Hao, R. Liu, and D. Zhao, “Solution combustion synthesis and visible light-induced photocatalytic activity of mixed amorphous and crystalline $MgAl_2O_4$ nanopowders,” *Chem. Eng. J.*, vol. 173, no. 3, pp. 750–759, 2011.

[63] J. Bai, J. Liu, C. Li, G. Li, and Q. Du, “Mixture of fuels approach for solution combustion synthesis of nanoscale $MgAl_2O_4$ powders,” *Adv. Powder Technol.*, vol. 22, no. 1, pp. 72–76, 2011.

[64] D. Kovacheva, H. Gadjov, K. Petrov, S. Mandal, M. G. Lazarraga, L. Pascual, J. M. Amarilla, R. M. Rojas, P. Herrero, and J. M. Rojo, "Synthesizing nanocrystalline $LiMn_2O_4$ by a combustion route," *J. Mater. Chem.*, vol. 12, no. 4, pp. 1184–1188, 2002.

[65] C.Z. Lu and G.T.K. Fey, "Nanocrystalline and long cycling $LiMn_2O_4$ cathode material derived by a solution combustion method for lithium ion batteries," *J. Phys. Chem. Solids*, vol. 67, pp. 756–761, 2006.

[66] S. Rodrigues, N. Munichandraiah, and A. K. Shukla, "Novel solution-combustion synthesis of $LiCoO_2$ and its characterization as cathode material for lithium-ion cells," *J. Power Sources*, vol. 102, no. 1–2, pp. 322–325, 2001.

[67] S. Vivekanandhan, M. Venkateswarlu, and N. Satyanarayana, "Ammonium carboxylates assisted combustion process for the synthesis of nanocrystalline $LiCoO_2$ powders," *Mater. Chem. Phys.*, vol. 109, no. 2–3, pp. 241–248, 2008.

[68] R. Ianoş, I. Lazău, and C. Păcurariu, "Metal nitrate/fuel mixture reactivity and its influence on the solution combustion synthesis of γ-$LiAlO_2$," *J. Therm. Anal. Calorim.*, vol. 97, no. 1, pp. 209–214, 2009.

[69] S. Dimitrovska-Lazova, V. Mireski, D. Kovacheva, and S. Aleksovska, "Solution combustion synthesis of $YCoO_3$ and investigation of its catalytic properties by cyclic voltammetery," *J. Solid State Electrochem.*, vol. 16, no. 1, pp. 219–225, 2011.

[70] H. Jiang, H. Endo, H. Natori, M. Nagai, and K. Kobayashi, "Fabrication and photoactivities of spherical-shaped $BiVO_4$ photocatalysts through solution combustion synthesis method," *J. Eur. Ceram. Soc.*, vol. 28, no. 15, pp. 2955–2962, 2008.

[71] U. M. García Pérez, S. Sepúlveda-Guzmán, a. Martínez-de la Cruz, and U. Ortiz Méndez, "Photocatalytic activity of $BiVO_4$ nanospheres obtained by solution combustion synthesis using sodium carboxymethylcellulose," *J. Mol. Catal. A Chem.*, vol. 335, no. 1–2, pp. 169–175, 2011.

[72] J. Chandradass and K. H. Kim, “Mixture of fuels approach for the solution combustion synthesis of $LaAlO_3$ nanopowders,” *Adv. Powder Technol.*, vol. 21, no. 2, pp. 100–105, 2010.

[73] S. Shikao, “Combustion synthesis of $Eu^{3+}$ activated $Y_3Al_5O_{12}$ phosphor nanoparticles,” *J. Alloys Compd.*, vol. 327, no. 1–2, pp. 82–86, 2001.

[74] G. Xia, S. Zhou, J. Zhang, S. Wang, and J. Xu, “Solution combustion synthesis, structure and luminescence of $Y_3Al_5O_{12}$:$Tb^{3+}$ phosphors,” *J. Alloys Compd.*, vol. 421, no. 1–2, pp. 294–297, 2006.

[75] H. M. H. Fadlalla, C. C. Tang, A. Elsanousi, X. X. Ding, and S. R. Qi, “Solution-combustion synthesis of $Tb^{3+}$-doped $Y_3Al_5O_{12}$ nanoparticles,” *J. Lumin.*, vol. 129, no. 4, pp. 401–405, 2009.

[76] H. Wang, J. Han, and S. Du, “Efect of nitrogen pressure and oxygen-containing impurities on self-propagating high temperature synthesis of $Si_3N_4$,” *J. Eur. Ceram. Soc.*, vol. 21, pp. 297–302, 2001.

[77] Q. Wang, G. Liu, J. Yang, Y. Chen, and J. Li, “Preheating-assisted combustion synthesis of β-$Si_3N_4$ powders at low $N_2$ pressure,” *Mater. Res. Bull.*, vol. 48, pp. 1321–1323, 2012.

[78] T. Matsuzawa and Y. Aoki, “A New Long Phosphorescent Phosphor with High Brightness, $SrAl_2O_4$: $Eu^{2+}$, $Dy^{3+}$,” *J. Electrochem. Soc.*, vol. 143, no. 8, pp. 2670–2673, 1996.

[79] J. Dong-Dong, W. Bo-Qun, and Z. Jing, “Phase dependence of luminescent emission of $Eu^{2+}$ doped $SrAl_2O_4$,” *Chinese Phys.*, vol. 9, p. 69-72, 2000.

[80] H. Tanaka, H. Wada, and O. Odawara, “Structure formation of $SrAl_2O_4$ synthesized by solution combustion synthesis,” *Int. J. Self-Propagating High-Temperature Synth.*, vol.14, no. 3, pp. 199-208, 2005.

[81] H. Tanaka, A. V. Gubarevich, H. Wada and O. Odawara, “Process stages during solution combustion synthesis of strontium aluminates,” *Int. J. Self-Propagating High-Temperature Synth.*, vol. 22, no. 3, pp. 151–156, 2013.

[82] R. Ianoş, R. Istratie, C. Păcurariu, and R. Lazău, “Solution combustion synthesis of strontium aluminate, $SrAl_2O_4$, powders: single-fuel versus fuel-mixture approach,” *Phys. Chem, Chem. Phys*, vol. 18, no. 2, pp. 1150-1157, 2016.

[83] R.N. Bhargava, D. Gallagher, X. Hong, and A. Nurmikko, “Optical properties of manganese-doped nanocrystals of ZnS,” *Phys. Rev. Lett*., vol. 72, no. 3, pp. 416–419, 1994.

[84] R. N. Bhargava, “Doped nanocrystalline materials-physics and applications,” *Spec. Iso. Assem. Semicon. Nanocryst.*, vol.70, pp.85-94, 1996.

[85] R. N. Bhargava, “The role of impurity in doped nanocrystals,” *J. Lumin*., vol.72-74, pp.46-48, 1997.

[86] M. Tanaka, J. Qi, and Y. Masumoto, "Comparison of energy levels of $Mn^{2+}$ in nanosized- and bulk-ZnS crystals,” *J. Lumin.*, vol.87-89, pp.472-474, 2000.

[87] S. Adachi, Optical constants of crystalline and amorphous semiconductors, pp. 445-448, Kluwer academic publishers, 1999.

[88] N. Ishiwada, T. Ueda, and T. Yokomori, “Characteristics of rare earth (RE = Eu, Tb, Tm)-doped $Y_2O_3$ phosphors for thermometry,” *Lumin.*, vol. 26, no. 6, pp. 381–9, 2011.

[89]S. Shikao, “Combustion synthesis of $Eu^{3+}$ activated $Y_3Al_5O_{12}$ phosphor nanoparticles,” *J. Alloys Compd.*, vol. 327, no. 1–2, pp. 82–86, 2001.

[90] K. Van den Eeckhout, P. P. F. Smet, D. Poelman, and K. Van den Eeckhout, “Persistent luminescence in $Eu^{2+}$-doped compounds: a review,” *Materials (Basel).*, vol. 3, no. 4, pp. 2536–2566, 2010.

[91] J. Hölsä, T. Laamanen, M. Lastusaari, J. Niittykoski, and P. Novák, "Electronic structure of the $SrAl_2O_4:Eu^{2+}$ persistent luminescence material," *J. Rare Earths*, vol. 27, no. 4, p. 550-554, 2009.

[92] S. Ito, S. Banno, K. Suzuki, and M. Inagaki, "Phase Transition in $SrAl_2O_4$," *Z. Physik. Chem. Neue Folge*, vol.105, no. 3-4, pp. 173-178, 1977.

[93] K. Fukuda and K. Fukushima, "Crystal structure of hexagonal $SrAl_2O_4$ at 1073K," *J. Solid State Chem.*, vol. 178, pp. 2709–2714, 2005.

[94] National Bureau of Standards, *NBS monograph 25 pattern 20*, A United States Department of Commerce Publication, pp.91, 1984.

[95] K. Momma, and F. Izumi, "VESTA 3 for three-dimensional visualization of crystal, volumetric and morphology data," *J. Appl.Cryst.*, vol. 44, no. 6, pp. 1272–1276, 2011.

[96] A. Douy, and M. Capron, "Crystallisation of spray-dried amorphous precursors in the $SrO\text{-}Al_2O_3$ system," *J. Eur. Cer. Soc*., vol.23, no.12, pp.2075-2081, 2002

[97] Y. Lu, and Y. UXiong, "$SrAl_2O_4:Eu^{2+}$, $Dy^{3+}$ phosphors derived from a new sol-gel route," *Microelectronic J.*, vol.35, pp.379-382, 2004.

[98] Q. Xiao, L. Xiao, Y. Liu, X. Chen, and Y. Li, "Synthesis and luminescence properties of needle-like $SrAl_2O_4$:Eu, Dy phosphor via a hydrothermal co-precipitation method," *J. Phys. Chem. Solids*, vol. 71, pp. 1026–1030, 2010.

[99] T. Peng, H. Yang, X. Pu, B. Hu, Z. Jiang, and C. Yan "Combustion synthesis and photoluminescence of $SrAl_2O_4$:Eu, Dy phosphor nanoparticles," *Matt. Let.*, vol. 58, pp.352-356, 2004.

[100] F. Ganits, T. Yu. Chemekova, and Yu. P. Udalov, "The phase diagram of $SrO\text{-}Al_2O_3$ systems," *Zh. Neorg. Khim.*, vol. 24, no. 2, pp 471-475, 1979.

[101] Phase Equilibria Diagrams Online Database (NIST Standard Reference Database 31), The American Ceramic Society and the National Institute of Standards and Technology, Figure No. 6427, 2016.

[102] M. Binnewies and E. Milke, *Thermochemical data of elements and compounds*, Weinheim, Wiley-VCH, 1999.

[103] Nensyougousei kenkyukai, *The chemistry of combustion synthesis*, pp. 32, TIC, Co. ltd., 1992 (In Japanese).

[104] S.Yuvaraj, L. Fan-Yuan,C. Tsong-Huei, and Y.Chuin-Tih, "Thermal Decomposition of Metal Nitrates in Air and Hydrogen Environments," *J. Phys. Chem.B*, vol. 107, no. 4, pp. 1044–1047, 2003.

[105] E. EI-Shereafy, M. M. Abousekkina, A. Mashaly, and M. EI-Ashry, "Mechanism of thermal decomposition and γ-pyrolysis of aluminum nitrate nonahydrate [$AI(NO_3)_3.9H_2O$]," *J. Radioanal. Nucl. Chem.*, vol. 237, no. 1–2, pp. 183–186, 1998.

[106] P. M. Schaber, J. Colson, S. Higgins, D. Thielen, B. Anspach, and J. Brauer, "Thermal decomposition (pyrolysis) of urea in an open reaction vessel," T*hermochim. Acta*, vol. 424, no. 1–2, pp. 131–142, 2004.

[107] National Bureau of Standards, *NBS monograph 25 pattern 10*, A United States Department of Commerce Publication, pp. 52, 1972.

[108] N.A. Sirazhiddinov and P.A. Arifov, "Solid-phase reactions in the formation of strontium aluminate," *Rus. J. Inorg. Chem.*, vol.16, no.1, pp. 40-42, 1971.

[109] H.P. Klug and L.E. Alexander, *X-ray diffraction procedures 2nd ed*, pp.531-536, John Wiley and Sons, New York, 1974.

[110] M.J. Buerger, *X-Ray Crystallography*, pp.181-182, John Wiley and Sons, New York, 1966.

[111] A. K. Prodjosantoso and B. J. Kennedy, “Synthesis and Evolution of the Crystalline Phases in $Ca_{1-x}Sr_xAl_2O_4$,” *J. Solid State Chem.*, vol. 236, no. 2002, pp. 229–236, 2006.

[112] M. Avdeev, S. Yakovlev, A. A. Yaremchenko, and V. V Kharton, “Transitions between $P2_1$, $P6_3$ ($\sqrt{3}A$), and $P6_322$ modifications of $SrAl_2O_4$ by in situ high-temperature X-ray and neutron diffraction,” *J. Solid State Chem.*, vol. 180, no. 12, pp. 3535–3544, 2007.

[113] K. Machida, G. Adachi, J. Shiokawa, M. Shimada, and M. Koizumi, “Structure of strontium tetraaluminate β-$SrAl_4O_7$,” *Acta Crystallogr. B*, vol. 38, no. 3, pp. 889–891, 1982.

[114] F.H.Chung, ”Quantitative interpretation of X-ray diffraction patterns of mixtures. I. Matrix-flushing method for quantitative multicomponent analysis,” *J. Appl. Cryst*., vol. 7, pp. 519-525, 1974.

[115] F.H.Chung, ”Quantitative interpretation of X-ray diffraction patterns of mixtures. II. Adiabatic principle of X-ray Diffraction Analysis of Mixuters,” *J. Appl. Cryst.*, vol. 7, pp.519-530, 1974.

[116] B.L. Davis, R. Kath, and M. Michael Spilde, “The Reference Intensity Ratio: Its Measurement and Significance,” *Powder Diffr*., vol. 5, no. 2, pp .76-78, 1990.

[117] S. Shionoya, “Review of luminescence in II-VI compounds,” *J. Lumin.*, vol. 1-2, pp. 17–38, 1970.

[118] R. Mach and G. O. MuLLer, “Physical Concepts of High-Field, Thin-Film Electroluminescence Devices”, *Physica Status Solidi (a)*, vol. 69, no. 1, pp. 11-66, 1982.

[119] M. A. Haase, J. Qiu, J. M. DePuydt, and H. Cheng, “Blue-Green Laser Diodes”, *Appl. Phys. Lett.*, vol. 59, pp. 1272-1274, 1991.

[120] S. Taniguchi, T. Hino, S. Itoh, K. Nakano, N. Nakayama, A. Ishibashi, M. Ikeda, and Y. Mori, "Room temperature continuous operation of blue-green laser diodes," *Elec. Lett.*, vol. 29, no .25, pp. 2194-2195, 1993.

[121] D. Gallagher, W.E. Heady, J.M. Racz, and R.N. Bhargava, "Doped zinc sulfide nanocrystals precipitated within a poly(ethylene oxide) matrix - processing and optical characteristics," *J. Cryst. Growth*, vol. 138, no. 1-4, pp. 970–975, 1994.

[122] S. V. Kozitsky and a. N. Krasnov, "Formation of 'gigantic' crystallites in ZnS obtained by self-propagating high-temperature synthesis," *J. Cryst. Growth*, vol. 165, no. 1–2, pp. 166–168, 1996.

[123] S. V. Kozitsky, V. P. Pisarskii, and O. O. Ulanova, "Structure and phase composition of zinc sulfide produced by self-propagating high-temperature synthesis," *Combust. Explos. Shock Waves*, vol. 34, no. 1, pp. 34–39, 1998.

[124] C.W. Won, H.H. Nersisyan, H.I. Won, D.Y. Jeon, and J.Y. Han, "Combustion synthesis and photoluminescence of ZnS: $Mn^{+2}$ particles," *J. Lumin.*, vol. 130, pp. 1026–1031, 2010.

[125] V.S. Ban and E.A.D. White, "Mass spectrometric study of processes in the closed tube vapor growth of CdS and ZnS," *J. Cryst. Growth*, vol. 33, pp. 365-370, 1976.

[126] J. E. Nicholls, J. J. Davies, B. C. Cavenett, J. R. James and D. J. Dunstan, "Spin-Dependent Donor-Acceptor Pair Recombination in ZnS Crystals Showing the Self-Activated Emission," *J. phys. C*, vol.12, pp. 361-365, 1979.

[127] C. Benecke, W. Busse, H.E. Gumlich, H. Hoffmann, S. Hofmman, A. Krost, and H. Waldmann, "On the excitation and emission of the infrared luminescence of wide band gap Mn II-VI Semimagnetic Semiconductors," *Phys. Stat. Solid.(b)*, vol. 153, pp. 391-396, 1989.

# Acknowledgements

I would particularly like to thank Professor O. Odawara for his great support and mentoring over the years and giving me the opportunity to work on the study and joining international meetings.

I also have acknowledged for Professor H. Wada and Dr. J. Habasaki for many advices. I also grateful to Dr. A. V. Gubarevich. She advised me with encouragement and assisted my research very much.

I am also grateful to all judges, Professor M. Yoshimoto, Professor M. Azuma, Professor and K. Nagai. I appreciate greatly holding examination meeting many times.

For my TG/DTA measurements, I would like to thank Professor S. Hata. He assisted my thermal analysis. For my FE-SEM measurements, I would also like to thank Professor Y. Kitamoto for supporting measurements.

I am grateful to all my laboratory students for advices in seminar, and I am also grateful to Secretary Emiko Izumi with her encouragements.

Finally, I would like to thank my family for their support over the years, which made graduate school experience.

# List of Publications

**(Chapter 5)**

[1] H. Tanaka, E. Miyazaki, and O. Odawara,

"Combustion Synthesis of Zinc-Manganese-Sulfur Compound Systems,"

*Internal journal of self-propagating high-temperature synthesis*, vol. 13, no. 3, pp. 227-232, 2004.

**(Chapter 2 and 3)**

[2] H. Tanaka, H. Wada, and O. Odawara,

"Structure Formation of $SrAl_2O_4$ Synthesized by Solution Combustion Synthesis,"

*Internal journal of self-propagating high-temperature synthesis*, vol. 14, no. 3, pp. 199-208, 2005.

**(Chapter 4)**

[3] H. Tanaka, A.V. Gubarevich, H. Wada, and O. Odawara,

"Process Stages During Solution Combustion Synthesis of Strontium Aluminates,"

*Internal journal of self-propagating high-temperature synthesis*, vol. 22, no. 3, pp. 151-156, 2013.

# List of Presentations

[1] H. Tanaka, H. Wada, and O. Odawara, “Solution combustion synthesis of strontium aluminates,” *The 44th Symposium on Basic Science of Ceramics*, Kochi (Japan), January, 2006.

[2] H. Tanaka, A.V. Gubarevich, H. Wada, O. Odawara, “Combustion Synthesis and Structure Changes of Strontium Aluminates”, *9th International Symposium of Self-Propagating High Temperature Synthesis*, Anavyssos (Greece), September, 2011.